Final Technical Report

Project Title: Biorefinery and Carbon Cycling Research Project

Award Number: DE-FG36-08GO88144

Recipient: University of Georgia Research Foundation, Inc.

Project Location(s): University of Georgia, Athens GA 30602

Project Period: 1 Jan 2009 to 30 Sept 2011
Date of Report: April 2012
Written by: K.C. Das
Program Manager: K.C. Das

Principal Investigators: K.C. Das, Thomas T. Adams, Mark A. Eiteman, James R. Kastner, Sudhagar Mani, Ryan Adolophson.

Subcontractors: None.

Cost-Sharing Partners: The University of Georgia, Athens GA 30602

DOE Project Team *[Ask the Project Officer or Monitor if you need any of the following information] [Include phone number and email for each]*

DOE-HQ contact: Gina Lynch
DOE Field Project Officer: Paul Grabowski
DOE Contract Specialist: Molly Hames
DOE Project Engineer:

Acknowledgment: This material is based upon work supported by the Department of Energy under Award Number DE-FG36-08GO88144.

Executive Summary

In this project we focused on several aspects of technology development that advances the formation of an integrated biorefinery. These focus areas include: [1] pretreatment of biomass to enhance quality of products from thermochemical conversion; [2] characterization of and development of coproduct uses; [3] advancement in fermentation of lignocellulosics and particularly C5 and C6 sugars simultaneously, and [4] development of algal biomass as a potential substrate for the biorefinery. These advancements are intended to provide a diverse set of product choices within the biorefinery, thus improving the cost effectiveness of the system.

Technical effectiveness was demonstrated in the thermochemical product quality in the form of lower tar production, simultaneous of use of multiple sugars in fermentation, use of biochar in environmental (ammonia adsorption) and agricultural applications, and production of algal biomass in wastewaters. Economic feasibility of algal biomass production systems seems attractive, relative to the other options. However, further optimization in all paths, and testing/demonstration at larger scales are required to fully understand the economic viabilities. The coproducts provide a clear picture that multiple streams of value can be generated within an integrated biorefinery, and these include fuels and products.

Table of Contents

Introduction

This project focuses on biorefinery and carbon cycling technologies for production of liquid fuels and value added products from forest, agricultural and other biomass in Georgia. Biorefining provides major opportunities for economic development, particularly in rural areas. Georgia is a leading producer of biomass from forest, agriculture and other industries.

Our overall goals were to develop technologies for (1) thermochemical conversion of biomass to liquid fuels, focusing on preprocessing (torrefaction), upgrading products and catalytic production of fuels, (2) fermentation processes emphasizing cellulosic ethanol, (3) development of uses for co-product biochar, and (4) feedstock development and management, including new feedstocks (such as algae) to support biomass based industry in Georgia. Additionally, we contributed to the development of the industry through educational outreach programs.

The state of Georgia is a leading producer of biomass and biorefining provides opportunities for economic development and job creation, particularly in rural areas. Outcomes from this project include new technologies for production of fuels and co-products from biomass; developments in biomass production (algae) methods, pretreatment technologies, and education of a workforce familiar with biorefining. A team of researchers from multiple disciplines were brought together at UGA and worked on various aspects of the biomass to biofuels pathways. This was accomplished by establishing a program titled Biorefining and Carbon Cycling Program with a vision as outlined in Figure 1.

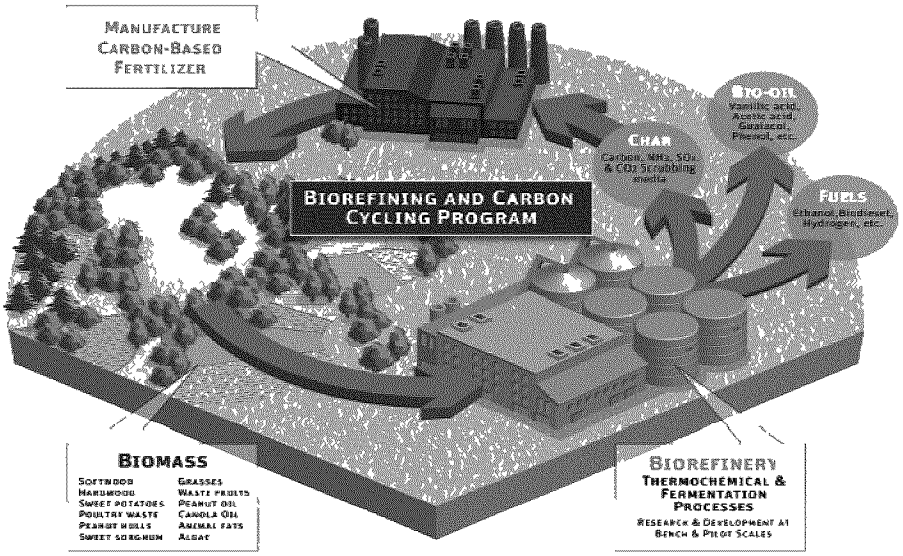

Figure 1. Schematic description of the University of Georgia Biorefining and Carbon Cycling Program R&D activities.

Task A – Development of Torrefaction technology and preprocessing for effective use of biomass and for generating clean intermediates from biomass for the production of liquid and gaseous fuels.

Our overall goal in this task was to develop thermochemical approaches to improve biomass conversion to liquid fuels. Particularly we focused on pretreatment using torrefaction as a first approach, with the hypothesis that this pretreatment would remove reactive components of biomass thereby providing a more stable product after thermal conversion. We also conducted work on reactive condensation of pyrolysis oils, which provide improved properties for the BioOil; and the use of carbon-based catalysts for tar removal from Syngas. These studies were done using a model compound, toluene.

Subtask A.1: Selectively altering biomass structure for improved pyrolysis and gasification

Our overall goal was to improve the quality of the liquid fuel product from pyrolysis. This was done using pretreatment with torrefaction that is expected to selectively alter the biomass structure. Torrefaction is known to reduce certain components of biomass thus increasing its energy density. It is known that these components could be the more reactive fractions of the biomass, and in its absence, BioOil properties would be improved.

Methodology

Freshly harvested loblolly pine logs (delimbed and debarked) were cut into sections prior to being chipped in a Vermeer 1230 brush chipper. Material was then sorted in a Royer Model 42 Power screener utilizing a ¼" screen to collect reject material. Particles larger than 2" were hand removed. The wood chips were stored for torrefaction and gasification experiments. The fuel composition of wood chips was summarized in Table A.1.

Table A.1. Loblolly Pine Properties

	Avg. ± S.D.
Moisture (%)	6.89 ± 0.08
Volatiles (wt% daf)	75.13 ± 0.38
Fixed Carbon (wt% daf)	17.84 ± 0.30
Ash (%wt daf)	0.24 ± 0.16
C (%wt daf)	49.12 ± 0.81
H (%wt daf)	5.59 ± 0.13
N (%wt daf)	0.16 ± 0.02
S (%wt daf)	0.04 ± 0.02
O (%wt daf)	45.09 ± 0.83
Hemicellulose (%wt daf)	15.64 ± 2.14
Cellulose (%wt daf)	40.54 ± 7.89

Lignin (%wt daf)	28.76 ± 1.72
HHV [MJ kg^{-1}]	18.72 ± 0.43
LHV [MJ kg^{-1}]	17.47

Approximately 100 kg of dried pine was loaded in a rotary kiln for the torrefaction process (Figure A.1). The kiln was a batch system with a 3 m^3 octagonal shaped mild steel reactor (1) externally heated by a 1.3 mmBtu hr^{-1} natural gas burner (2). The reactor rotates on its axis with ports allowing inert gas through one end (3) and a 16" pipe to allow exhaust to escape (4). Nitrogen was supplied concentric to the axis of rotation via a rotary union inlet from a liquid tank at 8-17m^3 h^{-1} (3). An external motor drives the reactor rotation from the gas inlet end (4). Rotation was set at 0.75 rpm by a Teco Speecon 7300CU controller to minimize size reduction of the material and fine dust formation. The burner (2) was equipped with a Honeywell burner control UV flam amplifier. Temperature was monitored at the wall of the reactor (5). Additional temperature readings were recorded at 15, 30, and 45cm from the axis of rotation inside the reactor to analyze the temperature distribution in the feedstock. An additional controller monitored the kiln upper set point with a thermocouple at the opposite end. Vapors generated was incinerated with a Midco Incinomite 0.1-0.8mmBtu hr^{-1} burner before exhausting (6). The material was torrefied at various temperatures and hold times (Table A.2) in triplicate. Mass balances, temperature, and residence time were analyzed. Temperature was monitored with a Campbell Scientific CR21X data logger. A ramp procedure involved 5 hours of drying at 120°C followed by 30 minutes at 200°C (with nitrogen), and then target temperature for desired hold time. A control sample was generated at 120°C for 5 hours. Nitrogen flow during shutdown was set at 8m^3 hr^{-1} with closed flap on exhaust during cooling to prevent air intrusion and combustion.

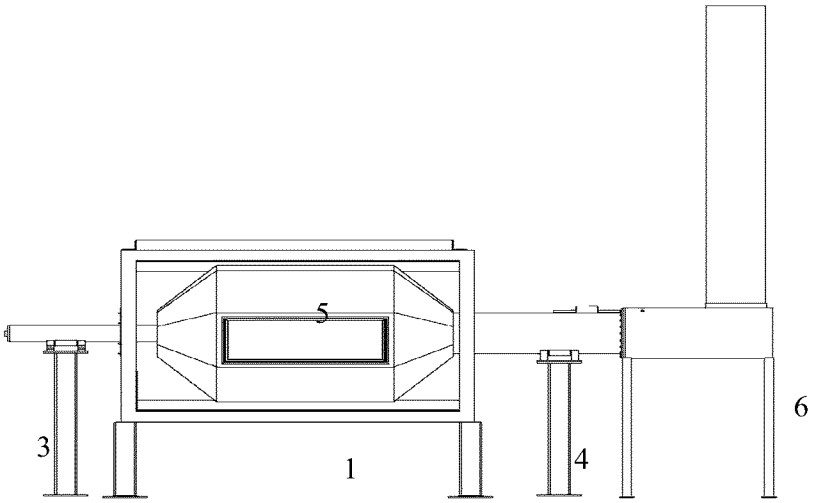

Figure A.1. Rotary Kiln used for torrefaction and drying. (1) Reactor, (2) Natural Gas Burner, (3) Nitrogen Inlet and Drive Motor, (4) Exhaust, (5) Reactor Wall and temperature reading, (6) Exhaust and incineration

Table A.2. Torrefaction experimental plan with temperatures and hold times

Run	Temperature (˚C)	Hold Time (min)
1	250	30
2	275	30
3	300	30
4	250	60
5	275	60
6	300	60
7 (Control)	120	300

Feedstock and Torrefied Material Chemical Analysis

All analytical techniques used were either ASTM standards or widely recognized methods from the literature. Random sampling of byproducts was then ground in a Tecator cyclone mill for further analysis. Elemental carbon, hydrogen, nitrogen, sulfur, and oxygen (ultimate analysis) were accomplished using a LECO brand (Model CHNS-932) with optional pyrolysis furnace (Model VTF-900) following protocols outlined in ASTM D5291 and D3176. Analysis of moisture, volatiles, and ash were analyzed thermogravimetrically using a LECO brand TGA (Model TGA701) following ASTM D5142 and E1131. Metals analysis was conducted with an Elmer (Model - Elan 6000) inductively coupled plasma (argon) spectrometer (ICP) equipped with a mass spectrometer (MS) detector system. Samples were first digested as described by EPA Method 3051.

Gasification experiment

Material was gasified in a 10 kg hr^{-1} 45kW fixed bed down draft wood gasifier shown in Figure A.2. The system is a two-stage gasifier fitted with a cyclone and exhaust flare. The hopper can hold approximately 0.4 m^3 (~70kg dry wood) allowing over 6 hours of operation time. Thermocouples were positioned along the reaction zones, below the grate, along the gas line, and at the flare. Pressure transducers recorded the pressure drop across the material bed to monitor any backpressure build up. Syngas flow was measured with a Dwyer DS-300 averaging pitot static tube.

Gasification was initiated by igniting a starter material (i.e. Char) with a propane torch. An air compressor provided air flow of 7.0 and 8.4 Nm^3 hr^{-1} in stages 1 and 2 respectively. Vibration of hopper and grate occurred for 6 seconds approximately every 4 minutes to break apart any material bridging. At two hour intervals of operation, inlet gas was shut off to allow collection of char accumulation below the grate and clean out of exhaust lines. Gasifier performance was evaluated using the following parameter:

1. The air to fuel ratio is also known as the Equivalence Ratio (ER) was calculated on the entirety of the run by summing up the total air input and total feed consumed.

$$Air{:}\,Fuel\ Ratio = \frac{O_2\ feed\ rate\ (mol\ min^{-1})}{Total\ fuel\ feed\ rate\ (mol_{carbon} min^{-1})}$$

2. The conversion of gas on a carbon basis indicated the efficiency to utilize the feedstock's potential energy.

$$Conversion\ to\ gas\ (\%, carbon\ basis) = \frac{Produced\ carbonaceous\ gas\ (mol_{carbon})}{Total\ feed\ carbon\ (mol_{carbon})} * 100\%$$

3. Cold gas efficiency is a metric to determine the effective energy transfer of the feedstock to combustible syngas.

$$Cold\ gas\ efficiency\ (\%) = \frac{Produced\ gas(mol) * HHV\ (MJ\ mol^{-1})}{Feedstock\ (kg_{d.b.} * HHV(MJ\ mol^{-1})} * 100\%$$

Other metrics evaluated during the gasification runs include dry chip feed rate (kg h^{-1}), chip moisture content (%,wet basis), dry gas HHV (MJ m^{-3}), gas yield (m^3 kg^{-1}, db), char yield (%), dry air in (kg kg^{-1}, db feed), energy yield (MJ kg^{-1}, db feed), total energy out rate (MJ h^{-1}), and mass conversion efficiency (%).

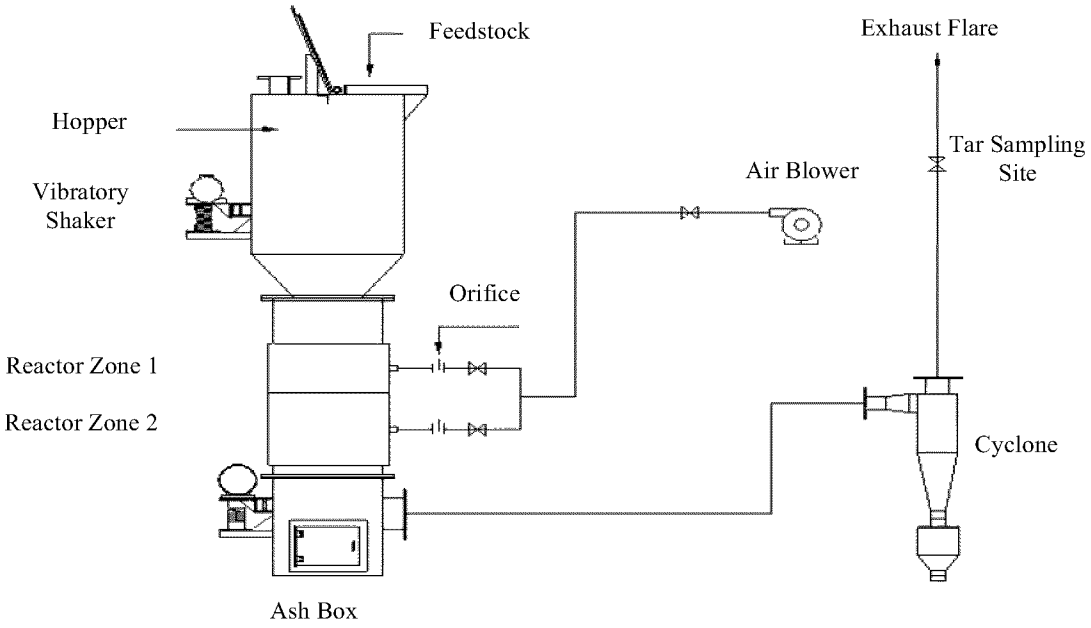

Figure A.2. Two stage downdraft wood gasifier schematic

Micro-GC Analysis

During steady state operation of gasifier (0.25 < ER < 0.4), gases were directly sampled at two minute intervals and analyzed by a Micro-GC (Agilent 3000A micro-GC) to determine the concentration of gases (H_2, CO, CO_2, CH_4, and other C_2-C_6) after the tar

impinger train. Columns on the GC include an MS 5A PLOT (10 m length x 32 mm diameter), a PLOT U (8 m x 0.32 mm), an alumina PLOT (10 m x 0.32), and an OV-1 (10 m x 0.15 mm x 2.0 μm). After column separation, compounds were detected and quantified with thermal conductivity detectors that are calibrated using a refinery gas calibration mix (Agilent, part #5184-3543) and comparable syngas mixture (2.27% CH_4, 1.925% O_2, 13.93% CO_2, 14.89% H_2, 24.08% CO, and N_2 by balance). Molar-% concentrations of gases were averaged over the course of the sampling interval for analysis.

Results and Discussions

All torrefaction conditions outlined in the experimental plan were performed and replicated in triplicate. Temperatures, and product yields were recorded throughout each process. Figure A.3 shows an example of the internal reactor temperature of the biomass for torrefaction at 300°C held for 60 minutes. The preliminary ramp conditions were held at 120°C for 5 hours to dry the material as the moisture content average ranged from 19.97% to 40.35% as received. Once the drying process was complete, the reactor was set to 200°C. This step was performed to allow all material in the reactor to absorb sufficient heat and reach obtain even temperature distribution throughout the reactor. This was held for 30 minutes before ramping up to target conditions. During the ramp phase to the target temperature, settings were monitored manually to prevent overshooting in the system. The residence time began when the average temperature of all thermocouples inside the reactor were ±5°C of target temperature (Fig. A.3: 380 minutes to 440 minutes). Temperatures were held ±5°C of target temperature for their respective durations as hysteresis was observed. Once the residence time was achieved, the natural gas burner system was shutdown, exhaust valves were closed off to prevent oxygen combusting the material, and doors to the reactor open to cool the reactor. Rotation of the kiln continued for two hours after the operation to facilitate cooling and prevent hotspots. Nitrogen continued to purge into the system at a flow rate of 3 m^3 hr^{-1}. The subsequent day, the reactor was opened and the solid material was collected and weighed.

Solids Yields

Figure A.4 shows the solid yields of torrefied pine as a function of residence time and temperature. Percentage changes within replications of each treatment were consistent within ±5% standard deviations of the average value. Torrefaction at 250°C yielded 87.01% and 81.89% for 30 and 60 minute residence times respectively. Torrefaction at 275°C yielded 66.00% and 61.40% for the different times. Treatment at 300°C resulted in yields of 46.58% and 2.70%. Higher temperature and longer residence times result in decreased solids yield.

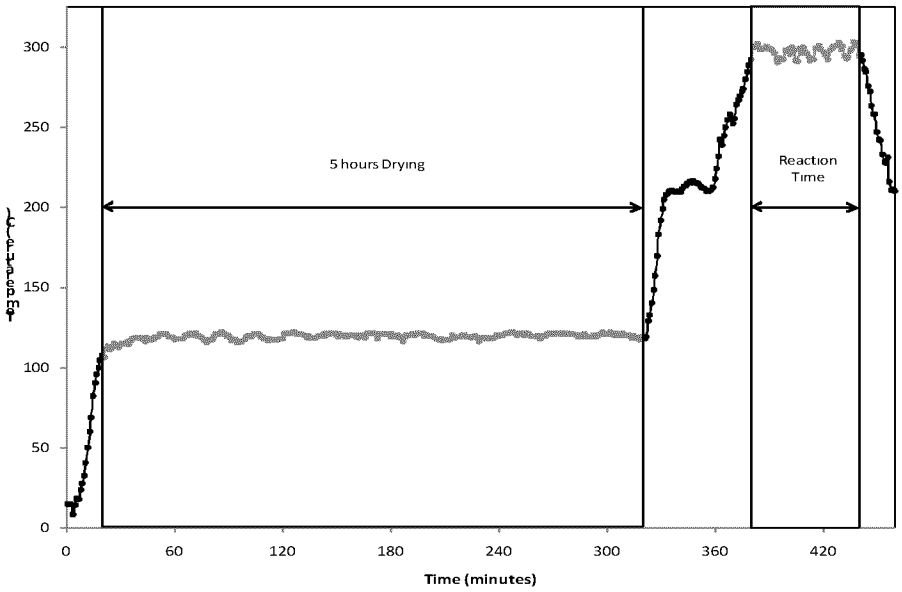

Figure A.3. Temperature profile in batch rotary kiln

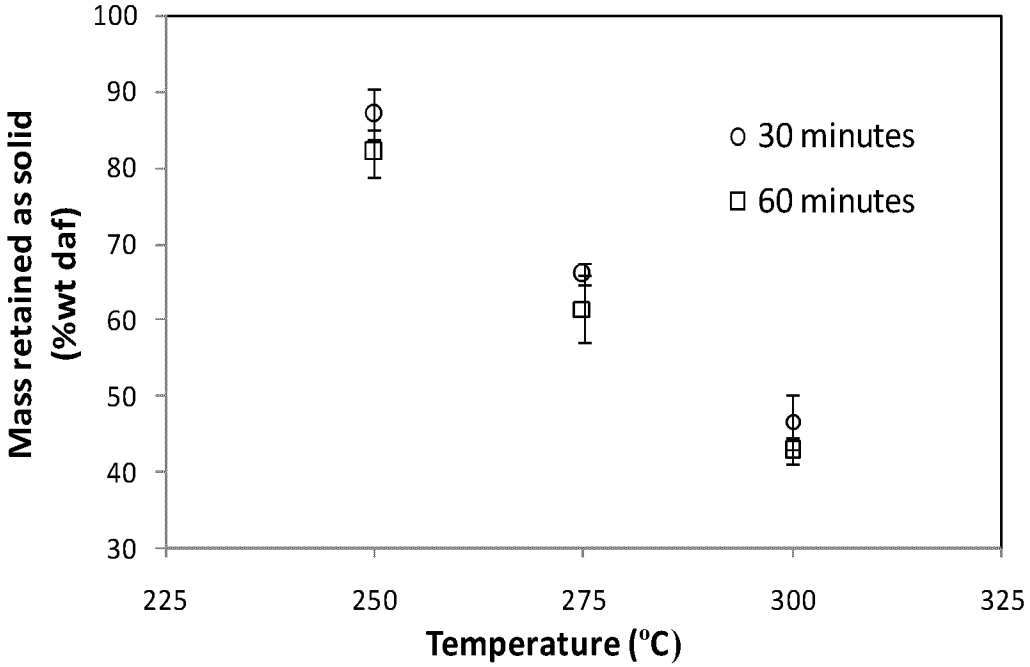

Figure A.4. Yield of torrefied loblolly pine

Torrefied Material Properties

Table A.3 shows the physical and chemical properties of selected torrefied pine under different treatments of temperature and residence time. Moisture content remained

below 3% for 250ºC and fell below 2% for 300ºC treatments. Volatile content declined from 75.13% from dried wood to as low as 44.70% in 300°C for 60 minutes torrefied wood. Composition of hemicellulose, cellulose, and lignin experienced changes in composition between torrefaction treatments. In general, hemicellulose and cellulose decreased and lignin increased with increased temperature and residence time.

Table A.3. Properties of selected Torrefied Loblolly Pine

	250ºC		**300ºC**	
	30 minutes	**60 minutes**	**30 minutes**	**60 minutes**
	Avg. ± S.D.	**Avg. ± S.D.**	**Avg. ± S.D.**	**Avg. ± S.D.**
Moisture (%)	2.65 ± 0.16	2.57 ± 0.36	2.01 ± 0.02	1.75 ± 0.02
Volatiles (wt% daf)	74.01 ± 0.79	73.63 ± 1.24	51.97 ± 0.14	44.70 ± 0.32
Fixed Carbon (wt% daf)	23.07 ± 0.55	24.07 ± 0.68	45.59 ± 0.14	53.20 ± 0.34
Ash (%wt daf)	0.37 ± 0.30	0.29 ± 1.18	0.44 ± 0.04	0.38 ± 0.11
C (%wt daf)	54.80 ± 0.44	55.21 ± 0.48	68.82 ± 0.70	73.02 ± 0.35
H (%wt daf)	5.77 ± 0.23	5.94 ± 0.28	5.26 ± 0.26	5.06 ± 0.20
N (%wt daf)	1.03 ± 0.45	0.81 ± 0.36	0.52 ± 0.17	0.29 ± 0.02
S (%wt daf)	0.05 ± 0.04	0.04 ± 0.02	0.05 ± 0.05	0.03 ± 0.01
O (%wt daf)	38.35 ± 0.74	38.00 ± 0.94	25.35 ± 0.86	21.61 ± 0.47
Hemicellulose (%wt daf)	4.27 ± 4.29	1.66 ± 0.16	4.86 ± 2.31	3.07 ± 0.58
Cellulose (%wt daf)	35.74 ± 2.04	34.48 ± 1.73	4.46 ± 0.09	1.41 ± 0.97
Lignin (%wt daf)	33.61 ± 7.76	32.35 ± 4.71	38.28 ± 6.08	50.72 ± 0.37
Bulk Density (kg m^{-3})	168.25 ± 3.68	165.96 ± 7.92	137.31 ± 11.41	139.03 ± 22.41
HHV (MJ kg^{-1})	21.59 ± 0.49	22.02 ± 0.54	27.32 ± 0.64	28.96 ± 0.39
LHV (MJ kg^{-1})	20.96	21.41	26.67	28.35
O/C	0.70	0.69	0.37	0.30
H/C	0.11	0.11	0.08	0.07

Downdraft Gasification

All torrefied material and dried wood (control) were gasified as outlined in the experimental plan for a total of 22 runs. Detailed results are being analyzed and written in a form a peer-reviewed publication. A key summary of the work is presented here.

Gasification runs were approached by controlling the input parameters such as equivalence ration (ER) to approximately 0.25 and gasification zone temperature to approximately 800ºC to maintain consistency. ER values were determined prior to each run based on the compositional property values provided in the ultimate analysis data of the feedstock. This calculation was then used to determine the required air input rates to maintain an ER value of 0.25. Although the intent of controlling the airflow to maintain consistency was there, the gasifier system occasionally limited the operators' ability to manipulate air flow due to pressure drop across the reactor bed or increased pressure in the system adding resistance to the air blower.

Figure A.5 shows carbon monoxide molar-% in the syngas of the different materials. Values were scattered and on initial observation do not show any apparent trends. All concentrations ranged between 5% and 30% with an average of 20.55±2.02%. Torrefied material at 300°C had several values below 15%. Torrefied material at 275°C showed hydrogen concentrations greater than 25%. The control and treatments at 250°C had values ranging between 17% and 27.

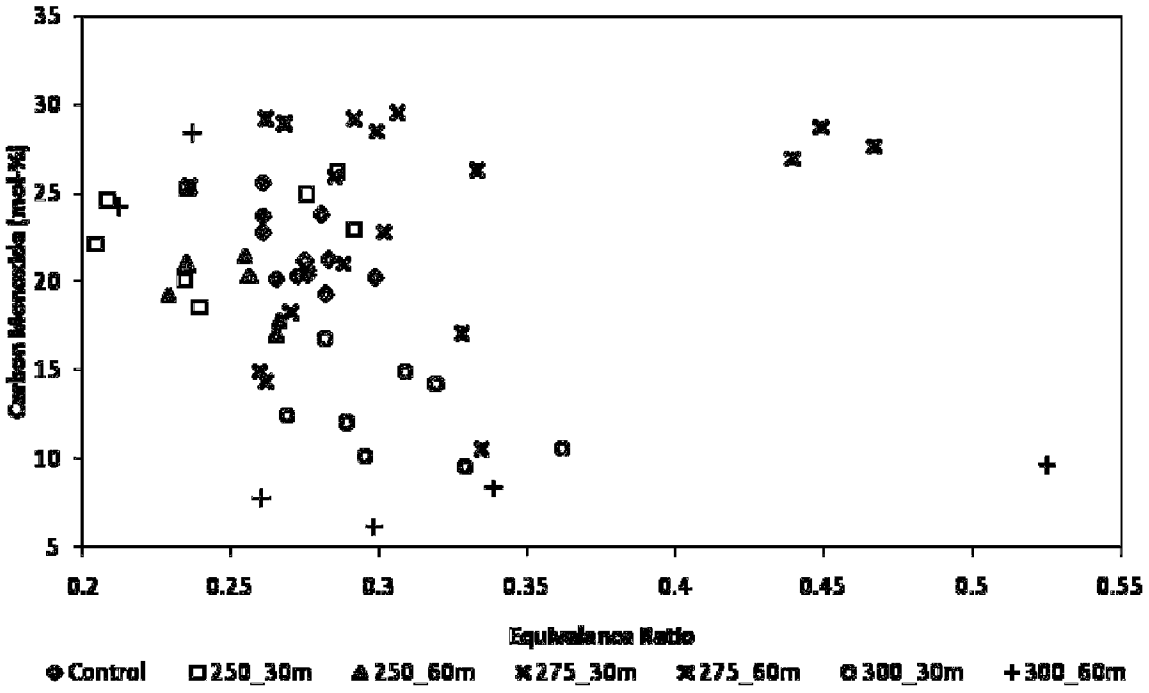

Figure A.5. Carbon monoxide yield as expressed in molar-% of syngas

Figure A.6 shows the molar-% of hydrogen in the syngas for the gasification runs. Hydrogen concentration ranged from 12-16% with a few points falling below 10% but had an average of 13.95±0.78%. Overall, values were fairly consistent within this range

as moisture content and elemental hydrogen as a percentage of the feedstock remained consistent. Figure A.7 shows the total measured tar concentration of all runs versus the equivalence ratio of the respective sampling interval. Values averaged 0.438±0.428 g Nm^{-3} and ranged from 0.090±0.20 g Nm^{-3} for Torr275_60m Rep 2 to as high as 0.833±0.38 g Nm^{-3} for Control Rep 1. In general, tar compounds were reduced with increased torrefaction temperature and time.

Toluene showed significant differences being higher between the control and torrefied pine at 250ºC with torrefied pine at 300ºC. Naphthalene was higher in the control, torrefied material at 250ºC at 30 minutes, torrefied material at 275ºC for 30 minutes with all torrefied material at 300ºC. Similar differences were observed with p-Xylene, Indene, and Styrene with the control and torrefied treatment of 250ºC at 30 minutes having higher values than all torrefied material at 300ºC. Figure A.8 shows the tar concentrations of all identified species for the three sample intervals collected in Control Rep 1. ER values remained consistent through each sample interval at 0.261. Toluene was the most abundant species followed by Naphthalene. P-Xylene, Styrene, and Indene were relatively similar in concentration values and were the lowest of the identified compounds. Total tar concentrations for samples 1, 2, and 3 were 0.916±0.139 g Nm^{-3}, 0.826±0.38 g Nm^{-3}, and 0.295±0.018 g Nm^{-3} respectively, indicating significant reduction in total tar relative to controls.

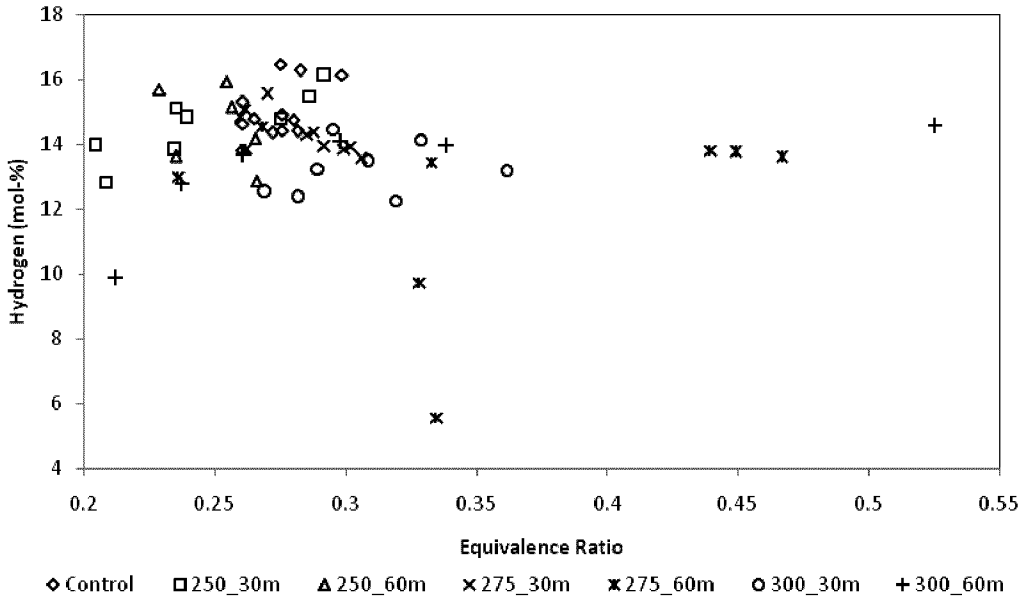

Figure A.6. Hydrogen yield as expressed in molar-% of syngas

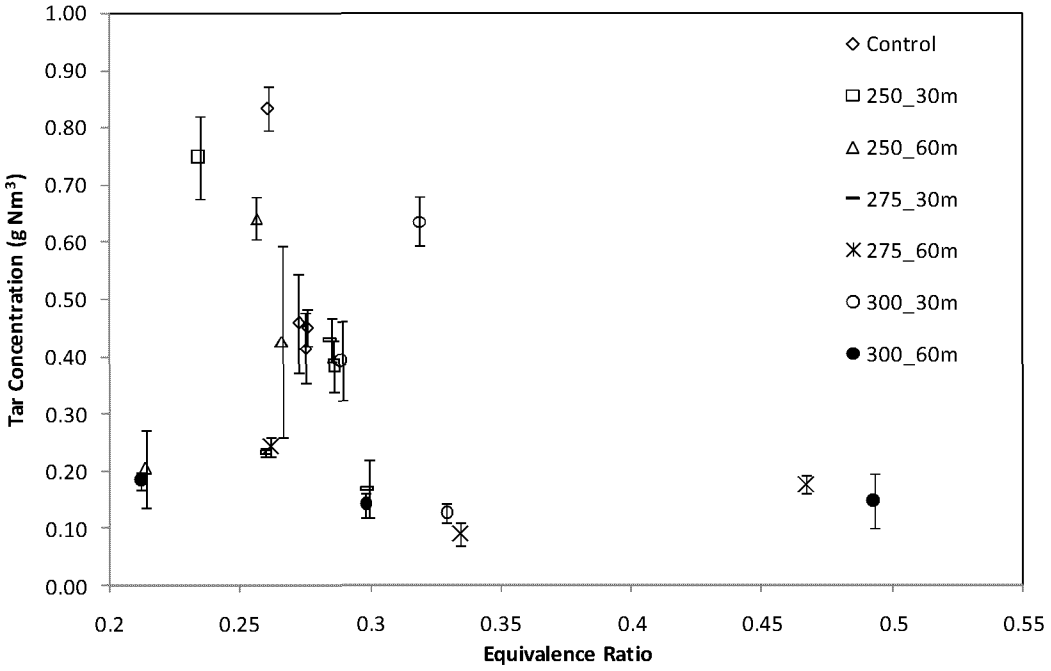

Figure A.7. Total tar concentration of syngas from sample interval 2

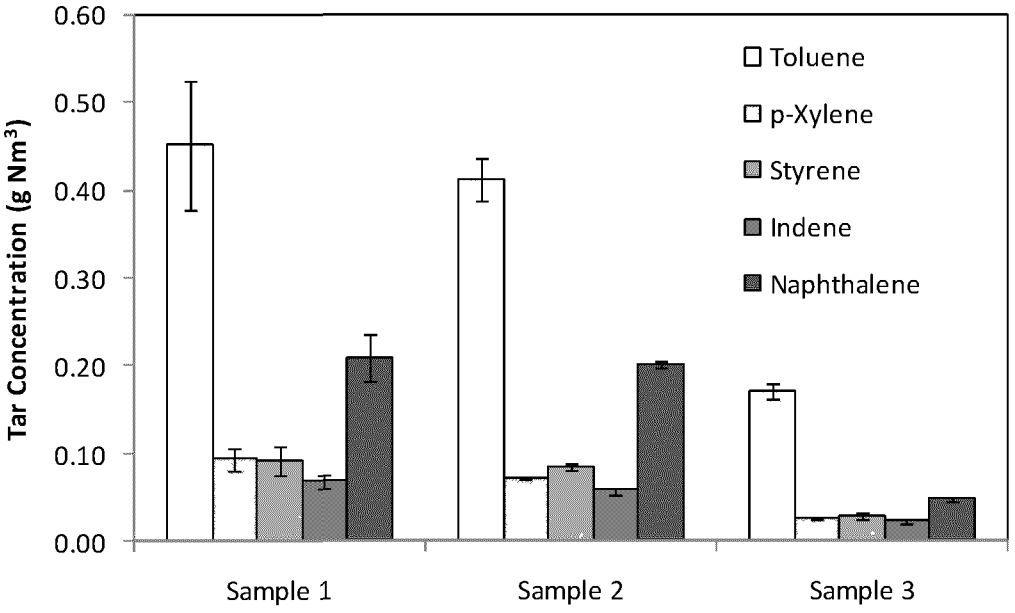

Figure A.8. Syngas tar concentration of Control Rep 1

Based on the decline in total tar concentration between the three sample intervals highlighted in Figure A.8, it can be assumed that the tar concentration changes during gasification. It was observed during collection of these samples that the coloration of the tar was dark yellow in sample 1 and progressively became clearer with each subsequent

sample collection. During intervals 1, 2, and 3, syngas sample port temperature averaged 294.86°C, 308.85°C, and 329.17°C respectively. Gasification temperature average 749.51°C, 786.41°C, and 793.07°C during these intervals as well. It can be assumed that with a constant ER value, the increase in gasification temperature reduced the tar concentration in the sample.

Subtask A.2: Catalytic tar removal to produce clean intermediates

Tars are defined as higher molecular weight hydrocarbons larger than benzene produced during thermal conversion of biomass into syngas or BioOil. They pose major problems using syngas for producing power, fuels and chemical products as they condense and corrode metal surfaces and inactivate catalysts. One of the solutions to this problem is to decompose tar compounds using catalysts before the syngas can be used for various applications. Our work focused on catalytically decomposing tar compounds or a specific tar compound using biochar as a catalyst. Among various tar compounds present in syngas, toluene was one of the least reactive compounds and was considered as a model tar compound in this study. Biochar was produced from pyrolysis of pine bark chips at 950°C and was used as an experimental catalyst.

Methodology

Catalyst preparation and characterization

Char was prepared by pyrolysing pine bark at 950°C for 2 hours retention time. The pyrolysed char was then crushed in the knife mill and passed through set of sieves to obtain a particular particle size of 212-420mm. The pine bark referred here is Southern pine bark (Varn Wood Products Ltd., Waycross, GA). The pyrolysis was done in a batch reactor with nitrogen supply of 1.5 L/min.

Table A.4. Elemental composition of char

Volatile %	Ash %	Fixed carbon %	Carbon %	Hydrogen %	Nitrogen %	Sulfur %
4.51	2.73	92.77	88.18	0.48	1.05	0.02

Apparatus and operation parameters

The experimental setup consists of 2 syringe pumps and a stainless steel fixed tube reactor externally heated by a furnace equipped with gas analysis devices. The schematic diagram of the setup is shown in Figure A.9. Two Cole Parmer syringe pumps were used to pump toluene and water respectively. The internal diameter and length of the reactor was 23 mm and 450 mm respectively. Catalyst is placed in the reaction zone supported by a quartz grid and glass wool. The fixed tube reactor is placed inside a furnace (Lindberg) for external heating. Two k-type thermocouples are used to measure the temperature of inlet and exit gas. Five additional thermocouples were placed over the length of the reactor to measure the temperature profile with the height if reactor. Two manometers are installed at the top and bottom of the reactor to record the pressure difference across the bed. Nitrogen was used as the carrier gas. Toluene and water are

pumped into the gas stream using the syringe pumps. An inline static mixer was placed at the inlet of reactor to enable proper mixing of nitrogen, steam and toluene. The exit gas was cooled using ice bath and exhausted. The two sampling ports were placed right before and after the gas passes the reactor. It was assumed that there are no horizontal temperature gradient between the inner wall of reactor and center of reaction zone.

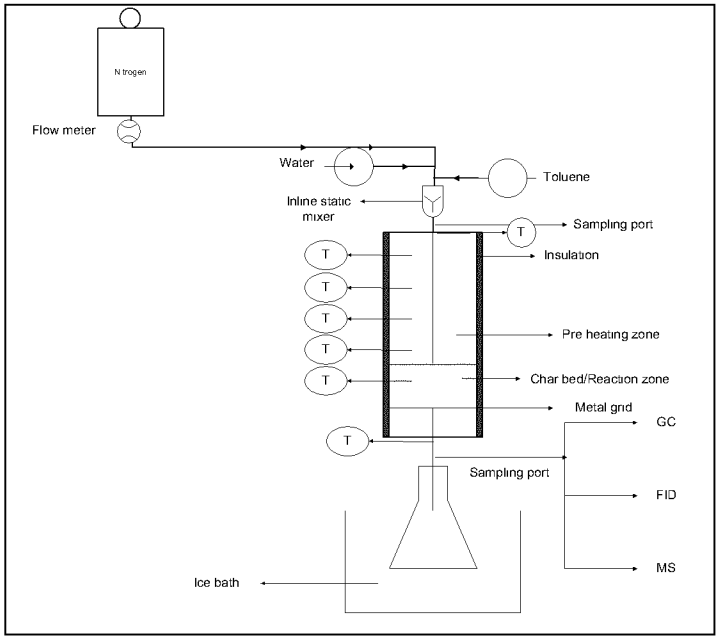

Figure A.9. Experimental setup for toluene steam reforming

GC-FID was used to find the toluene conversion using a pre-made calibration curve. 200 ml of sample was injected in GC-FID for observing toluene concentration. GC in line with TCD gave the CO_2 production from the exit gas. The conversion of toluene was obtained at four levels of temperature (550, 650, 750 and 850°C) and four levels of inlet toluene concentration (1100–4600 ppm). The toluene conversion is calculated using the formula

$$X_c(\%) = \frac{[C_{t,in} - C_{t,out}]}{[C_{t,in}]} * 100 \qquad (1)$$

Toluene steam reforming was performed in order to study the effect of operational parameters on catalytic activity of char. Before start of each experimental reading, time of 75-150 minutes was given for adsorption and desorption. The operating conditions are summarized in Table A.5.

Table A.5. Operational parameters for toluene steam reforming

Temperature	°C	600-900
Initial tar concentration	ppm	1100-4600
Pressure	Atm	1
Gas residence time	S	1.15

Catalyst bed volume	cm^3	13.14
Catalyst bed height	Cm	3
Space time	$kg\text{-}hr/m^3$	0.09
H_2O concentration		2.5*toluene concentration

During steam reforming, there are many parallel reactions going on. Main gaseous products of toluene steam reforming are H_2, CO, CO_2 and benzene (Taralas, 2000). The dealkylation reaction of toluene by water is

$$C_7H8 + 2\,H_2O \longrightarrow C_6H_6 + CO_2 + 3H_2O \quad (2)$$
$$\Delta H_{r\ (1173K)} = -90KJ\ mol^{-1}$$

$$C_7H_8 + 3H_2O \longrightarrow C_6H_6 + CO + 2H_2 \quad (3)$$
$$\Delta H_{r\ (1173K)} = -123KJ\ mol^{-1}$$

The net reaction is

$$2C_7H_8 + 3H_2O \longrightarrow 2C_6H_6 + CO_2 + 5H_2 + CO \quad (4)$$
$$\Delta H_{r\ (1173K)} = -213KJ\ mol^{-1}$$

The other compounds were calculated by

$$X_{CO_2}(\%) = \frac{[C_{CO_2}]}{7[C_{t,in} - C_{t,out}]} * 100 \quad (5)$$

$$(Benzene)X_b(\%) = \frac{[C_b]}{[C_{t,in} - C_{t,out}]} * 100 \quad (6)$$

Results and Discussions

Toluene fractional conversion - Reaction Temperature

Two types of experiments were performed: thermal and catalytic toluene reduction. The thermal experiments were performed in an empty reactor to study the stability of toluene. Experiments of steam reforming of toluene were performed during a temperature range of 600-900°C for inlet concentration of 2500 ppm and residence time of 1.15 seconds. No catalyst deactivation was observed after 8 hours of run on stream. The summary of the experimental results is shown in figure A.10.

The carbon balance for experiments with char as catalyst was not verified because biomass char is not an inert material and it reacts with the steam in feed gas. At these times, it is difficult to measure carbon loss of the char. Toluene seemed to be quite stable till 700°C with only 6% conversion. However, it loses its stability as temperature increases. The conversion increased to 23% at 800°C and 64% at 900°C. From the results, there was a significant difference in toluene conversion with and without catalyst. This shows activity of char towards toluene reforming. There is a slight increase in conversion with temperature from 600°C to 800°C but a drastic increase from 800-900°C. The selectivity of benzene was observed to be increasing steadily with temperature till 800°C but the increasing rate decreased from 800 to 900°C.

Toluene concentration

Inlet concentration of toluene was changed by changing the toluene feed rate in same flow of nitrogen. The operating parameters were same as char except for different range of temperatures (550-700°C). Inlet toluene concentration was observed to have a significant effect on the toluene conversion and rate of reaction. Increase in toluene inlet concentration increased the conversion from 550 to 700°C (table A.6). Char has already shown the trend of increasing tar conversion with increased inlet loadings with naphthalene as model compound (Abu El-Rub *et al.*, 2008).

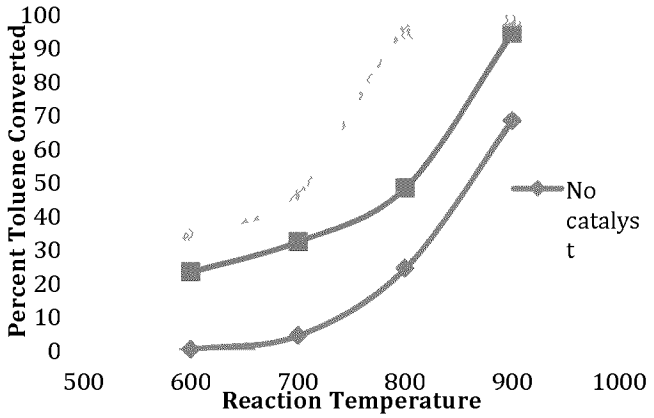

Figure A.10. Toluene conversion on Char and Fe/Char

Table A.6. The influence of inlet concentration on toluene conversion at different temperature char (w_{cat}/ $F_{toluene}$=0.09 kg_{cat} h m^3 at 25 °C).

Inlet concentration (ppm)		100	2500	3100	4600
Conversion %	550°C	9	11	14	18
	600°C	11	13	17	19
	650°C	16	20	22	25
	700°C	21	26	28	32

Toluene Kinetic Model

The reactor used in the study is considered plug flow reactor with no gas expansion (constant flow rate through it). Assumption of no mass and heat transfer are adopted. The apparent rate constant and apparent activation energy for steam reforming of toluene can be expressed as

$$-r_T = kC_T^n C_{H_2O}^m \qquad (9)$$

The steam/toluene provided (2.5) is much higher than the stoichiometric requirement (1.7), therefore, it is assumed that it has no effect on toluene conversion (Yamaguchi *et al.*, 1986; Swierczynski *et al.*, 2008). So, the binary reaction with H_2O can be expressed

as a pseudo-order reaction with respect to only toluene concentration. According to the experiments conducted in this study at different concentrations and temperatures, the rate of decomposition of tar was found to be first order. Then the equation can be expressed as

$$-r_T = k_{app} C_T \qquad (10)$$

The first order rate constants can be calculated according to the equation (11) derived from an integral plug flow reactor model (Levenspiel, 1975).

$$k' = \frac{-ln(1 - X_T)}{W_{cat}/q} \qquad (11)$$

The temperature dependence of the rate constant is determined by Arrhenius equation, from which activation energy and pre-exponential factor can be calculated. To plot the Arrhenius equation, experiments were performed in a temperature range of 600-900°C with gas composition (2500 ppm toluene diluted with nitrogen, S/C = 2.5). The activation energy was calculated from the plot in figure 3 and are shown in Table A.7.

Table A.7. Estimates of the kinetic parameters for toluene steam reforming on char (toluene 2500 ppm diluted by Nitrogen, S/C: 2.5, temperature from 600-900 °C, $w_{cat}/F_{toluene}$=0.09 kg_{cat} h m^{-3} at 25 °C).

Parameters	Estimated Values
A(m^3 kg_{cat}^{-1} h^{-1})	81.6
E_a(kJ mol^{-1})	2.27 * 10^5

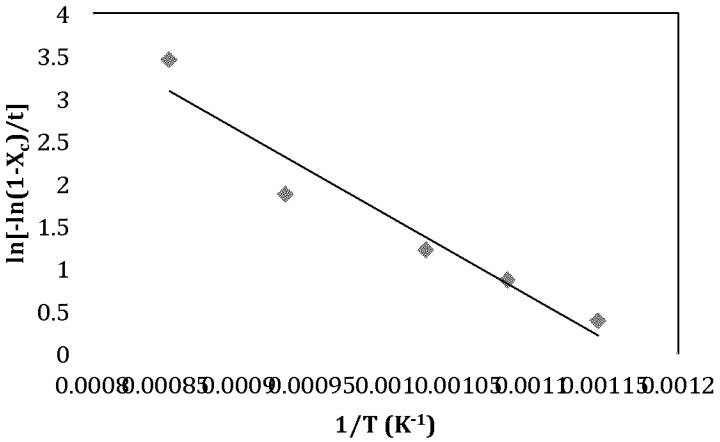

Figure A.11. Arrhenius plot for calculation of apparent activation energy, T: 600-900°C; space time: 0.09 kg_{cat} h m^{-3}.

The values were in accordance with literature. Activation energy for decomposition of naphthalene with char as catalyst was reported to be 61KJ/mol. Activation energies to steam reform toluene calculated for different catalysts reported by different authors are reported in table A.8.

Table A.8. Activation energies for toluene steam reforming from literature

Catalyst	Activation Energy	Reference
No catalyst (Thermal cracking)	365±5KJ/mol	(Taralas *et al.*, 2003)
Ni/mayenite	80.24 KJ/mol	(Li *et al.*, 2009)
Ni/Olivine	196 KJ/mol	(Swierczynski *et al.*, 2008)
Char	81.6 KJ/mol	This study

Conclusion

Biochar can be used as a renewable catalyst to thermally crack tar compounds present in syngas. In this study, toluene was decomposed at low temperature when biochar was acting as a catalyst. The apparent rate constant and apparent activation energy were calculated for toluene steam reforming over char assuming first order reaction with respect to toluene. Activation energy of 81.6KJ/mol was determined for toluene catalytic cracking reaction using biochar as a catalyst.

Subtask A.3: Upgrading of BioOil by de-oxygenation and increasing stability

The high level of reactive species and water content of bio-oil makes it unstable under normal storage conditions, which lead to increased viscosity over time. In addition, high oxygen and water content also lower the heating value of the fuel. During aging, bio-oil viscosity and chemical composition change dramatically mainly due to polymerization reactions. Polymerization reactions that lead to viscosity increases are accelerated at higher storage temperatures. Adding solvents after pyrolysis can increase the stability of bio-oil during aging. Solvents reported in the literature include ethyl acetate, a mixture of methyl isobutyl ketone and methanol, acetone, methanol, a mixture of acetone and methanol, and ethanol. Findings reveal that 10% (w/w) methanol enhanced bio-oil stability most effectively. Esterifying bio-oil can significantly improve the quality of bio-oil by lowering water content, viscosity, and the free-acid content.

Fischer esterification is proposed to be the reaction pathway in conversion to esters. The esterification reaction follows the equation, $RCOOH + C_nH_{2n+1}OH \leftrightarrow RCOOC_nH_{2n+1} + H_2O$, leading to the formation of water and an ester. The simplest ester that can be produced is methyl formate, $HCOOCH_3$, when methanol (CH_3OH) is used as the alcohol and is reacted with formic acid, HCOOH. In our work, ethanol was atomized into a stream of uncondensed bio-oil vapor in order to quickly cool and condense, while simultaneously esterifying carboxylic acids in the vapor phase. The intent was to increase the quality of bio-oil by effectively removing the undesired acidic compounds.

Methodology and results described and summarized below have independently been reported in the following peer-reviewed publications:

1. *Hilten, R., B. Bibens, J.R. Kastner and K.C. Das. 2010. In-line esterification of pyrolysis vapor with ethanol improves bio-oil quality. Energy & Fuel 24(1):673-682.*

Methodology

Pine wood pellets were used for all experiments and directly pyrolyzed "as received" with no pre-processing such as drying or grinding. Figure A.12 shows the schematic of the transported-bed pyrolysis reactor used in the study. The reactor consisted of a 100 mm diameter stainless steel tube containing an auger driven by a ¼ hp electric motor. The auger continuously transported biomass feedstock through the reactor, which was externally-heated using a tube furnace (Lindberg/Blue M, model HTF55322A). Auger speed was maintained at 1.5 rpm that translated to a solid retention time of 8.3 min in the auger (residence time in the heated zone: 5.9 min).

For pyrolysis experiments, the biomass feed rate was held constant to ensure consistent pyrolysis conditions. Pyrolysis vapors leaving the reactor were directed through a reactive condensation unit where ethanol (EtOH) was injected and then through a series of five ice-bath traps to condense any remaining bio-oil. An inert atmosphere was maintained in the reactor and char collector by supplying nitrogen to various inlets in the system.

Figure A.13 shows the schematic for the reactor used in the experiments to condense and esterify acidic components in the pyrolysis vapor using ethanol. The reactive condensation unit consisted of a 102 mm I.D. stainless steel tube with a reaction zone length, L=457 mm, meaning the reaction zone volume was 3.8 L. In the reactor, vapors were contacted with atomized 100 % (200 proof) ethanol (C_2H_5OH, abbr. EtOH, supplied by Thermo Fisher Scientific) that was supplied using a peristaltic pump and input to the reactor by a small-bore (0.015 mm diameter) cone-spray atomizer nozzle. In order to achieve adequate atomization of EtOH at low flow rates (1.5 – 2.0 mL min^{-1}), 0.1 L min^{-1} pressurized N_2 at 377 kPa (40 psig) was mixed with the EtOH prior to entering the atomizer nozzle. At a carrier gas flow rate of 3.6 L min^{-1}, the effective reactor volume (3.8 L) translated to a vapor residence time of 63.3 s in the reaction zone before entering the drip trap. Un-condensed vapor and non-condensable gases were routed through a series of five ice-bath traps that collected the remaining condensable vapor. Since the reaction equilibrium constant in liquid phase is 4 compared to 367 in vapor phase, we have made the assumption that once bio-oil leaves the heated reaction zone and condenses, esterification essentially ceases.

Product Yield

The quantity of biomass in the hopper was weighed before and after each pyrolysis run to determine the total amount supplied to the reactor. Biomass feed rate was steady throughout each run. Solid product char and condensed liquids were collected and weighed to determine product yield. A simple mass balance was used to calculate the quantity of non-condensable gases. For the experimental runs, the biomass feed rate was kept constant to ensure equivalent characteristics for the vapor feed entering the reactive condensing unit, while EtOH atomization rate was varied from 0 to 6 mL/min. These runs produced samples with a WHSV from 8.3 – 33 (7.3 - 23.2 % EtOH, w/w). Total yield of bio-oil was determined by weighing the whole product then subtracting the weight of EtOH added during the run. After total yield was determined, oily phase material from the drip and ice-bath traps was separated from aqueous phase by decanting, combined, quantified, and stored in a 4 °C refrigerator until characterized. In all, five

samples were generated during five one-hour pyrolysis runs. From the five samples, no less than three subsamples were taken for each characterization technique described below.

Characterization Methods

The pelletized pine feedstock used to generate bio-oil was extensively characterized prior to pyrolysis. Moisture, volatiles, ash content and elemental C, H, N, S, and O were analyzed using standard methods. Please see above cited reference for additional details. Table A.10 shows the characterization of the pine pellet biomass (PP BM) and pine pellet char (PP CH) produced during continuous pyrolysis at 500 ˚C.

Bio-oils produced by the five pyrolysis runs underwent several analyses in addition to those performed on the biomass and char. These include water content in the oils (Karl Fischer titration), higher heating value, dynamic viscosity (η in cP), and other parameters. Differential scanning calorimeter (oxidation onset temperature) method was used to determine bio-oil stability.

Formation of esters was verified and quantified using a Hewlett-Packard (Model HP-6890) gas chromatograph containing an HP-5 MS column, 30 m in length, with a 0.25 mm I.D. and 0.25 μm film thickness in conjunction with a Hewlett-Packard mass spectrometer (Model HP-5973) with a mass selective detector. An internal standard, heptane, was added to each sample-acetone mixture at 0.0625 % (v/v). Two model compounds in the bio-oil, acetic acid (AcOH, for acetyl hydroxide) and ethyl acetate (EA) were selected to represent an acid and an ester for quantification. Peak height ratios were calculated for AcOH and EA with the internal standard, heptane. A quantification method was developed by producing a five-point standard curve using standard solutions containing mixtures of AcOH, EA, and heptane in acetone. The standard curve yielded a least-squares best-fit line showing the concentration of AcOH and EA versus peak height ratio with heptane. This correlation was then used to predict the concentration of each of the two compounds in the bio-oil samples based on the peak height ratio with heptane calculated for the bio-oils.

Results and Discussion

The condensing system effectively lowered bio-oil vapor temperature such that a liquid formed in the collector below the condenser (drip trap) prior to the ice bath traps. Figure A.14 shows the temperature profile obtained during the run producing a bio-oil condensed with 7.4 % EtOH (w/w). Figure A.15 shows the temperature difference between the condenser inlet and the upper and lower zones in the condensers. The relationship is strongly linear, showing that as EtOH atomization rate increases, temperature drop decreases. We assume this is due to the fact that higher atomization rates of EtOH cool the incoming vapor very quickly at the reactive condensing unit's inlet prior to the reaction zone. WHSV significantly affects lower condenser zone temperature at $\alpha = 0.9$. Despite linearity, the relationship between WHSV and upper condenser zone temperature is not statistically significant at $\alpha = 0.9$. The relationship between lower condenser zone temperature (˚C) and ethanol atomization rate (kg h^{-1}) is statistically significant at $\alpha = 0.95$. These are useful observations, since condensation temperature can be controlled by EtOH and biomass feed rate to selectively condense various bio-oil components. For example, if it is desired to prevent water from

condensing in the drip trap, spray volume can be adjusted such that the condenser temperature is higher than the condensing temperature of water.

Yield of Pyrolysis Products

Table A.9 lists the yield of bio-oil components in % of original biomass (w/w) and % of total bio-oil (w/w) at each WHSV. From Figure A.16, it is evident that with increasing WHSV, total oily phase yield (% of biomass, w/w) decreases while aqueous phase increases. Although it appears that with increasing WHSV the oily phase increased and the aqueous phase decreased, neither relationship was significant at $\alpha = 0.95$. However, the apparent increase in aqueous phase supports the hypothesis that esterification occurred.

Pyrolysis runs with the lowest WHSV (8.3 or 26.2 % EtOH (w/w)) produced a two-phase oil in the drip trap, although oily phase material condensed in the ice bath traps, as well. The aqueous phase yield in the drip trap indicated that the temperature in the reactive condensation unit was below the boiling point of some of the aqueous phase components. If desired, the temperature in the reactive condensing unit could be controlled using only EtOH in order to condense desired products in the drip trap.

Product Characterization

Table A.11 shows characterization data for the bio-oil for each of the five pyrolysis experiments including a control run where no EtOH was added. Results indicate that the oily phase water content generally decreases with higher EtOH atomization rate, although the relationship is not statistically significant. In addition, as evidenced by the ultimate analysis of the oils, elemental oxygen content seemed to increase with increasing EtOH. A reduction in elemental oxygen would be consistent with formation of esters assuming that no ethanol remained unreacted in the product. If carboxylic acids react with EtOH to form esters as hypothesized, the oxygen content should decrease. In the reaction of one mole of AcOH at 53.3 % oxygen (w/w), theoretical with one mole of EtOH at 34.8 % oxygen (w/w), theoretical, one mole of ethyl acetate (EA) is formed with an oxygen content of 36.4 % (w/w) which is lower than that of AcOH. Some of the oxygen from AcOH is concentrated in the reaction by-product, water, and should partition in the aqueous phase of the condensed product and thus increase the aqueous phase yield, as seen in Figure A.16 with decreasing WHSV. Since oxygen concentration does not decrease with increasing EtOH, it is likely that some ethanol remains unreacted in the bio-oil or that other reactions such as acetalizations generate higher oxygen content products.

Results indicated that as the % EtOH (w/w) was increased the water content decreased. This was mainly due to the fact that less water was condensed with the oils directly after the reactor. Table A.11 provides water content for oil collected and combined from both drip and ice bath traps. Results are consistent with the formation of a more non-polar bio-oil and esters. Although lower biomass feed to ethanol spray ratios (i.e., WHSV) lowered the water content at an undetermined threshold WHSV (denoted as the single-phase threshold) between 3.8 and 8.2, the bio-oil produced existed as a single phase with high water content. This was observed during a previous experiment in which two single-phase bio-oils were generated with WHSV at 1.5 and 4.8 (57 and 28 wt % EtOH) with water content at 11.5 and 26.2 wt %, respectively. HHV in the bio-oil

increases with increasing EtOH feed rate. The sample produced at WHSV 8.3 (23.2 wt % EtOH) showed similar HHV to EtOH. Since esters, particularly ethyl acetate (HHV = 25 MJ kg^{-1}), are formed in relatively high concentrations (1.89 to 3.42 μL mL^{-1}), it is expected that the increase in heating value is partially due to their presence. Additionally with decreasing water content, HHV should increase. For bio-oil collected from all traps, HHV ranged from 24.5 to 27.6 MJ kg^{-1} indicating little change in HHV due to esterification.

Kinematic viscosity decreased substantially as more EtOH was added to the reactor relative to the whole oil. This is clearly evident in Figure A.17 showing a non-linear decrease in viscosity at 40 and 60 °C as a function of EtOH concentration. An interesting phenomenon to note is that although water content in the oily phase is lower at lower WHSV which generally results in higher viscosity, we have shown the opposite to be true of the esterified oils. Using fast pyrolysis bio-oil as the reactant, Zhang et al. (2006) saw a decrease in viscosity from 49 to 4.9 cSt when measured at 20 °C after the bio-oil was esterified with ethanol.

Table A.12 shows OOT (oxidation onset temperature) and cloud point (both in °C) for the reactively-condensed bio-oils. The trend for oxidation onset temperature is unclear. We expected that OOT would increase with increasing EtOH indicating an increase in stability. One measure of stability is the resistance to polymerization as evidenced by a viscosity increase. Despite the lack of evidence for an increase in stability in the current study, cold flow properties were improved as evidences by the linear decrease in cloud point as WHSV decreases (EtOH increases). A linear regression best-fit line showed an R^2=0.79 and a p-value<0.05. Thus, the relationship between cloud point and EtOH content is significant at $\alpha = 0.05$.

Figure A.18 shows the chromatogram for one of the calibration samples in which the EA, AcOH, and heptane peaks are clearly evident at retention times of 1.99, 2.05, and 2.8 min, respectively. For five calibration standards, peak height ratios for AcOH and EtOH with heptane were determined and used to calculate concentration in experimental samples. Although ethanol likely reacts with other carboxylic acids in the bio-oil (e.g., formic, propionic, butyric acid), with aldehydes (e.g., acetaldehyde, formaldehyde, propionaldehyde, furfural) and with ketones (e.g., acetone, propanone, butanone), forming multiple products, only the effects of EtOH addition on the yield of ethyl acetate are quantified here. Though not quantified, acetals, products of the reaction between ethanol and aldehydes, were identified in the chromatograms.

Fractional conversion of acetic acid in % (v/v) shown in Figure A.19 is calculated as the change in concentration (in mmol mL^{-1}) divided by the concentration of acetic acid (mmol mL^{-1}) in the control sample for which no ethanol was added during condensation. Both reaction temperature and EtOH concentration relative to the whole oil significantly affect (at $\alpha = 0.95$) the conversion of acetic acid. With better control of reaction zone temperature to achieve higher temperatures, it is expected that fractional conversion of acetic acid could be increased. Figure A.20 shows the fractional yield (%, v/v) of ethyl acetate assuming that the expected yield is equivalent to the fractional conversion of acetic acid. The concentration of EtOH is a significant predictor of EA fractional conversion at $\alpha = 0.9$ while reaction temperature is not. It is assumed that losses of ethyl acetate during storage and transfer of bio-oil due to high volatility of ethyl acetate

account for some of the variability in fractional conversion. This is likely true of other esters, as well. However, the highest yield of EA was at 23.2 % EtOH and was 19 % which compares well with other studies reported in the literature. Our method successfully generated esters without a catalyst in reaction times at around 60 s.

It is clear from Figures A.19 and A.20 that the esterification reaction is a function of temperature and reactant concentration, since the conversion of acetic acid increased with reaction temperature (Figure A.19) and as more EtOH is added, acetic acid conversion EA formation (Figure A.20) increased. Ultimately, the reaction will be limited by the amount of reactants in the bio-oil vapor available for esterification. Since the reaction is reversible, it will reach equilibrium between products and reactants. The removal of water shifts the equilibrium towards products. Equilibrium for esterification reactions lie far to the right, especially if conducted in vapor phase, for which the thermodynamic equilibrium constant is 367 for the reaction of ethanol and acetic acid to form ethyl acetate.

Key conclusions

We have developed a novel method to improve the quality of bio-oil. By atomizing ethanol into uncondensed bio-oil vapor produced during pyrolysis, a single-step, combined condensation and esterification process has been developed. Using a reactive condensation unit, we esterified bio-oil vapor with ethanol (EtOH) at elevated temperature (114-127 °C) at reactor residence times around 60 s without the use of a catalyst, although any primary alcohol could conceivably be used. GC-MS results demonstrated the formation of esters including ethyl acetate and ethyl propionate and acetals including diethoxymethane and 1,1-diethoxyethane. Quantitative GC-MS results indicated that acetic acid concentration decreased by as much as 42 %, subsequently improving the pH, viscosity, and cold flow properties of the resultant bio-oil. Experiments showed the following improvements for bio-oil condensed with 23.2 % EtOH (w/w) relative to the control:

1. pH was increased from 2.5±0.01 to 3.1±0.01
2. viscosity was reduced from 24.4± to 9.7± cSt (measured at 40 °C)
3. water content was reduced from 10±0.8 to 8.4± 2.3% (w/w)
4. the cloud point was reduced from -4.7±0.2 to -12.1±0.4 °C

Table A.9. Product yield for reactive condensation experiments

Product	% Yield (w/w) at % EtOH				
	0.0	7.3	10.3	16.4	23.2
Char	21.8	23.5	23.5	24.4	24.4
Gases	20.6	17.8	17.0	27.2	13.9
Bio-oil	57.7	58.7	59.5	48.4	61.7

Oily Phase					
(% of BO[a])	17.5	21.6	17.1	19.2	9.0
(% of BM[b])	9.0	11.6	9.6	9.5	6.0
Aqueous Phase					
(% of BO)	82.5	78.4	82.9	80.8	91.0
(% of BM)	42.4	42.0	36.5	40.0	40.4

[a]Bio-oil; [b]Biomass

Table A.10. Characterization of solid feedstock and pyrolysis char.

Analysis[a]	Biomass	Char
Moisture (w.b.)	7.45	3.20
Volatiles	74.83	27.58
Ash	0.13	2.70
Fixed Carbon	17.59	69.12
C	52.60	79.1
H	5.66	3.1
N	0.18	0.2
S	0.02	0.0
O[b]	38.90	12.6
HHV (MJ/kg)	20.6	34.1

[a]Measured as a % (w/w, d.b.) unless otherwise stated.,

[b]By difference.

Table A.11. Characterization data for oily-phase bio-oils produced at various WHSV. Can we provide statistics for the results, especially for the pH and the viscosity data?

Parameter	Oily Phase Characteristics at WHSV					
	?	33 3	25	16 7	8 3	0
EtOH (wt %)	0	7 4	10 3	16 4	23 2	100
C	64 9 ± 1 7[b]	57 9 ± 2 0	56 ± 0 5	56 6 ± 0 4	55 8 ± 1 4	46 6 ± 3 4
H	7 1 ± 0 4	5 6 ± 0 6	5 6 ± 0 4	6 4 ± 0 1	6 ± 0 1	11 7 ± 0 7
N	0 2 ± 0 03	0 2 ± 0 01	0 3 ± 0 02	0 2 ± 0 02	0 2 ± 0 03	0 ± 0 01
S	0 ± 0 02	0 ± 0 01	0 ± 0 01	0 ± 0 00	0 ± 0 01	0 ± 0 01
O[a]	27 8 ± 1 4	36 3 ± 1 9	38 1 ± 0 5	36 7 ± 0 4	38 ± 1 6	41 7 ± 0 00
HHV (MJ/kg)	27 6 ± 0 2	24 5 ± 0 1	25 7 ± 0 6	25 2 ± 0 05	27 ± 0 2	27 2 ± 3 8
% H_2O	10 ± 0 8	16 2 ± 2 6	11 2 ± 0 2	14 ± 0 9	8 4 ± 2 3	0 4 ± 0 01
pH	2 48 ± 0 01	2 65 ± 0 02	2 74 ± 0 03	2 82 ± 0 02	3 05 ± 0 01	5 29 ± 0 4
Viscosity (cSt)						
40 °C	300 1 ±	151 2 ±	41 3 ±	37 2 ±	49 2 ±	3 75[b] ±
60 °C	24 4 ±	13 7 ±	13 5 ±	11 2 ±	9 7 ±	3 99[c] ±
SG (g/mL)	1 18 ± 0 2	1 19 ± 0 2	1 15 ± 0 1	1 11 ± 0 2	1 06 ± 0 1	0 8 ± 0 01

[a]By difference

[b]"± XX X" indicates ± one standard deviation

Table A.12. Oxidation onset temperature (°C) and cloud point temperature (°C) for EtOH-condensed bio-oils.

EtOH [wt %]	Oxidation Onset Temperature [°C]		Cloud Point [°C]	
	Ave	S.D.	Ave	S.D.
0	174.3	1.1	-4.7	0.2
7.4	167.7	0.5	-7.3	0.4
10.3	157.1	3.1	-7.9	0.3
16.4	169.9	2.5	-6.7	1.0
23.2	172.2	1.6	-12.1	0.3

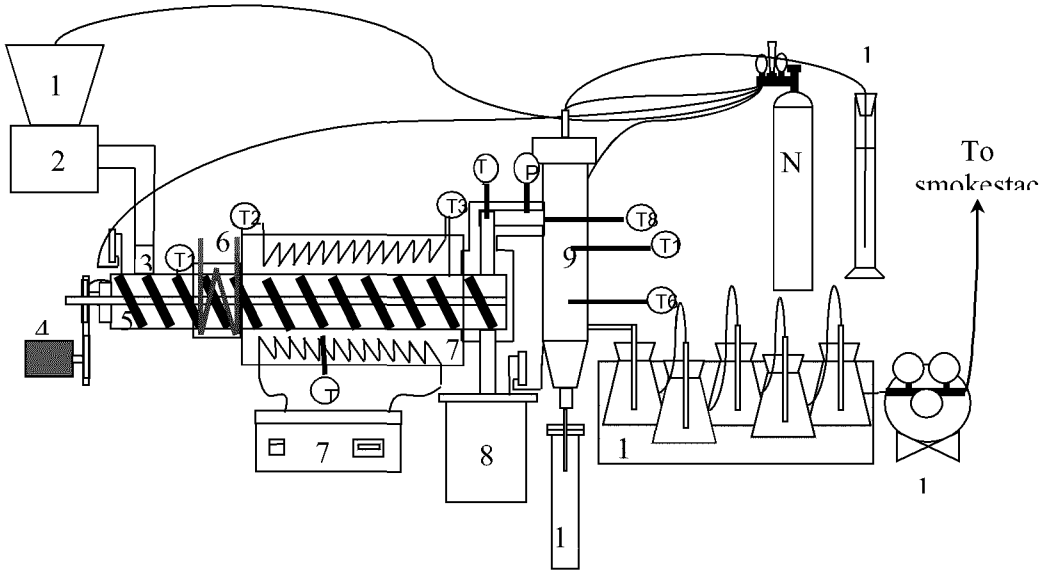

Figure A.12. Continuous pyrolysis reactor including components; (1) biomass hopper, (2) vibratory feeder, (3) reactor inlet, (4) auger motor, (5) auger conveyer, (6) water cooler, (7) furnace and furnace control, (8) char collector, (9) reactive condensation unit, (10) bio-oil drip trap, (11) ice bath trap, (12) vacuum pump, (13) ethanol container.

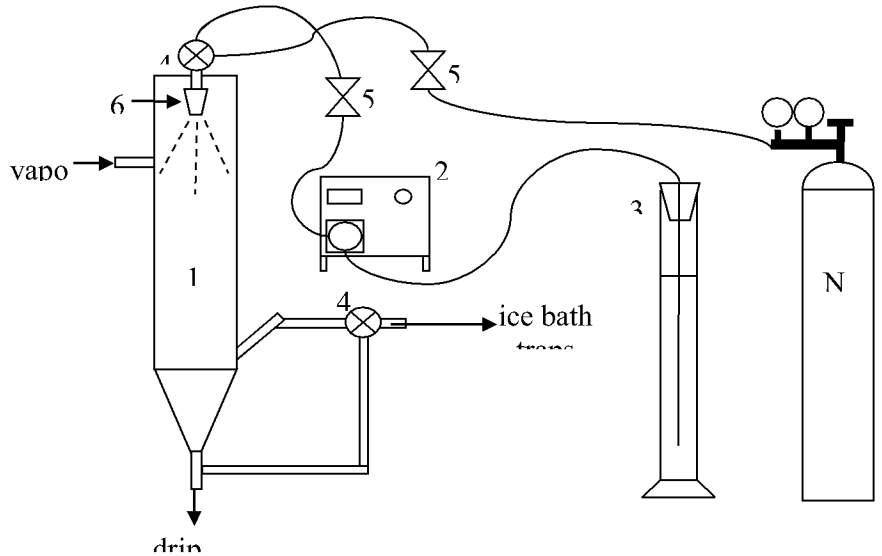

Figure A.13. Condensing system for pyrolysis unit shown in Fig. 1. Items shown figure include; (1) reactive condensation unit, (2) peristaltic pump, (3) graduated cylinder containing ethanol, (4) junction, (5) one-way valve, and (6) atomizing nozzle.

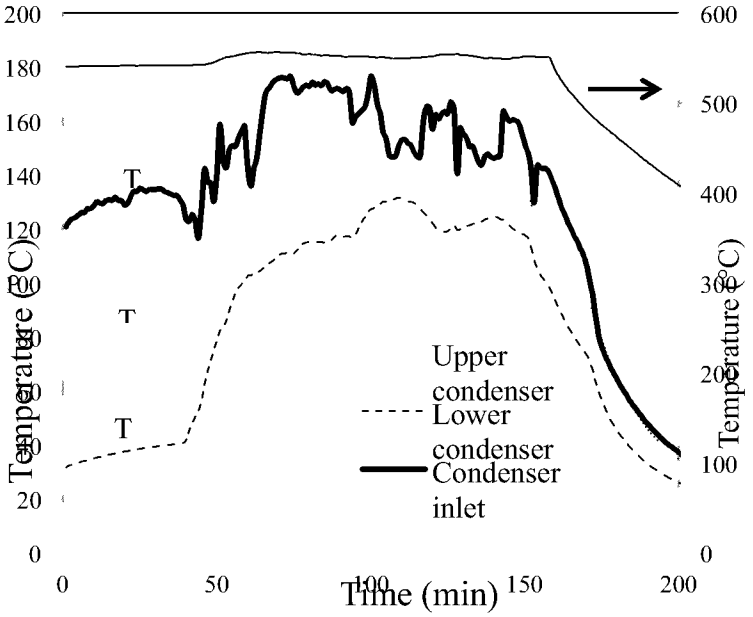

Figure A.14. Cooling profile for bio-oil condensed with 7.4 % EtOH (w/w) injected at 1.5 mL min^{-1}. Furnace temperature (thin, solid line) is shown on secondary vertical axis.

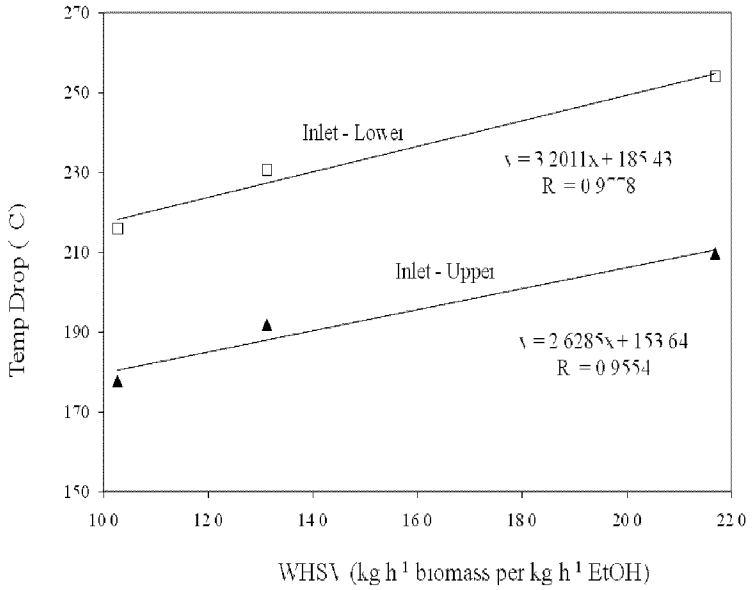

Figure A.15. Temperature difference between condenser inlet and upper (▲) and lower (□)
condenser zones.

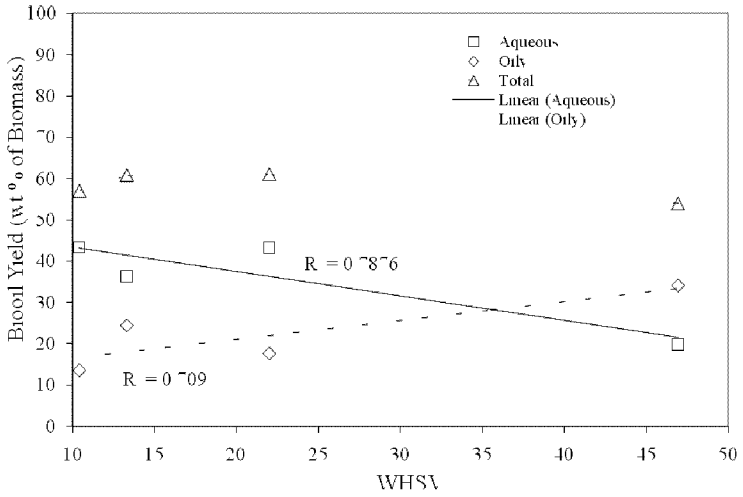

Figure A.16. Relationship between WHSV and yield (wt % of original biomass) of whole oil (open triangles), oily phase (open diamonds, R^2=0.71, p-value>0.05) and aqueous phase (open squares, R^2=0.79, p-value>0.05).

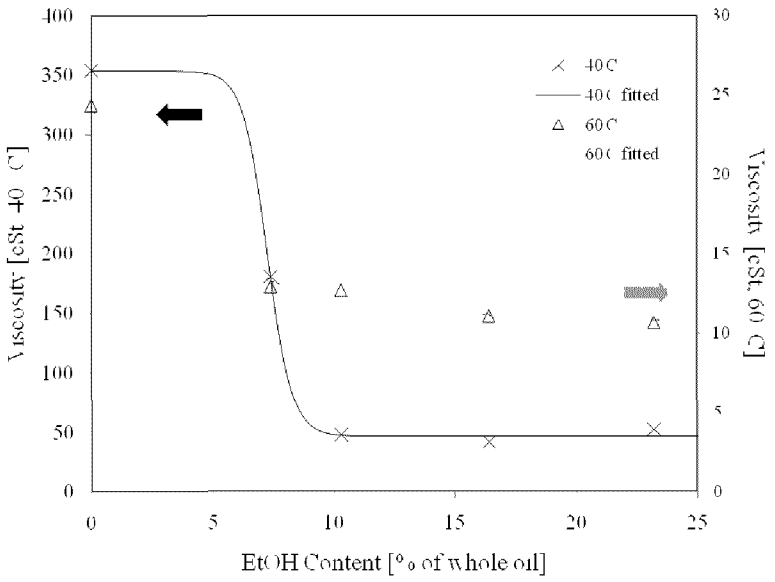

Figure A.17. Viscosity as a function of EtOH fitted with a 5-parameter sigmoidal line at 40 °C (R^2=0.999) and 60 °C (R^2=0.996, $p<0.05$).

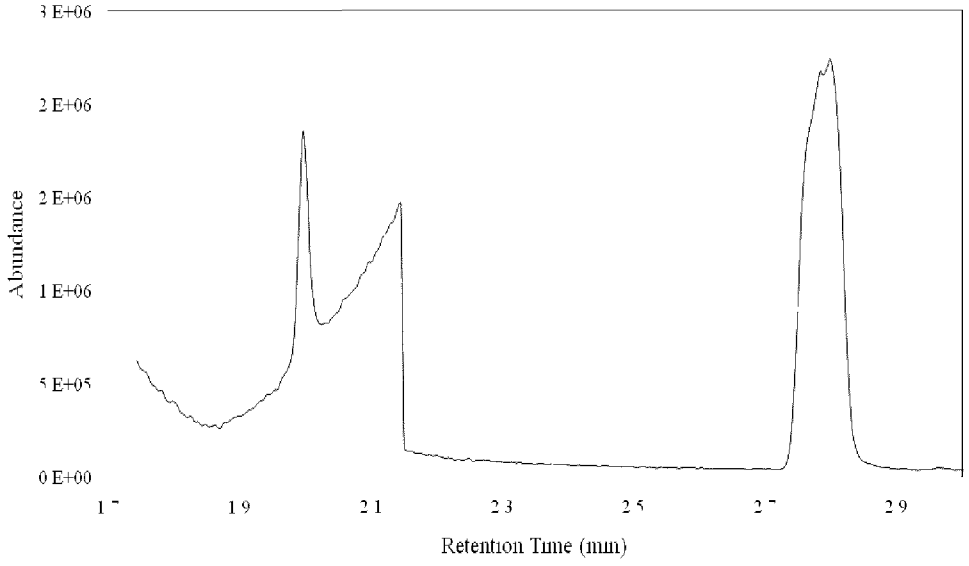

Figure A.18. Gas chromatogram for calibration standard containing EA (rt=1.999, quality:72), AcOH (rt=2.142, quality: 90), and heptane (rt=2.8, quality: 90).

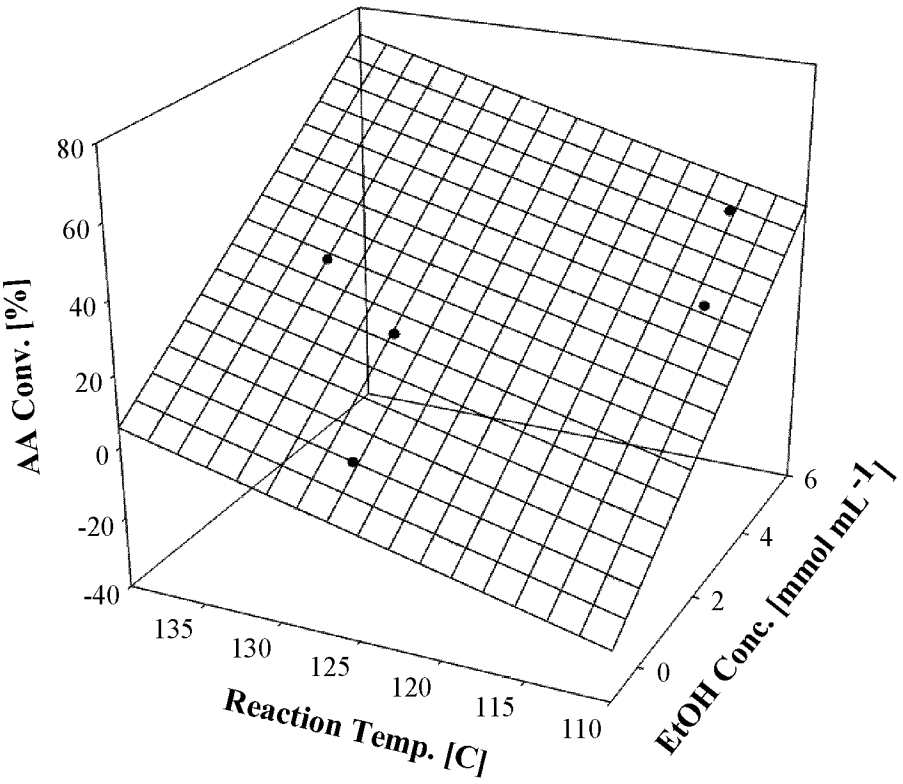

Figure A.19. Fractional conversion of acetic acid (AA) as a function of reaction temperature [°C] and EtOH concentration [mmol mL^{-1}] (R^2=0.996, $p<0.01$).

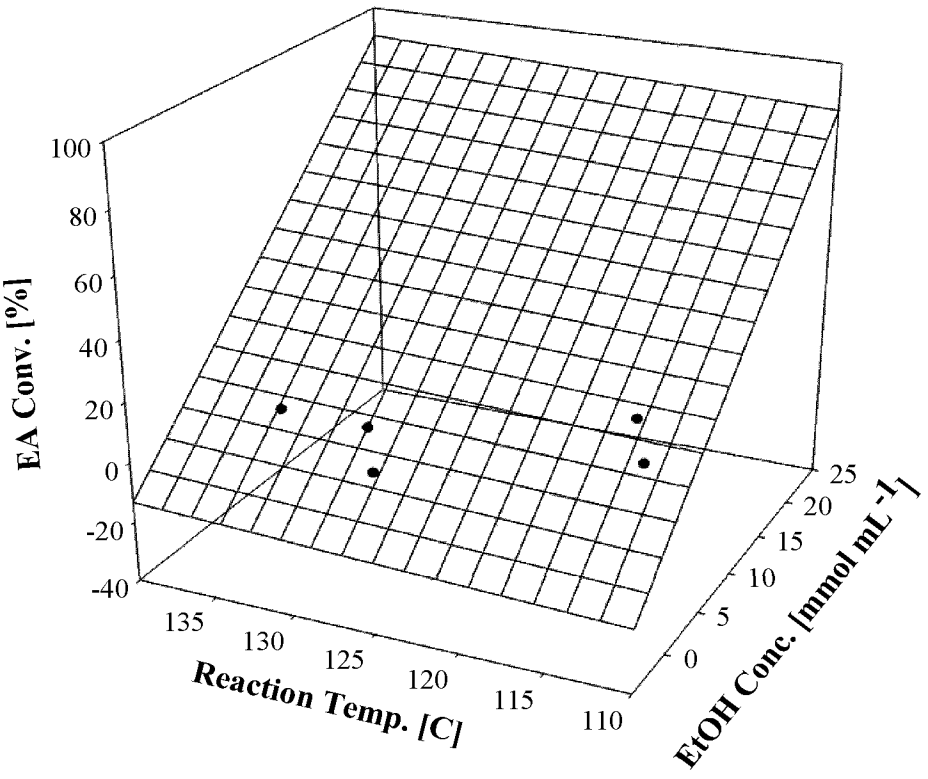

Figure A.20. Fractional conversion of acetic acid to ethyl acetate (EA) as a function of reaction temperature [°C] and EtOH concentration [mmol mL^{-1}] (R^2=0.89, $p<0.1$).

Subtask A.4: Production and characterization of pyrolysis char for environmental catalysis and adsorbent application

Our goal was to increase the value of char co-product by exploring novel applications in the environmental area. This task was intended to include characterization and application in ammonia adsorption, and further to extend to soil applications (described later in this report under subtask E.3). Ammonia adsorbents were generated via pyrolysis of biomass (peanut hulls, palm oil shells, and poultry litter) over a range of temperatures and compared to a commercially available activated carbon (AC) and solid biomass residuals, wood and poultry litter fly ash. Dynamic ammonia adsorption studies (i.e., breakthrough curves) were performed using these adsorbents at 23°C from 6 to 17 ppmv NH_3. These results indicate the feasibility of using a low temperature (and thus low energy input) pyrolysis and activation process for the generation of NH_3 adsorbents from biomass residuals.

Methodology and results described and summarized below have independently been reported in the following peer-reviewed publications:

2. *Kastner .J.R, J. Miller, and K.C. Das. 2009. Pyrolysis conditions and ozone oxidation effects on ammonia adsorption in biomass generated chars. Journal of Hazardous Materials, 164(2-3):1420-1427.*

Methodology

Wood fly ash from a pulp mill and poultry litter fly ash (from the combustion of poultry litter) was used in this study. The physical and chemical characteristics of the wood fly ash, including pH, surface area, bulk density, and the elemental composition were previously determined and are reported in Table A.13. Activated carbon (Darco™ granular, untreated 4-12 mesh, Sigma-Aldrich) was obtained from Sigma-Aldrich (Table 1) and used as a benchmark in this research.

Pelletized peanut hulls were used to generate char, and were typically 0.5-1 inches (1.3-2.54 cm) in length and 0.32 inches (0.8 cm) in diameter. The composition of typical pelletized peanut hulls has been reported to consist of 2-4% ash, 35-45% cellulose, and 27-33% lignin, with a bulk density ranging from 609-720 kg/m^3 and pH 5-6. In addition to peanut hulls, palm oil shells and poultry litter were used as feed stocks for pyrolysis and char generation.

The pyrolysis unit consisted of a gas preheater (1/4 OD inch stainless steel tube wrapped in heating tape [Thermolyne, Barnstead Inc, La] and was packed with fine steel mesh to provide turbulent mixing), followed by a tube furnace and condensation unit. Preheat temperature was controlled via a solid-state relay connection to a maximum temperature of 700°C. The furnace was a tube type (1 in ID, x 16 in length, Type 55035, Lindberg, WS), with an actual heating length of 12 inches and installed thermocouple for temperature control. Detailed description of the system and methods of pyrolysis are reported in section A.4.

In the case of the commercially available activated carbon (AC), poultry litter ash (PLA), wood fly ash (WFA), and palm oil char (POC), these materials were used in the adsorption experiments as received or generated. The poultry litter char (PLC) and peanut hull char (PHC)

were crushed and passed through 4 and 12 mesh screens (4.75 - 1.7 mm); the fraction that passed the #4 mesh and remained on the #12 mesh were used in the experiments (Table A.14).

Fixed Bed Adsorption

The dynamic adsorption of ammonia was measured in a fixed-bed reactor, packed with a defined mass of the adsorbent (5 g, except where noted). Breakthrough curves for ammonia and the different absorbents were measured in a continuous flow system in which compressed air was mixed with ammonia vapor of a defined concentration using a standard tank of ammonia (2500 ± 50 ppmv) and passed downward through the reactor column (Kimax, 2.5 cm i.d., 30.0 cm length, Ace Glass Vineland, NJ). The wood fly ash and poultry litter ash were distributed throughout the glass wool. A series of breakthrough curves was performed at different inlet NH_3 concentrations for each adsorbent; initially, breakthrough was performed at 6-7 ppmv, followed by desorption using air, then the inlet concentration was measured in a duplicate blank reactor system (glass wool only), and subsequently the next series of inlet concentrations were identically tested (8.5-9.5, 11-13, and 13-17 ppmv). Inlet and outlet NH_3 concentrations were measured using an online chemiluminesence detector (ThermoEnvironmental, Model 17C, Chemiluminescent Analyzer, Franklin, MA).

Adsorption Isotherms

Ammonia isotherms with the different materials were determined at 23°C from breakthrough curves. A defined mass (m) and height (H) of adsorbent was packed in between the glass wool, and ammonia of a defined inlet concentration (C_{in}) and total flowrate (Q) was passed downward across the bed. The outlet NH_3 concentration (C_{out}) was measured in real time using the chemiluminesence detector, and the inlet concentration was verified after each test. The resultant normalized concentration versus time profile (C_{out}/C_{in}) was fit to a sigmodal function and the mass of ammonia adsorbed (M_{ads}) was calculated from integration of equation 1.

$$M_{ads} = Q_T C_m \int_0^t (1 - \frac{C_{out}}{C_m}) dt \qquad (1)$$

Thus, for each particular inlet NH_3 concentration the mass adsorbed per amount of adsorbent or the adsorption capacity was calculated as $q = m/M_{ads}$ (mg NH_3/g adsorbent) allowing for an isotherm to be developed (plot of q versus the equilibrium NH_3 concentration).

Results and discussions

In general, the ammonia breakthrough curves (Q_T = 6.1 L/min; m = 5 g, H = 2.5 cm) indicated a very long mass transfer zone and the curves were greatly extended, suggesting much of bed was not utilized for mass transfer (data not shown here). Close inspection of the breakthrough curves between activated carbon (AC) and the palm oil shell char (500°C) did suggest that this char had an overall NH_3 adsorption capacity (proportional to the area behind the curve) similar to AC. Except for char generated from palm oil shell at 500°C, ammonia adsorption capacities were significantly higher on activated carbon. Palm oil chars generated via pyrolysis at temperatures below and above 500°C (ie., 400°C and 600°C), peanut hull chars at all temperatures (375°C, 400°C, 500°C, 600°C, 700°C), and poultry litter char at 500°C, had very low NH_3 adsorption capacities (Table 2 and some data are not shown).

Research indicates that acidic, polar functional groups on the carbon surface are responsible for adsorption of NH_3 and combined with a high surface area enhance adsorption. Most processes to activate carbon involve heating the carbon (or char) in the presence of an oxidizing agent either as a vapor (e.g., H_2O or steam, CO_2) or via wet impregnation (e.g., H_2SO_4, ZnCl). Alternatively, a gaseous oxidizing agent, such as ozone (O_3), could be used which would allow more uniform surface treatment (compared to wet impregnation), under lower temperatures. Ozone treatment of activated carbon has been shown to increase the number of acidic surface groups on the carbon. Subsequently, char and activated carbon were treated with ozone at defined concentrations and contact time (additional details provided in reference cited above). Ozone treatment clearly increased the ammonia adsorption capacity of the carbons with the greatest effect observed in the activated carbon, since the area behind the breakthrough curve increased and the resultant adsorption capacity, q (mg/g) increased by ~ 2, 6, and 10 times for palm oil char, peanut hull char (pyrolysis only), and activated carbon respectively (Table 3). Similar results were observed for peanut hull char generated using steam at 400°C.

There has been limited research on ammonia adsorption at concentrations relevant to agricultural operations (i.e., 0-50 ppmv) that would be important for design purposes, since adsorption capacities can decrease with decreasing equilibrium gas phase concentrations. Palm oil shell char or POC (generated at 500°C) had an NH_3 adsorption capacity, q, similar to untreated activated carbon and ranged from 0.70 to 0.95 mg/g for 6-14 ppmv NH_3 (23°C). These results are similar to NH_3 adsorption studies using untreated activated carbon from coconut shells (480 m^2/g) in which q ranged from 0.2 to 2 mg/g from 600 to 2400 ppmv NH_3 at 40°C (Rodrigues et al., 2002). However, our reported NH_3 adsorption capacities for the untreated carbon were significantly lower than activated carbon from palm-shells via acid oxidation or CO_2 activation (70-130 mg/g for 2000 ppmv NH_3 at 50°C – Guo et al., 2005). The significantly higher NH_3 adsorption capacities for the acid and CO_2 activated chars may have been due to the higher surface areas (1000 vs. 1-5 m^2/g in our work), the presence of acidic functional groups, and the higher NH_3 gas phase concentration (Guo et al., 2005).

The high NH_3 adsorption capacity of the palm shell char generated at 500°C relative to the other chars in our work, may have been due to the formation of acidic functional groups in semi-volatile condensation products located on the char; the pH of this material was 5.89 compared to 10-10.5 in the other chars (Table A.13).

Conclusion

Chars generated from biomass via low temperature pyrolysis (400-500°C) were demonstrated to be feasible ammonia adsorbents, if acidic functional groups or low pH was imparted to the char. In the case of palm shells pyrolyzed at 500°C, the resultant adsorption capacity was similar to commercially available activated carbon, even though the surface area was 400X lower than the AC. Steam activation during pyrolysis and ozone oxidation of the carbon surface significantly increased ammonia adsorption indicating that either treatment could be used to enhance NH_3 adsorption capacity. We anticipate that extending the pyrolysis holding time (>40 min) would increase the surface area of the chars and when coupled with steam activation or ozone treatment would greatly increase ammonia adsorption capacity; ozone treatment is potentially more attractive given it ability to functionalize the carbon at room temperature.

References cited in this section:

1. Guo, J.; Xu, W.S.; Chen, Y-L.; Lua, A-C. 2005. Adsorption of NH_3 onto activate d carbon prepared from palm shells impregnated with H_2SO_4. *Journal Colloid Interface Science*. 281:285-290.

2. Rodrigues, C.C.; Moraes, Jr., D. 2002. Control of Ammonia through Adsorption in a Fixed Bed of Activated Carbon. *Adsorption Science and Technology* 20(10): 1013-1022.

Table A.13. Physical and chemical characteristics of adsorbents used in ammonia adsorption studies (Mean ± SD where presented).

Properties	Activated Carbon	Peanut Hull Char (700°C)	Palm Oil Char (500°C)	Poultry Litter Char (500°C)	Poultry Litter Ash	Wood Fly Ash
Surface Area, m^2/g	425 ± 52	4.1 ± 0.8	0.9 ± 0.6		3.7	44.89 ± 8.34
pH	4.6	10.5	5.89	9.99	10.46	12.13 ± 0.17
Bulk Density, g/cm^3	ND	0.61-0.72	ND	ND	ND	0.54
Carbon, % (dry)	ND	64-68			ND	18.75 ±1.87
Pore Vol. (ml/g)	0.90	ND	ND	ND	ND	ND

Table A.14. Particle size analysis of adsorbents used in the ammonia adsorption studies.

Sieve/Adsorbent	Activated Carbon[a] (%, w/w)	Palm Oil Shell Char (%, w/w)	Peanut Hull Char (%, w/w)	Poultry Litter Char (%, w/w)
4 (4.75 mm)	5	0.00	0.00	9.03
6 (3.35 mm)	NP	2.24	32.32	26.16
7 (2.80 mm)	NP	13.06	11.92	13.19
8 (2.36 mm)	NP	45.15	6.87	34.03
10 (2.00 mm)	5	9.33	10.71	17.59
>12 (1.70 mm)	NP	30.22	38.18	9.03

[a], taken from Norit Americas website (http://www.norit-americas.com/1.6.cfm?type=TDS); NP, not performed

Table A.15. Ammonia adsorption capacities of different adsorbents at 23°C and a relative humidity of 10%, except where noted.

Adsorbent	Pyrolysis Temperature (°C)	Activation Method	Ammonia Concentration (ppmv)	q, NH_3 (mg/g)
Activated Carbon	unknown	steam	17	1.1
Activated Carbon	unknown	steam	6.5	0.61
Activated Carbon, 73% RH	unknown	steam	5.6	0.46
Palm Oil Shell Char	500	none	13.3	0.67
Palm Oil Shell Char	500	none	6.0	0.70
Palm Oil Shell Char, 73% RH	500	none	6.74	4.0
Peanut Hull Char	400	steam	14.6	0.22
Peanut Hull Char	400	steam	6.65	0.14
Peanut Hull Char, 73% RH	400	steam	6.65	0.0092
Peanut Hull Char	500	none	12.5	0.028
Peanut Hull Char	500	none	6.36	0.045
Poultry Litter Char	500	none	13	0.027
Wood Fly Ash	NA	NA	14.3	0.043
Poultry Litter Ash	NA	NA	15.0	0.032
Activated Carbon	unknown	steam/O_3[a]	6.0	6.61
Palm Oil Shell Char	500	O_3[a]	6.0	1.26
Peanut Hull Char	500	O_3[a]	6.0	0.12
Peanut Hull Char	500	O_3[b]	6.0	0.16
Peanut Hull Char	400/Steam	O_3[a]	5.9	0.18

[a], 30 minute treatment at 33 g/m^3 of ozone at 23°C

[b], 1 hour treatment at 33 g/m^3 of ozone at 23°C

Table A.16. Effect of Pyrolysis and Activation Process on Ammonia adsorption capacities of different adsorbents at 23°C and a relative humidity of 10%, except where noted.

Adsorbent	Pyrolysis Temperature (°C)	Activation Method	Ammonia Concentration (ppmv)	q, NH_3 (mg/g)
Activated Carbon	unknown	steam	6.5	0.61
Palm Oil Shell Char	500	none	6.0	0.70
Peanut Hull Char	500	none	6.36	0.045
Poultry Litter Char (longer holding time or LHT)	500	none	6.27	0.009
Poultry Litter Char (steam pyrolysis or SP)	500	Single Step (SS)	5.7	0.12
Poultry Litter Char (pyrolysis/steam activation)	500	Two-Step (TS)	6.3	0.05
Activated Carbon	unknown	Steam/O_3[a]	6.0	6.61
Palm Oil Shell Char	500	O_3[a]	6.0	1.26
Peanut Hull Char	500	O_3[a]	6.0	0.12
Peanut Hull Char	500	O_3[b]	6.0	0.16
Peanut Hull Char	400/Steam	O_3[a]	5.9	0.18
Poultry Litter Char (LHT)	500	None, O_3[a]	5.3	0.21
Poultry Litter Char (SP)	500	SS, O_3[a]		
Poultry Litter Char (P/S)	500	TS, O_3[a]		

[a], 30 minute treatment at 33 g/m^3 of ozone at 23°C

[b], 1 hour treatment at 33 g/m^3 of ozone at 23°C

Task B – Mixed Fermentation Technology for 5- and 6- Sugar Utilization

Summary of achievements

The efficient and simultaneous conversion of pentoses and hexoses is a significant hurdle to the economic utilization of biomass hydrolysates. The formation of any fermentation products (ethanol, butanol, succinic acid, lactic acid, pyruvic acid, etc.) from sugar mixtures would be greatly enhanced by designing a process which uses both type of sugars effectively. In this research we have demonstrated that the simultaneous consumption of sugar mixtures is feasible using a consortium of organisms which are each "designed" to consume only one sugar. By using this collection of organisms simultaneously, each organism is able to transform the particular sugar into the desired fuel or biochemical product without interference from other organisms. The technology was demonstrated using *Escherichia coli* an organism commonly used in industrial production.

Subtask B.1: Identify E. coli strains that have very fast growth rates

The initial working hypothesis was that various strains of *E. coli* would should vastly different abilities to consume the individual sugars principally found in lignocellulosic hydrolysate: D-(+)-glucose, D-(+)-xylose, L-(+)-arabinose, D-(+)-galactose, D-(+)-mannose.

A comparison of specific growth rates was completed by first growing cells at 37°C with agitation of 250 rpm (19 mm pitch) in 250 mL shake flasks containing 30 mL basal medium with 5 g/L of a single sugar. When the OD of this culture reached approximately 1, 5 mL was transferred to a second shake flask containing 45 mL basal medium with 5 g/L of a single sugar from which optical density was measured at 0.5 – 1.0 h intervals to determine growth rates.

The basal medium used in all experiments contained (per L): 13.3 g KH_2PO_4, 4.0 g $(NH_4)_2HPO_4$, 1.2 g $MgSO_4 \cdot 7H_2O$, 13.0 mg $Zn(CH_3COO)_2 \cdot 2H_2O$, 1.5 mg $CuCl_2 \cdot 2H_2O$, 15.0 mg $MnCl_2 \cdot 4H_2O$, 2.5 mg $CoCl_2 \cdot 6H_2O$, 3.0 mg H_3BO_3, 2.5 mg $Na_2MoO_4 \cdot 2H_2O$, 100 mg Fe(III)citrate, 8.4 mg $Na_2EDTA \cdot 2H_2O$, 1.7 g citric acid, 4.5 mg thiamine·HCl, and 5 g sugars (D-(+)-glucose, D-(+)-xylose, L-(+)-arabinose, D-(+)-galactose, D-(+)-mannose). The OD measured at 600 nm (DU-650 spectrophotometer, Beckman Instruments, San Jose, CA) was used to monitor cell growth.

Seven different *E. coli* strains were used to compare their growth rates on each of the five monosaccharides found in lignocellulosic hydrolysates. Generally K-12 derivatives *E. coli* MC4100 and MG1655 showed lower growth rates on monosaccharides than strains W, C and B (Table B.1). *E. coli* W showed the highest growth rate on glucose or arabinose, while ATCC8739 (C strain) was the fastest growing strain on xylose. In general, this C strain and W were both 'fast growing', and therefore these strains were selected for detailed study. We were surprised that the well-characterized *E. coli* strain MG1655 performed poorly.

Table B.1. Specific growth rates (h^{-1}) of *E. coli* strains on different carbon sources.

Substrate	W	B	C ATCC8739	C ATCC13706	C CGSC3121	MC4100	MG1655
D-Xylose	0.84	0.78	0.89	0.78	0.73	0.72	0.55
D-Glucose	1.00	0.97	0.96	0.85	0.73	0.88	0.72
L-Arabinose	0.94	0.86	0.93	0.80	0.75	0.67	0.68
D-Mannose	0.46	0.33	0.46	0.51	0.44	0.45	0.26
D-Galactose	0.66	0.79	0.75	0.45	0.25	0.83	0.33

Subtask B.2: Construct gene knockouts to create improved glucose/xylose-utilization strains

In parallel with subtask B.1, we initially chose MG1655 because its genome has been completely sequenced, and this strain has become the strain of choice for physiological studies in *E. coli.* (As shown in Table B.1, other strains were subsequently shown to be superior for this specific research.)

To construct a MG1655 derivative that could not consume glucose, all of the routes to metabolize glucose had to be eliminated. Like many sugars, glucose must first be phosphorylated before it can be further metabolized by *E. coli*. The principal route to phosphorylate glucose is by the phosphotransferase system (PTS). Because the PTS phosphorylates several sugars, some of the enzymes involved have broad specificities and can phosphorylate more than one sugar. Glucose can be phosphorylated by two different enzymes of the PTS, glucosephosphotransferase and mannosephosphotransferase encoded respectively by the *ptsG* and *manZ* genes (originally designated as *gpt* and *mpt*). Furthermore, glucose can be phosphorylated by the enzyme glucokinase which is encoded by the *glk* gene. A MG1655 derivative that could not consume glucose was constructed by knocking out the genes encoding for glucosephosphotransferase (*ptsG*), mannosephosphotransferase (*manZ*) and glucokinase (*glk*).

To construct a MG1655 derivative that could not consume xylose, either the *xylA* or *xylB* genes could be eliminated. Xylose is transported into *E. coli* by the xylose transport system and once internalized must be isomerized to xylulose by xylose isomerase (*xylA*) and phosphorylated to xylulose-phosphate by xylose kinase (*xylB*) before it can be metabolized. A MG1655 derivative that could not consume glucose was constructed by knocking out the gene encoding for xylose isomerase (*xylA*). The four knockouts described above were constructed using the straightforward "Keio protocol". A large number of strains were constructed from MG1655, and these are listed in Table B.2.

Table B.2. Knockouts derived from *E. coli* MG1655. Glu = glucose, Xyl = xylose. "Glu-" indicates the strain has very limited growth on glucose.

ALS1038	MG1655 *xylA*	Xyl-
ALS1048	MG1655 *ptsG manZ glk*	Glu-
ALS1060	MG1655 *ptsG manZ glk xylA*	Glu- Xyl-
ALS1122	MG1655 *ptsG manZ glk xylA crr*	Glu- Xyl-
ALS1155	MG1655 *crr*	
ALS1220	MG1655 *ptsI*	
ALS1226	MG1655 *ptsI glk*	
ALS1235	MG1655 *ptsI glk xylA*	Xyl-
ALS1253	MG1655 *crr manX glk*	
ALS 1291	MG1655 *ptsG manZ glk crr*	Glu-
KD894	MG1655 *crr manX glk*	

The W strain was subsequently selected for study because of its superior growth rate on sugars found in lignocellulosic hydrolysate (Table B.1), but this proved challenging because the Keio protocol for constructing knockouts was ineffective. We therefore focused on construction of glucose-knockouts strains derived from the W strain as described in Table B.3. These two strains, KD777 and KD915 were used to study the elimination of glucose consumption, which is the key part of the mixed sugar fermentation technology. Because the number of knockouts we could generate in W strains was limited, we subsequently selected the C strain (ATCC 8739) to create other strains which involved arabinose or xylose utilization.

Table B.3. Knockouts derived from *E. coli* W. Glu = glucose, Xyl = xylose. "Glu-" indicates the strain has very limited growth on glucose.

ALS1097	W *xylA*	Xyl-
KD777	W *ptsG*::tet *glk*::kan *manZ*::cam	Glu-
KD915	W *ptsG*::FRT *manZ*::cam *glk*::FRT *crr*::FRT	Glu-

We are presently constructing W *ptsG glk manZ galK*. This strain has been a challenge to construct (compared to MG1655 or C derivatives) because as noted above the W strain knockouts are not amenable to the 'Keio protocol' which greatly simplifies obtaining knockouts. The strain will have four antibiotic resistances, including gentamycin. We are constructing this strain because each derivative containing the *ptsG glk manZ* knockouts is surprisingly able to consume glucose slowly. Although glucose consumption only occurs after other substances (e.g.,

xylose) are depleted and therefore would not significantly affect this approach to treat lignocellulosic hydrolysates, we want to understand what process is allowing glucose uptake. Based on discussions with other scientists (though not completely consistent with our results), our current hypothesis is that galactokinase encoded by the *galK* gene is phosphorylating glucose. Because our detailed studies used derivatives from the W strain and because (inexplicably) the *glk* gene must be the final gene knocked out, we have to go back and reconstruct strains from W *ptsG manZ* (i.e., first W *ptsG manZ galK* then W *ptsG glk manZ galK*).

We also have constructed a variety of knockouts derived from the C strain, and these are listed in Table B.4.

Table B.4. Knockouts derived from *E. coli* C. Glu = glucose, Xyl = xylose, Ara = Arabinose. "Glu-" indicates the strain has very limited growth on glucose.

ALS1363	C *ptsG glk manZ*::Kan	Glu-
ALS1364	C *ptsG glk manZ crr*::Kan	Glu-
ALS1370	C *ptsG glk manZ crr xylA*	Glu- Xyl-
ALS1371	C *ptsG glk manZ crr araA*	Glu- Ara-
ALS1391	C *xylA araA*::kan	Xyl- Ara-

The strains ALS1363 and ALS1364 are hindered in their ability to consume glucose. ALS1370 is hindered in ability to consume glucose and unable to consume xylose. Therefore, ALS1370 should consume only arabinose in a mixture of glucose, xylose and arabinose. ALS1371 is hindered in its ability to consume glucose and unable to consume arabinose. Therefore, ALS1371 should consume only xylose in a mixture of glucose, xylose and arabinose. ALS1391 is unable to consume either xylose or arabinose. We hypothesize that if we grew ALS1370, ALS1371 and ALS1391 together on a mixture of xylose, glucose and arabinose, ALS1370 would consume the arabinose, ALS1371 would consume the xylose and ALS1391 would consume the arabinose.

Subtask B.3: Introduce ethanol-generating capability into strains from earlier subtasks.

Our working hypothesis was that insertion of ethanol producing plasmids into the various sugar-specific strains would permit that strain to convert exclusively the one sugar into ethanol. We obtained the pLOI295 and pLOI297 plasmids constructed years ago by Lonni Ingram's laboratory (Univ. Florida) for this purpose. These two plasmids contain the pyruvate dehydrogenase (*pdh*) and alcohol dehydrogenase (*adhE*) genes from *Zymomonas mobilis*. The presence of these two enzymes has been previously shown to endow *E. coli* with the ability to accumulate significant ethanol (Ingram and Conway 1988 *Appl. Env. Microbiol.* 54(2):397-404). Because we had

not yet fully learned that W and C strains were superior in growth on particular sugars, we examined ethanol production in a derivative of MG1655. Furthermore, we believed strains having an additional knockout in the *pflB* would be necessary to achieve high ethanol concentrations since this knockout prevents the formation of formate, the major metabolic product of *E. coli* under normal (anaerobic) conditions.

Unfortunately, we found that neither pLOI295 or pLOI297, the two pET plasmids that we tested, were capable of producing high levels of ethanol. With pLOI295 we could only obtain an ethanol yield of 25% from glucose, and much lower levels were obtained with the pLOI297 plasmid. Because other researchers have reported similar problems with the pET plasmids, we decided to reclone the pET genes into the widely used and more stable pTrc99A expression vector.

ALS1074 (MG1655 *xylA pflB*) contains a knockout of the *xylA* gene and therefore is expected in a mixture of glucose and xylose to be glucose-selective; i.e., the strain will consume glucose but not xylose. ALS1073 (MG1655 *ptsG manZ glk pflB*) contains three knockouts in glucose uptake and is therefore expected in a mixture of glucose and xylose to be xylose-selective; i.e., the strain will consume xylose but not glucose. These two strains were transformed with plasmid pTrc18A-*pdh.adhE*. ALS1073 and ALS1074 were individually and simultaneously grown in a medium containing nominally 15 g/L glucose and 10 g/L xylose. Specifically, 50 mL of medium was used in a 250 mL shake flask operating at a temperature of 37°C and an agitation of 250 rpm. The cultures were induced with 1 mM IPTG 8 h after inoculation. Anaerobic conditions were simulated 12 h after inoculation by reducing the agitation to 75 rpm. For each of the three experiments performed in duplicate (ALS1073 alone, ALS1074 alone, and ALS1073 and ALS1074 together), a sample was taken at the beginning of the experiment, and again at the end. The results are shown in Table B.5.

Table B.5. Production of ethanol by substrate-selective strains of *E. coli*

		ALS1074 alone		ALS1073 alone		ALS1073 + ALS1074	
		Exp 1	Exp 2	Exp 1	Exp 2	Exp 1	Exp 2
Xylose (g/L)	Start	9.8	10.0	9.2	8.9	8.6	8.8
	End	9.7	9.9	2.2	1.5	0.1	0
Glucose (g/L)	Start	13.1	13.5	14.0	13.6	12.8	13.1
	End	0.4	0.2	13.3	13.5	0.3	0.2
Ethanol (g/L)		2.8	2.9	2.2	2.4	5.7	5.8
Optical Density		9.0	7.6	2.0	2.2	8.7	9.1

For ALS1074, essentially all of the glucose was consumed and none of the xylose, resulting in an accumulation of about 2.8 g/L ethanol. For ALS1073,

essentially all of the xylose was consumed but none of the glucose, resulting in an accumulation of an average of 2.3 g/L ethanol. When both ALS1073 and ALS1074 were used together on this sugar mixture, both sugars were consumed with about 5.7 g/L ethanol generated. The results demonstrate that the two-strain approach, in which each strain is designed to be selective for one sugar but the strains otherwise are identical, can effectively generate ethanol. However, we were disappointed in the rate at which ethanol was produced by the cells. Also, the final yield of ethanol was only about 25%, about half of the theoretical maximum. Because of this fact, we and others have come to the conclusion that *E. coli* is more suitable for the production of other commodity chemicals such as organic and amino acids, where yields of over 100 g/L can be achieved.

Conclusions (Task B)

- Strains C and W were shown generally to have the greatest growth rates on individual sugars.
- A large number of strains derived from wild-type *E. coli* strains W, C and K-12 (MG1655) have been constructed which are unable to consume either glucose, xylose or arabinose (and which therefore are substrate selective).
- Knockouts in strain W could not be performed with a commonly used protocol, making strain construction in this background more difficult than in strains C or K-12 derivatives.

Although ethanol production was improved in glucose-xylose sugar mixtures using the consortium approach, the plasmids used to generate ethanol were not found to be satisfactory. Other products may be preferred using this technology.

Task C – Improve acetate utilization strains

Summary of accomplishments

An additional problem with the use of lignocellulosic hydrolysate arises from the presence of compounds which inhibit the conversion of sugars. In particular, since xylose is acetylated in lignocellulose, for example, acetic acid seems to be one unavoidable component of lignocellulose hydrolysates. Generally acetic acid reduces xylose conversion much more than it reduces glucose conversion. While acetic acid can be reduced by judicious design of the hydrolysis process or by improvements in the biomass itself, it does not appear feasible to eliminate this compound. In this research we have demonstrated that acetic acid can be selectively removed by extending the consortium approach. Specifically, an organism was designed which is unable to consume any sugars but which can consume acetic acid. The technology was demonstrated using *Escherichia coli* an organism commonly used in industrial production.

Subtask C.1: Mutagenesis to see if the acetate-utilization strain can be improved.

The initial working hypothesis was that various strains of *E. coli* would should vastly different abilities to consume acetic acid.

In order to examine different strains of *E. coli*, strains were grown on 50 mL defined medium with 5 g/L acetate as the carbon source in 250 mL shake flasks at 37°C and 350 rpm with a starting pH of 7. The defined medium contains (per liter): citric acid, 1.70 g; KH_2PO_4, 13.30 g; $(NH_4)_2HPO_4$, 4.50 g; $MgSO_4 \cdot 7H_2O$, 1.2 g; $Zn(CH_3COO)_2 \cdot 2H_2O$, 13 mg; $CuCl_2 \cdot 2H_2O$, 1.5 mg; $MnCl_2 \cdot 4H_2O$, 15 mg; $CoCl_2 \cdot 6H_2O$, 2.5 mg; H_3BO_3, 3.0 mg; $Na_2MoO_4 \cdot 2H_2O$, 2.5 mg; Fe(III) citrate, 100 mg; thiamine·HCl, 4.5 mg; $Na_2(EDTA) \cdot 2H_2O$, 8.4 mg. When the OD in a first flask was about 2.0, 5 mL of culture was transferred simultaneously to two identical 250 mL shake flasks composed of the same medium. The specific growth rates and the acetate consumption of these strains was measured and compared to identify the strains with the highest growth rate. Table C.1 shows the results.

The results demonstrate that *E. coli* strains show a wide range of abilities for the consumption of acetic acid. The fastest strain was the wild type C strain ATCC 8739 which has a growth rate of 0.405 h^{-1}, while the slowest strain was SCS-1 with a growth rate of 0.153 h^{-1}, less than half of the growth rate observed by C. We are currently very interested in learning why some strains of *E. coli* grow much better than others on acetic acid. Toward an answer to this question, online genome databases like xBASE and NCBI (National Center for Biotechnology Information) genome database and DNA library technology are being used to compare growth rates with the genome data to determine if a correlation exists between these two parameters. Presently we have not identified any 'markers' in these sequences which correlate with cell growth rate on acetate.

We have tried several different mutagenic approaches, but better *E. coli* acetate-utilization strains could not be obtained. This result is not a problem, however, as a growth rate of 0.405 h^{-1} on acetic acid is surprisingly high, and quite sufficient for an economic process for removing this inhibitor from lignocellulosic hydrolysate. As a comparison, this growth rate on acetate exceeds the maximum growth rate of the ethanol-producing yeast *Saccharomyces cerevisiae* on glucose.

Table C.1. Specific growth rates (h^{-1}) of *E. coli* strains on acetate.

Strain	Growth rate (h^{-1})
MG1655 (ATCC 700926)	0.292
MC4100	0.340
SCS-1 (Stratagene)	0.153
MACH1 (Invitrogen)	0.340
DH1 (ATCC 33849)	0.295
JM105 (Pharmacia)	0.304
B (ATCC 11303)	0.343
C (ATCC 8739)	0.405
C (ATCC 13706)	0.337

C (CGSC 3121)	0.265
BL21 (Stratagene)	0.301
JM101 (ATCC 33876)	0.328
W3110 (CSGC 4474)	0.255
W (ATCC 9637)	0.372

We initially chose MG1655 to examine acetate consumption in the presence of xylose and glucose because its genome has been completely sequenced, and this strain has become the strain of choice for physiological studies in *E. coli*. (As shown in Table 3.1.1, other strains were subsequently shown to be superior.) Strain ALS1060 contained Δ*ptsG*763::FRT, Δ*manZ*743::FRT, Δ*glk*-726::FRT, Δ*xylA*748::FRT deletions, which were generated by transducing MG1655 with the corresponding Keio (FRT)Kan deletion and then curing the Kan(R) using the pCP20 plasmid, which contains a temperature-inducible FLP recombinase as well as a temperature-sensitive replicon. The strain KD840 additionally contained the Δ*crr*-746::(FRT)Kan deletion. Medium contained (per L): 13.3 g KH_2PO_4, 4.0 g $(NH_4)_2HPO_4$, 1.2 g $MgSO_4 \cdot 7H_2O$, 13.0 mg $Zn(CH_3COO)_2 \cdot 2H_2O$, 1.5 mg $CuCl_2 \cdot 2H_2O$, 15.0 mg $MnCl_2 \cdot 4H_2O$, 2.5 mg $CoCl_2 \cdot 6H_2O$, 3.0 mg H_3BO_3, 2.5 mg $Na_2MoO_4 \cdot 2H_2O$, 100 mg Fe(III)citrate, 8.4 mg $Na_2EDTA \cdot 2H_2O$, 1.7 g citric acid, 0.0045 g thiamine·HCl, and acetate using $Na(CH_3COO) \cdot 3H_2O$. A wide range of acetate, glucose and xylose concentrations were examined, and these components were autoclaved separately, sterilely combined, and neutralized with NaOH to a pH of 7.0. Batch processes using 1.0 L medium were carried in a controlled 2.5 L bioreactor. Air was sparged into the fermenter at a flowrate of 1.0 L/min, and the agitation was 500 rpm to prevent oxygen limitation. The pH was controlled at 7.0 using 20% (w/v) NaOH and 20% (v/v) H_2SO_4, and the temperature was controlled at 37°C.

In the controlled bioreactor, MG1655 and KD840 each had growth rates on acetate (as sole carbon source) of about 0.22 h^{-1}, about 25% less than was observed in the shake flask studies used to examine growth rates reported in Table C.1. In various batch cultures we observed acetate consumption first, followed by very slow glucose and consumption of xylose (when present). This observation that ALS1060 grew slowly in the presence of glucose suggests that *E. coli* may have another means to transport and utilize glucose, and that mutations in the *ptsG manZ glk* genes are insufficient to prevent glucose consumption. With the goal of completely excluding glucose consumption, we next examined growth on glucose using strains having mutations additionally in one of several other genes encoding other PTS proteins: *fruA* or *fruB* encoding proteins of the fructose-specific PTS; the *bglF* gene involved in the PTS of β-glucosides, or *crr* which encodes the $EIIA^{glu}$. The strain with the *crr* knockout showed decreased glucose uptake, and we therefore used KD840 for additional study.

KD840 consumed acetate as a sole carbon source at a specific growth rate of 0.23 h^{-1}, identical to ALS1060, indicating that the additional knockout of the *crr* gene did

not curtail acetic acid consumption. We also examined batch growth of KD840 in BA10 medium with 20 g/L glucose and 10 g/L xylose. Similar to the growth of KD840 in the mixture of acetate and glucose, acetate was completely consumed by 40 h with a specific growth rate of 0.12 h^{-1}. Over the course of the subsequent 40-50 h, about 7 g/L glucose and 1 g/L xylose were consumed (Figure C.1), similar to the previous observations for ALS1060. During this period the OD also increased slowly at a growth rate less than 0.01 h^{-1}. The slow consumption of glucose and to a lesser extent xylose after acetic acid is exhausted will not pose a problem because the process of detoxifying the hydrolysate can just be halted immediately after acetic acid is removed (for example, at 38 h in the experiment shown in Figure C.1). This result provides compelling evidence that acetic acid can be removed selectively from a mixture of sugars, a process useful to the detoxification of lignocellulosic hydrolysate.

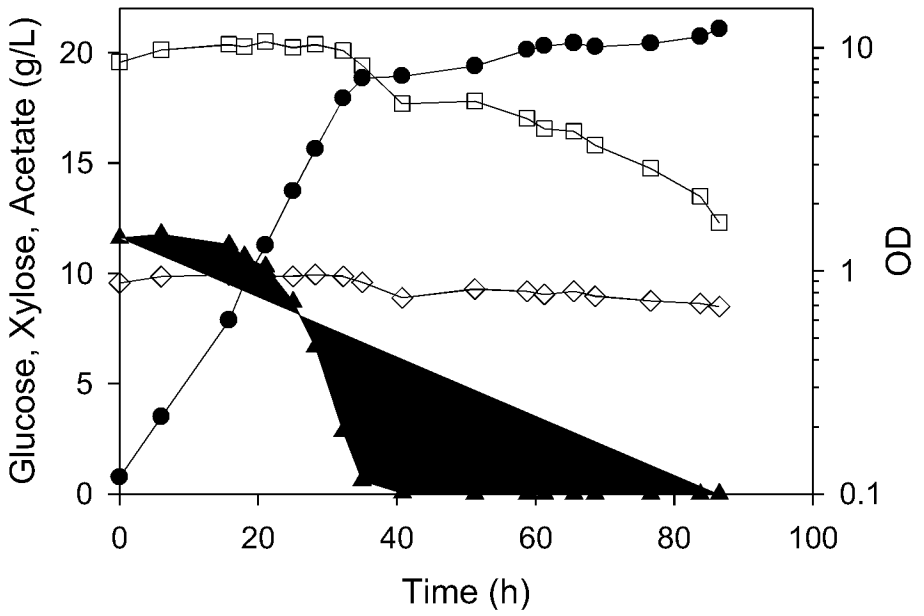

Figure C.1. Aerobic batch culture of *E. coli* KD840 on defined medium with 10 g/L acetate, 20 g/L glucose and 10 g/L xylose. Glucose (□), xylose (◇), acetate (▲) and the OD (●) were measured over the course of the process.

Subtask C.2: Two-step process for converting lignocellulosic hydrolysates into ethanol

Our initial working hypothesis was that a consortium of different strains of *E. coli* could be employed to first remove acetic acid and second to generate ethanol from the remaining sugars found in the lignocellulosic hydrolysate. We were disappointed that even after recloning of the ethanol-generating plasmids, ethanol production was so poor (reported in earlier subtask). However, we were pleased that acetic acid could

be consumed and leave glucose and xylose unconsumed. Because of the poor performance of ethanol generation, we selected lactic acid as a model product.

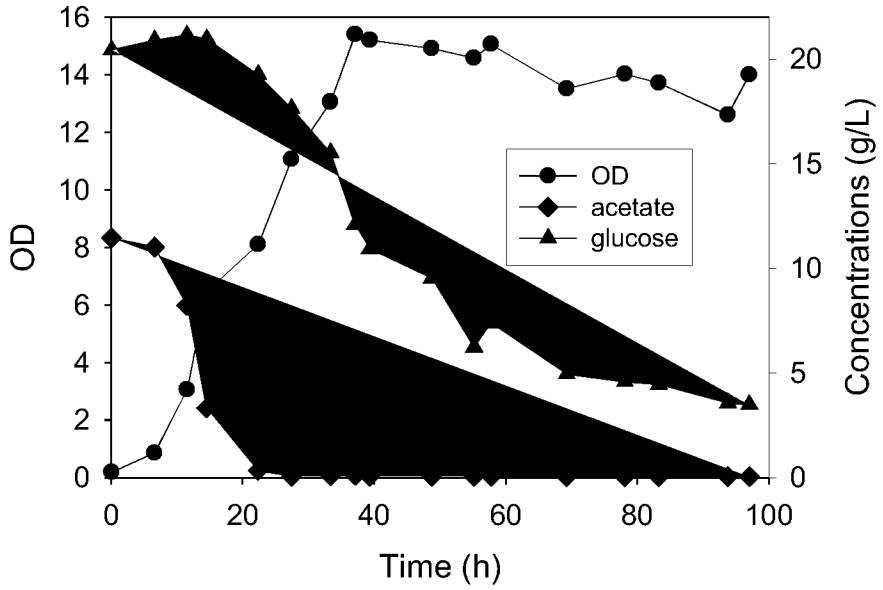

Figure C.2. Batch microbial process of C *ptsG manZ glk crr* in a mixture of acetate and glucose.

Because we had shown the C strain consumed acetic acid faster than any other strain, we constructed C *ptsG manZ glk* and C *ptsG manZ glk crr*, strains which should not consume glucose, but should not be hindered in consuming acetate. We examined the performance of this strain in a mixture of 20 g/L glucose and 10 g/L acetate (Figure C.2). The C strain consumes acetate extremely quickly, and has no difficulty exhausting 10 g/L acetate in less than 20 hours. After acetate is consumed, glucose is slowly consumed, similar to our observations previously. In this case, it is not clear whether glucose was consumed when acetate was present. Certainly during the first 15 hours when the acetate concentration decreased from 11 g/L to 3.3 g/L, no glucose was consumed.

In order to generate lactic acid as an example product from the resulting mixture of glucose and xylose, we used ALS1074 (MG1655 *xylA pflB*) and ALS1073 (MG1655 *ptsG manZ glk pflB*) that had been previously employed for ethanol generation. In addition to the basal medium containing (per liter): 13.3 g KH_2PO_4, 4.0 g $(NH_4)_2HPO_4$, 1.2 g $MgSO_4 \cdot 7H_2O$, 13.0 mg $Zn(CH_3COO)_2 \cdot 2H_2O$, 1.5 mg $CuCl_2 \cdot 2H_2O$, 15.0 mg $MnCl_2 \cdot 4H_2O$, 2.5 mg $CoCl_2 \cdot 6H_2O$, 3.0 mg H_3BO_3, 2.5 mg $Na_2MoO_4 \cdot 2H_2O$, 100 mg Fe(III)citrate, 8.4 mg $Na_2EDTA \cdot 2H_2O$, 1.7 g citric acid, and 4.5 mg thiamine·HCl, we used two different xylose-glucose mixtures: one called "B2X3G" medium which contained with nominally 20 g/L xylose and 30 g/L glucose, and one called "B3X2G" which nominally contained 30 g/L xylose and 20 g/L glucose. Batch experiments were carried out in a 2.5 L bioreactor containing 1.0 L medium. Each experiment consisted of two process phases maintained at 37°C.

During an initial aerobic growth phase with duration as reported in the results, air was sparged into the fermenter at a flowrate of 1.0 L/min, and the agitation was 1000 rpm to ensure no oxygen limitation. The pH was controlled at 6.7 using 28% (w/v) NH_4OH. During a second anaerobic 'production' phase, N_2 was supplied at 0.2 L/min, the agitation was reduced to 200 rpm, and the pH was controlled at 6.7 using 20% (w/v) NaOH.

ALS1073 and ALS1074 were first studied by growing each strain alone under aerobic conditions in B2X3G medium, then after 8 h switching to anaerobic conditions. ALS1074 consumed approximately 10 g/L glucose during the 8 h of growth to an OD of 11.5 (Figure C.3). After initiating anaerobic conditions, growth stopped and the remaining 17 g/L glucose was converted into about 14 g/L lactate within 3 h for a yield of 0.83 g/g (based on substrate consumed during the anaerobic production phase only). Lactate was formed at a constant specific rate of 1.2 g/g·h during the anaerobic phase, and throughout the process the xylose concentration remained unchanged. Similarly, ALS1073 consumed 4 g/L xylose during the 8 h aerobic growth phase to an OD of 4.5 (Figure C.4). During the anaerobic phase, the remaining 13.3 g/L xylose was converted to 13 g/L lactate at a yield near 1.0 g/g. The conversion of xylose to lactate was completed in 14 h. The rate of xylose consumption during the anaerobic phase by ALS1073 appears to be much slower than the rate of glucose consumption by ALS1074. However, the biomass concentration was appreciably different between the two experiments—the biomass concentration of ALS1073 after 8 h of growth on xylose was less than 40% of the biomass concentration using ALS1074 on glucose. The specific rate of xylose consumption was 0.92 g/g·h at the onset of the anaerobic phase, whereas the rate of xylose consumption was 0.49 g/g·h during the latter portion of the anaerobic phase.

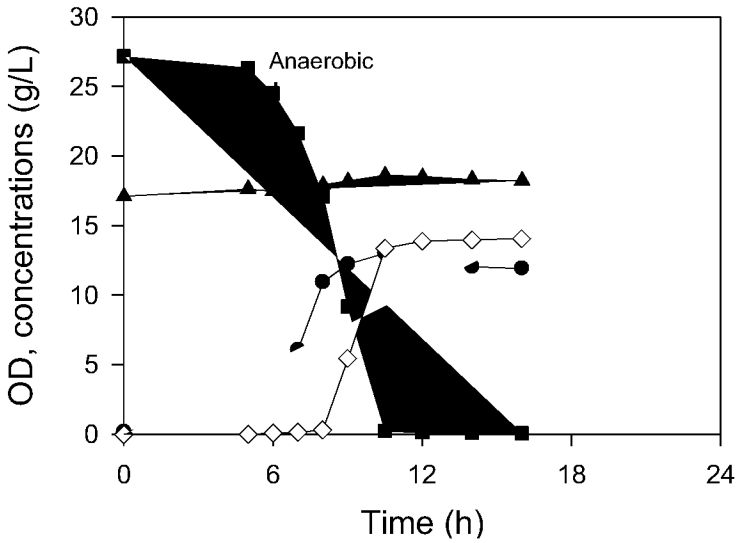

Figure C.3. Batch aerobic-anaerobic process of *Escherichia coli* ALS1074 on a mixture of glucose (■) and xylose (▲). After 8 h of aerobic growth, the culture was switched to anaerobic conditions as indicated. The OD (●) and lactate concentration (◇) were measured over the course of the fermentation.

In another experiment, *both* ALS1073 and ALS1074 were inoculated into a single bioreactor containing the same xylose-glucose defined medium B2X3G. In this two-strain co-fermentation, care was taken to ensure that each strain was inoculated at approximately the same cell density that was used in the two different one strain processes. After 8.5 h of growth the anaerobic phase was similarly initiated, and at this time the culture had consumed about 4 g/L xylose and 10 g/L glucose to achieve an OD of 16 (Figure C.5). During the anaerobic phase, the remaining glucose was consumed in less than 3 h, and the xylose was consumed in about 12 h. Assuming that the measured OD of 16 represents an OD of 11.5 for ALS1074 and an OD of 4.5 for ALS1073 (values observed in the single organism cases above), then the specific rate of glucose consumption during the anaerobic phase was 1.6 g/g·h, and the rate of xylose consumption was initially 1.2 g/g·h. The 17.5 g/L glucose and 13.3 g/L xylose present at the onset of the anaerobic phase were converted to 25.9 g/L lactate, for a yield of 0.84 g lactate/g total sugar.

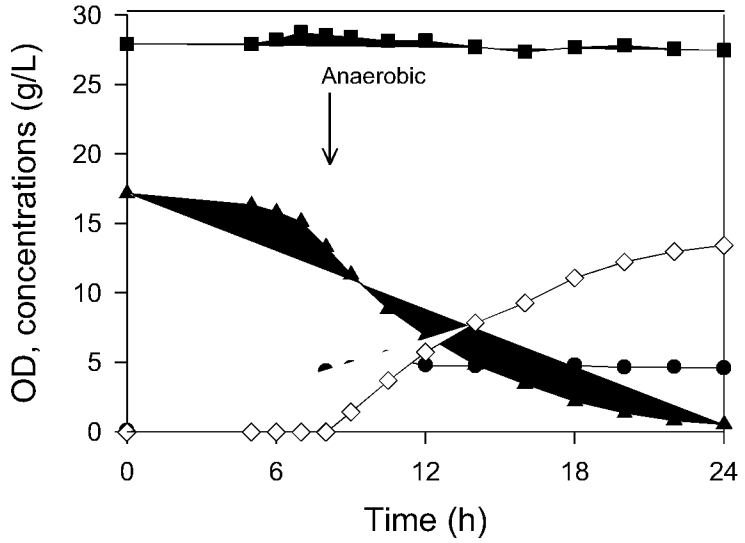

Figure C.4. Batch aerobic-anaerobic process of *Escherichia coli* ALS1073 on a mixture of glucose (■) and xylose (▲). After 8 h of aerobic growth, the culture was switched to anaerobic conditions as indicated. The OD (●) and lactate concentration (◇) were measured over the course of the fermentation.

Although the two-strain process as implemented (Figure C.5) performed exactly as each single strain process, the two-strain process exposed one important shortcoming. Under the conditions of the experiment, the volumetric rate of xylose consumption did not match the volumetric rate of glucose consumption. Specifically, because glucose exhaustion occurred in less than 3 h of anaerobic conditions but xylose consumption required over 12 hours, the process inefficiently consumed only one of two possible substrates for the final 10 h. The overall process was essentially limited by the volumetric rate of xylose consumption. To maximize overall productivity, the two consumption rates ideally would allow both glucose and xylose

to become exhausted at about the same time. Moreover, these two consumption rates should be adjustable so that this optimal productivity occurs regardless of the initial concentrations of xylose and glucose.

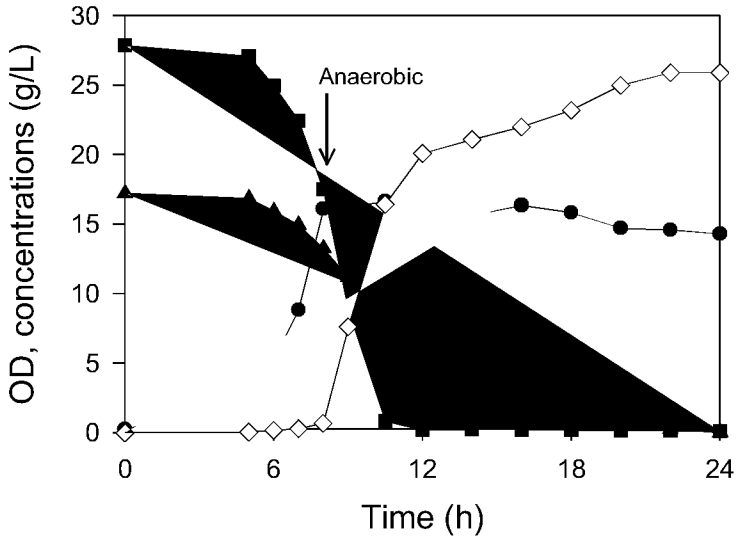

Figure C.5. Batch aerobic-anaerobic process of *Escherichia coli* ALS1073 and ALS1074 on a mixture of glucose (■) and xylose (▲). After 8 h of aerobic growth, the culture was switched to anaerobic conditions as indicated. The OD (●) and lactate concentration (◇) were measured over the course of the fermentation

The volumetric consumption rate (Q) is equal to the specific consumption rate (q) times the biomass concentration (X). So, for the xylose-selective strain $Q_{xylose} = q_{xylose}X_{xylose}$. One general method to increase Q is to increase q, for example using metabolic engineering approaches directed toward altering the pathways involving that substrate. Another general method to increase Q is to increase the biomass concentration of the strain. Because $q_{glucose}$ is about 30% greater than q_{xylose} during the anaerobic phase for the particular two-strain bioprocess we conducted, a higher cell density for the xylose-selective strain X_{xylose} is needed relative to $X_{glucose}$ in order to match the two values of Q. In a one-strain approach for the simultaneous consumption of xylose and glucose, only one biomass concentration exists, and the absence of this additional degree of flexibility prevents the matching of utilization rates for multiple substrates.

To confirm the flexibility in aligning consumption rates, we repeated the two-strain experiment using the same B2X3G medium. In this case, we increased the cell density of the xylose-consuming strain by providing this strain more time for growth prior to switching to the non-growth production phase. Specifically, using a nearly identical medium with 20 g/L xylose and 31 g/L glucose, at the start of the process (t=0) the bioreactor was only inoculated with the xylose-consuming strain ALS1073. Two hours after this inoculation, the bioreactor was inoculated with the glucose-consuming strain ALS1074, and at 8.5 h, anaerobic conditions commenced. Therefore, the xylose-consuming strain experienced 8.5 h of aerobic growth, while the glucose-consuming strain was allowed only 6.5 h of aerobic growth. At the time

that anaerobic conditions commenced, the OD of the culture was approximately 10.5 with 27.6 g/L glucose and 15.4 g/L xylose, and we estimate that about 60% of the biomass was ALS1073 while 40% of the biomass was ALS1074. In this experiment, the rates of glucose and xylose consumption were much more closely matched, and both sugars were consumed almost simultaneously. Thus, the two-sugar mixture was efficiently converted at a constant rate into 32 g/L lactate over the course of 8 h. We also observed about 2.5 g/L succinate and 0.5 g/L ethanol and acetate (yields based on xylose+glucose: 0.84 g lactate/g, 0.065 g succinate/g, 0.004 g acetate/g, 0.012 g ethanol/g). The small sacrifice made in the unnecessarily large glucose consumption rate was more than offset by the improvement in the xylose-consumption rate.

We next studied whether this approach can be "tailored" for other concentrations of xylose and glucose. In particular, we conducted a bioprocess using a medium with initially 33 g/L xylose and 22 g/L glucose (nominally B3X2G). Because this medium contains 50% more xylose than glucose, an even higher cell density of the xylose-selective strain ALS1073 relative to the glucose-selective strain ALS1074 is required compared to the previous process using B2X3G medium. Therefore, at the start of the process (t=0) the culture was inoculated with ALS1073, while the inoculation with ALS1074 occurred 3.1 h later. Anaerobic conditions commenced at 9.1 h; thus, ALS1073 experienced 9.1 h of growth while ALS1074 experienced 6 h of growth. At the onset of anaerobic conditions, the OD of the culture was approximately 12 with 19.5 g/L glucose and 20.4 g/L xylose (Figure C.6). Again, the rates of glucose and xylose consumption were closely matched, and the two-sugar mixture was efficiently converted into 37 g/L lactate with a lactate-sugar yield of 0.88 g/g. Other products generated during anaerobic conditions included 0.069 g succinate/g, 0.010 g acetate/g, 0.009 g ethanol/g.

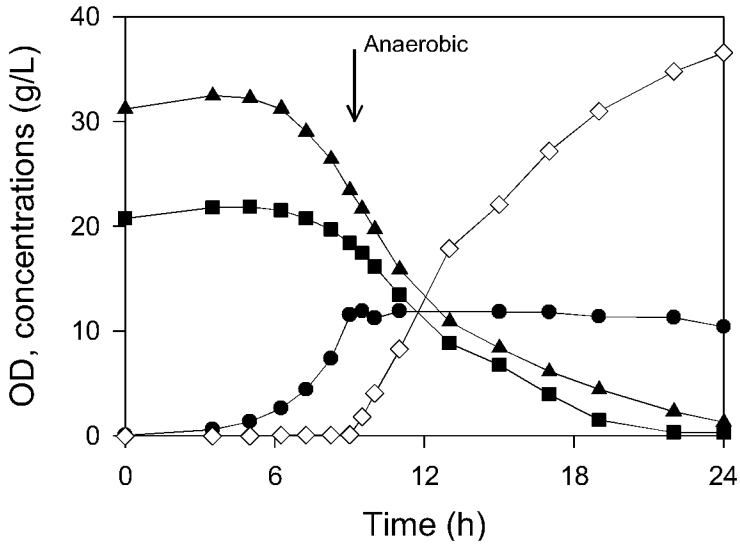

Figure C.6. Batch aerobic-anaerobic process of *Escherichia coli* ALS1073 and ALS1074 on a mixture of glucose (■) and xylose (▲). At the start of the process the bioreactor was inoculated with ALS1073, and after 3.1 hours the bioreactor was

inoculated with ALS1074. After 9.1 h of aerobic growth, the culture was switched to anaerobic conditions as indicated. The OD (●) and lactate concentration (◇) were measured over the course of the fermentation.

Conclusions (Task C)

- Acetate at concentrations of at least 10 g/L (1%) can be selectively removed from a mixture of xylose and glucose effectively. Slow metabolism of the sugars after acetate is exhausted would not pose a problem for a batch process.
- The resulting mixture of xylose and glucose can be simultaneously converted into a biochemical product such as lactic acid using the consortium approach.

Task D – Extend mixed fermentation approach to utilize other sugars in hydrolysates.

Summary of accomplishments

Previous tasks focused on xylose and glucose as the two dominant sugars found in lignocellulosic hydrolysate. Several other pentoses and hexoses occur in lignocellulosic hydrolysate, typically at a lower concentration. The goal of this task is to extend the consortium approach to these other sugars, with a focus on arabinose and galactose.

Subtask D.1: Constructing an arabinose-utilization E. coli strain.

We consider the system of interest to be the three-sugar mixture containing glucose-xylose-arabinose. Ultimately, in this mixture three strains would be necessary, a strain consuming xylose exclusively, a second strain consuming arabinose exclusively and a third consuming glucose exclusively. Both the xylose-utilizing strain and the arabinose-selective strain require (ideally) the complete elimination of glucose consumption. Once glucose consumption has been eliminated, then xylose consumption is readily eliminated by the *xylA* knockout, whereas arabinose consumption is readily eliminated by the *araA* knockout. The strains we have constructed which were anticipated to be prevented from glucose consumption were observed, however, to consume glucose slowly. An example of this is shown in Figure D.1.

In this experiment the *E. coli* strain KD915 (W *ptsG manZ glk crr*) was grown at 37°C with agitation of 250 rpm (19 mm pitch) in 500 mL shake flasks containing 100 mL basal medium with 7 g/L of xylose. When the OD of this culture reached approximately 3, the flask contents were diluted with fresh basal medium so that 100 mL having an effective OD of 1.5 was used to inoculate the bioreactor containing 0.9 L basal medium with both glucose and xylose present at 7 g/L. This batch experiment was carried out in a 2.5 L bioreactor (Bioflo 2000, New Brunswick Scientific Co., Edison, NJ) maintained at 37°C with air sparged at a flow rate of 1.0 L/min, an agitation of 500 rpm, and the pH controlled at 7.0 using 20% (w/v) NaOH.

Despite having four knockouts in key genes associated with glucose consumption, Figure D.1 shows that KD915 is able to consume glucose slowly. We furthermore

observed that the *crr* knockout does not make a significant difference in the consumption of glucose. That is, the strain without the *crr* knockout (KD777 = W *ptsG manZ glk*) had the same result. Fortunately, it appears that glucose consumption does not commence until *after* xylose is exhausted from the medium, although the results are not definitive. Experiments were also conducted with a wide range of glucose+other sugar mixtures, and the results were very similar for all but glucose-galactose mixtures (discussed under subtask earlier). In order to address the specific question of whether glucose is consumed by KD915 in the presence of xylose (for example), an additional set of experiments was conducted.

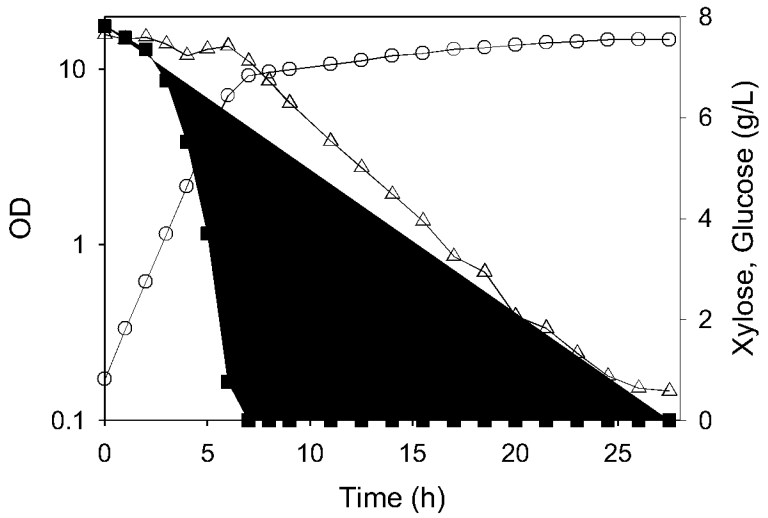

Figure D.1. Growth and substrate consumption of *E. coli* KD915 on a mixture of xylose and glucose. OD: ○; xylose: ■; glucose: △..

Steady-state cultures were carried out as chemostats in the same 2.5 L vessels used for batch cultures. After an initial batch phase, the medium was continuously supplied to achieve a dilution rate of 0.25 h^{-1}. The volume was maintained at 1.0 L, and steady-state was attained after 5 residence times (20 h). Although multiple experiments were completed, we highlight two different experiments using the mixture of xylose and glucose. In one case the system was carbon limited by having all other necessary nutrients like N and P in excess. Therefore, we would expect the xylose concentration to be zero while the glucose would be partly consumed (because its consumption is at a lower rate). In a second case the system was nitrogen limited. Therefore for this second case we would expect the xylose concentration *not* to be zero (because the cells exhausted nitrogen, and this carbon source is in excess). Because in the second case the cells would be in contact with xylose, we would be able to determine definitively whether glucose could be consumed in the presence of xylose.

For the carbon-limited case, the rate of xylose consumption was 3.80 mmol/gh while the rate of glucose consumption was 0.43 mmol/gh. For the nitrogen-limited case, the rate of xylose consumption was 4.94 mmol/gh, while glucose was not

consumed whatsoever. This very important result indicates that whatever mechanism is used by this strain for consuming glucose, is 'inhibited' by the presence of xylose. No such mechanism has ever been described in the literature previously. Furthermore, this result provides us with some guidance as to how we might operate the process of converting lignocellulosic hydrolysates into biochemical products. As long as xylose is present in the medium, the strain which is designed to consume only xylose will not consume glucose.

These same strains, unable to consume glucose, are able to consume arabinose selectively from a mixture of arabinose and glucose. For example, Figure D.2 show the growth of strain KD777 (W *ptsG manZ glk*) in an arabinose-glucose mixture using the same procedure described above. In this case, an additional does of arabinose was added 28 hours after inoculation, long after the initial arabinose had been consumed. At this later time, the cells rapidly consume the arabinose and briefly suspend their slow consumption of glucose.

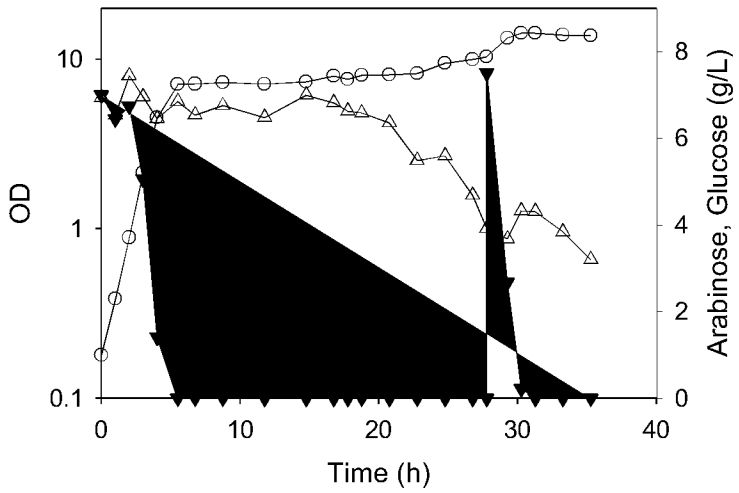

Figure D.2. Growth and substrate consumption of *E. coli* KD777 on a mixture of arabinose and glucose. OD: ○; arabinose: ▼; glucose: △.

We have recently constructed several strains that should be able to consume arabinose "exclusively" not only from a mixture of glucose and arabinose, but also from a mixture of glucose-xylose-arabinose. (Here "exclusively" is understood to mean that the strains will in fact consume glucose slowly after the arabinose is exhausted.) These are listed in Table D.1. We have not yet examined these strains in the three sugar mixture.

Another line of inquiry for this research has been to investigate further what is allowing glucose to be consumed slowly. With the goal of completely excluding glucose consumption, several other strains were constructed. These new strains had additional mutations in one of several other genes encoding other PTS proteins: *fruA* or *fruB* encoding proteins of the fructose-specific PTS, and the *bglF* gene involved in the PTS of β-glucosides. None of these individual knockouts had any effect on the slow glucose consumption observed in strains with *ptsG manZ glk* knockouts. Based

on discussions with other experts on glucose transport and phosphorylationg, we currently hypothesize that glucose can be transported by a wide variety of means, including a small amount of diffusion. However, in order to be metabolized, glucose must also be phosphorylated, and we currently hypothesize that glucose is being phosphorylated by galactokinase, encoded by the *galK* gene. β-D-Glucopyranose (a dominant form of glucose) and β-D-galactose differ only in the chirality of the C-4 hydroxyl, whereas the phosphorylation occurs at the C-6 hydroxyl, and therefore it seems possible that glucose is slowly phosphorylated by this enzyme. We are constructing the strain W *ptsG manZ glk galK* to test this hypothesis. It is interesting to recall that glucose consumption was not observed in W *ptsG manZ glk* in the presence of arabinose or xylose (or a few other sugars). If glucose is being phosphorylated by galactokinase, it is not clear why the presence of xylose, etc. would prevent this phosphorylation from occurring.

Table D.1. *E. coli* strains constructed which are curtailed in glucose and xylose consumption, and which therefore would be expected to consume predominantly arabinose in a three-sugar mixture of glucose-xylose-arabinose. Note that all strains listed consume glucose slowly under batch conditions.

ALS1060	MG1655 *ptsG manZ glk xylA*
ALS1122	MG1655 *ptsG manZ glk xylA crr*
ALS1370	C *ptsG glk manZ crr xylA*

Subtask D.2: Constructing a galactose-utilization *E. coli* strain.

In this case we consider the system of interest to be either the three-sugar mixture containing glucose-xylose-galactose or the four-sugar mixture glucose-xylose-galactose- arabinose. Ultimately, in this mixture four strains would be necessary, a strain consuming xylose exclusively, a second strain consuming arabinose exclusively, a third consuming glucose exclusively, and a fourth consuming galactose exclusively. As noted previously, elimination of xylose or arabinose utilization has been shown to be easy. So, the key aspect of this subtask is the elimination of glucose consumption in the presence of galactose.

For this study we again focused first on strains with *ptsG manZ glk* knockouts (KD777) or with *ptsG manZ glk crr* knockouts (KD915). In the presence of both galactose and glucose, these strains behave quite differently than we have observed in other sugar mixtures; an example result is shown in Figure D.3. Although galactose alone is metabolized readily and 'normally' by a strain with *ptsG manZ glk crr* knockouts, the consumption of galactose in the presence of glucose is slower. Moreover, in this case glucose is clearly metabolized at the same time as galactose rather than only after galactose has become exhausted. This observation was confirmed in *carbon-limited* chemostat experiments showing that galactose was consumed at 2.03 mmol/gh compared to glucose (in excess) at 1.56 mmol/gh. These results provide weight to the hypothesis that galactose and glucose are more

intimately related to each other than other sugars, and that specifically glucose is phosphorylated by galactokinase (as proposed in Subtask D.1).

This result also creates a question for the overall consortium approach of converting sugars found in lignocellulosic hydrolysate. It seems unlikely that a strain can be developed which metabolizes galactose exclusively from a mixture of sugars (specifically which contains glucose). Additional study is necessary to determine a process can be developed which will allow the strain which consumes glucose but not arabinose nor xylose to consume galactose effectively, or whether galactose will be inefficiently be converted only after glucose conversion is complete.

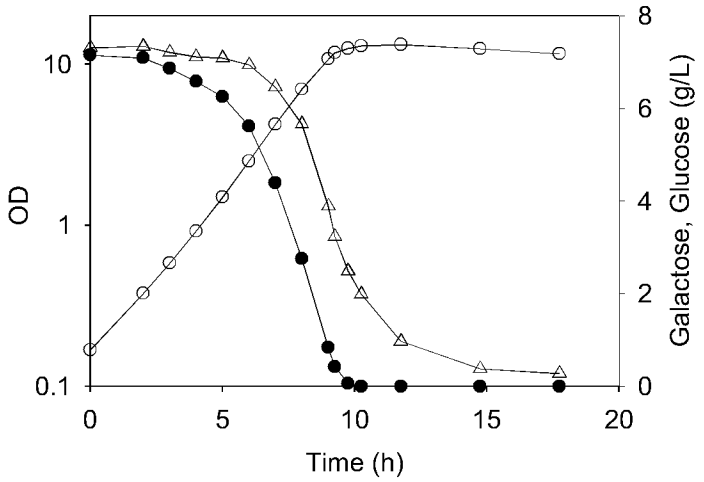

Figure D.3. Growth and substrate consumption of *E. coli* KD915 on a mixture of galactose and glucose. OD: ○; galactose: ●; glucose: △.

Conclusions (Task D)

- Elimination of glucose consumption has yet to be achieved. However, for the case of arabinose and xylose, glucose consumption can be prevented by maintaining either one of these other sugars in the medium.
- Strains have been developed which will consume only arabinose in a mixture of glucose-xylose-arabinose (with slow glucose metabolism after arabinose is exhausted).
- The consumption of galactose and glucose are intimately related, so that complete elimination of glucose consumption may be impossible without elimination of galactose consumption. It remains to be determined whether galactose and glucose can be simultaneously consumed by other strains (for example, which cannot metabolize xylose, etc.).

Task E – Production, characterization, modification and uses for pyrolysis char.

Subtask E.1: Characterization of pyrolysis-char
Subtask E.3: Agricultural applications of pyrolysis-char

Our overall plan was to evaluate agronomic properties of char from different feedstocks and processes. Carbonization produces char with unique properties. The particular features of pyrolysis-char such as recalcitrance, high carbon content and porosity, require specific analytical methods. We tested various properties and identified those chars most suitable for agricultural applications as biochar. The task started as E.1 further led into E.3 where actual applications were evaluated. The influence of pyrolysis char on nutrient retention, nutrient cycling, and nitrogen immobilization were assessed.

Methodology and results described and summarized below have independently been reported in the following peer-reviewed publications:

1. *Gaskin, J, K.C. Das, A. Tasistro, L. Sonon, K. Harris, and B. Hawkins. Characterization of biochar for agricultural use in the soils of the southeastern United States. In: Terra Preta Nova: A Tribute to Wim Sombroek. William Woods (Ed.), Springer Publishers.*

Char produced from the pyrolysis of biomass or biochar has potential as an agricultural amendment in low fertility soils. Much of the interest in its potential use as an agricultural amendment has been stimulated by research discussed in the above cited book and the previous volumes on the role of charcoal in Terra Preta soils. Results from studies conducted in South American and African tropics on acidic, highly-weathered Oxisols with low organic carbon, cation exchange capacity, and base saturation indicates that addition of charcoal has significantly influenced nutrient cycling, soil biology, and crop productivity.

The Southeastern United States is an important agricultural area. The state of Georgia alone has approximately 4.3 million hectares of corn (*Zea mays*), soybean (*Glycine max*), cotton (*Gossypium hirsutum*), and peanuts (*Arachis hypogaea*) in production and 9.6 million hectares of forestland largely in loblolly pine (*Pinus taeda*) production. The growing interest in biofuels is increasing demands on row crop production and may also increase demand on forestlands. The Ultisols of the Southeastern United States are similar to tropical Oxisols with low organic carbon contents of less than 1%, low cation exchange capacities of approximately 5 cmol kg^{-1}, and low base saturation of usually less than 30%. Biochar produced as a byproduct of energy production through pyrolysis may provide an opportunity to the productivity of Southeastern soils, similar to the way charcoal functions in Terra Preta.

Pyrolysis conditions and biochar characteristics

Charcoal or biochar corresponds to black carbons that result from the incomplete combustion of biomass. Black carbon consist of graphite-like planes (graphene layers), which show varying degrees of disorientation and the resulting spaces between these planes which constitute porosity. The capacity of biochar to remove impurities from solutions and gases has been known for many centuries. This is due

to the porous nature of the material and to the surface chemical properties including the type and number of functional groups.

Feedstocks and pyrolysis condition effects

Analyses of biochar from common feedstocks in the Southeastern US confirm the effect of feedstock and temperature on biochar composition. Total and Mehlich I extractable minerals were analyzed in biochars produced from peanut hull (PN), pine chip (PC), pine bark (PB), and hardwood (HW) feedstocks pyrolyzed at low temperatures (380, 400, and 420 °C) with steam in a small furnace, and poultry litter (PL) at 400 and 500 °C in a batch reactor in a steam flow environment (Table E.1). Feedstock had the largest affect on nutrient content when pyrolysis is conducted at low temperatures with biochar nutrient content mirroring that of the feedstock (Table E.1, Figure E.1).

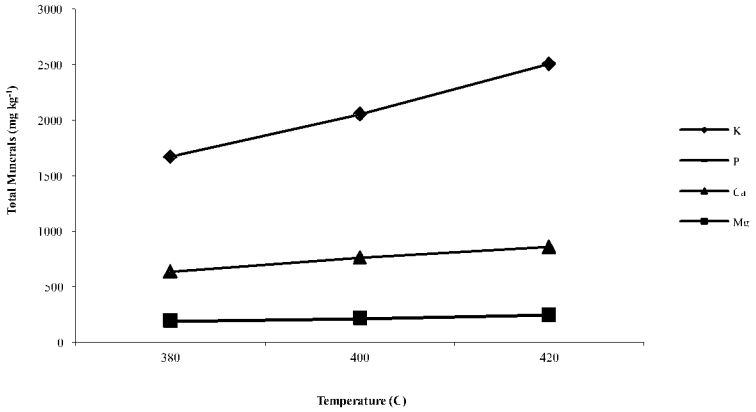

Figure E.1. Total mineral in biochar produced from pine chips pyrolized at three different temperatures.

Table E.1. Total carbon and nutrient concentrations for feedstocks and biochars produced from those feedstocks.

Constituent	Peanut hull Feedstock Biochar	Poultry Litter Feedstock Biochar	Pine chips Feedstock Biochar	Hardwood Feedstock Biochar
C (%)	65.5	41.7	67.0	70.3
N (%)	2.00	3.70	0.14	0.30
C:N	33	11	543	234
S (%)	0.13	1.18	0.02	0.02
P mg kg $^{-1}$	1,620		235	278
K mg kg $^{-1}$	15,372		1,973	2,409

Ca mg kg $^{-1}$	4,420	1,686	2,709

The total nitrogen concentrations of the PL and PN char was high at 4% and 2%, respectively. Although the nitrogen content of the PN biochar is potentially high enough to offer a substantial nitrogen input and the C:N ratio is relatively low (33), the nitrogen does not appear to be readily available. Nitrogen mineralization was very low in incubations of infertile, low C Tifton soils (fine-loamy, siliceous, thermic Plinthic Kandiudults) amended with PN and PC chars at 11 and 22 Mg ha^{-1} equivalent rate (Table E.2). Less than 2% of the total N was mineralized for both char types. There was no statistical difference in NH_4-N concentrations between the control and char amended soils (p=0.05). There was a trend for higher NO_3-N concentrations in the PN amended soils, but only the PN 11 Mg ha^{-1} rate was statistically different from the control.

Table E.2. Equivalent application rate, total initial nitrogen concentration, and ammonium- and nitrate-nitrogen concentrations mineralized from amendment of two Tifton soils with peanut hull (PN) and pine chip (PC) biochar at 11 and 22 Mg ha $^{-1}$. Letters within the same column indicate statistical difference at the p=0.05 level.

Feedstock	Equivalent Application Rate	Total Initial N	Mineralized NH_4-N	NO_3-N
	kg total N ha^{-1}	--%--	--------- mg kg $^{-1}$ -------	
PN 11	213	0.035	1.49 ∀ 0.24a	5.53 ∀ 0.65b
PN 22	436	0.044	0.94 ∀ 0.78a	5.08 ∀ 0.62a
PC 11	19	0.026	1.19 ∀ 0.36a	3.62 ∀ 0.51a
PC 22	28	0.027	1.44 ∀ 0.26a	4.41 ∀ 0.16a
Control	0	0.025	1.37∀ 0.38a	3.26 ∀ 1.66a

We saw similar indications that nitrogen in the high N biochar was not plant available in the first year of field trials on similar Tifton soils with corn (*Zea mays*). Peanut hull and PC char were incorporated to a depth of 15 cm in microplots (1.8 x 2.2 m) at rates of 11 and 22 Mg ha^{-1} in a factorial combination with two rates of nitrogen fertilizer (0 and 213 kg ha^{-1}) surface applied as ammonium nitrate. During the first growing season, corn growth and grain yield in the char-amended plots with no nitrogen fertilizer was significantly lower than in the char-amended plus nitrogen

fertilizer and nitrogen fertilizer/no char amendment check plots. The PN amended at 22 Mg ha-1 plots had significantly higher biomass, but not higher grain yields than the no nitrogen fertilizer/no char amendment control (Figure E.2). These preliminary data appear to indicate the N in the PN char is not readily available to microorganisms in the short–term (24-days) and is not highly plant available over a growing season (approximately 4 months).

a)

b)

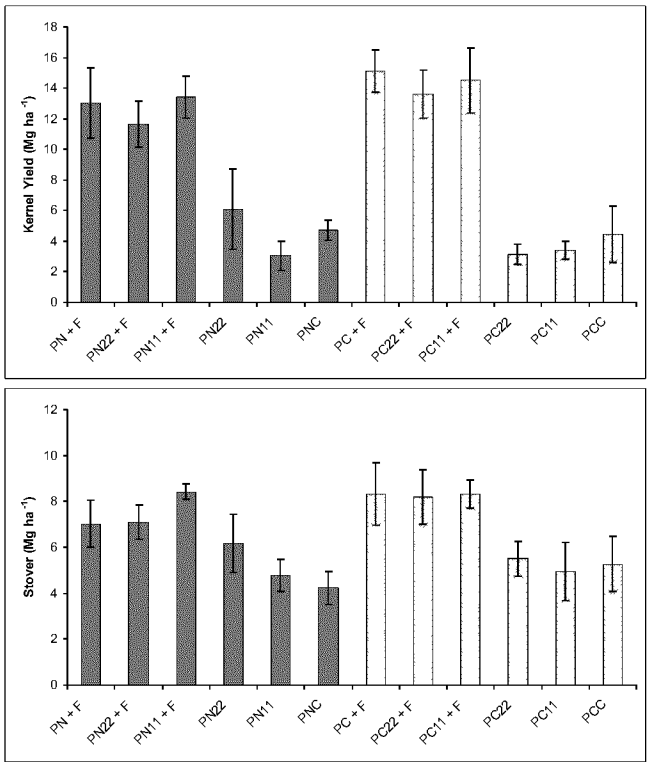

Figure E.2. Corn grain yield and stover (biomass) from Tifton soil plots amended with peanut hull (PN) and pine chip (PC) char. PNF – N fertilizer check, PN22+F- PN char at 22 Mg ha^{-1} +N fertilizer, PN11+F- PN char at 11 Mg ha^{-1} + N fertilizer, PN22- PN char at 22 Mg ha^{-1}, PN11 char at 11 Mg ha^{-1}, PNC- no amendment control, PCF – N fertilizer check, PC22+F- PC char at 22 Mg ha^{-1} +N fertilizer, PC11+F- PC char at 11 Mg ha^{-1} + N fertilizer, PC22- PN char at 22 Mg ha^{-1}, PC11 char at 11 Mg ha^{-1}, PCC- no amendment control.

Feedstock and Pyrolysis Condition Effects on Cation Exchange Capacity

The PN, PC, PB, SD, and HW biochars discussed above were analyzed for cation exchange capacity (CEC) using a modified Na-acetate /ethanol/NH_4-acetate compulsory replacement method with sodium analyzed by atomic absorption spectrophometry. Due to interference of the biochar ash, biochars were leached with deionized water before analysis to remove soluble salts. Cation exchange capacity of char ranged from 37.7 cmol kg^{-1} char for PN char produced at 380°C to 14.1 cmol kg^{-1} char for the PC pyrolyzed at 426 °C. Analysis of Tifton soils amended with PN and

PC biochar at 11 and 22 Mg ha^{-1} rates showed a 5 to 15 % increase in CEC versus the unamended control.

Feedstock and Pyrolysis Condition Effects on Sorption Properties

Biochars from PN, PC, HW, and PB pyrolyzed at 426°C were ground to <420 µm and washed with deionized water to remove soluble salts and air-dried. Biochars were then added to Tifton soils at the rate of 0.05 g char g^{-1} soil and phosphorus sorption isotherms were determined using batch techniques. Soil-biochar mixtures were equilibrated with five concentrations of P (0, 5, 20, 50, and 100 mg P L^{-1}) in 0.01M $CaCl_2$ matrix. The capacity and intensity of sorption by soil varied with the type of biochar added to soil. The amount of P sorbed was highest in soil amended with PN biochar, while the lowest P sorption occurred in unamended soil (data not shown). All systems showed a sharp increase in adsorption at low equilibrium P concentrations but sorption eventually reached a plateau, a characteristic of an L-*curve* isotherm. This is an indicative of a high relative affinity of the sorption surfaces for the adsorbate (P) at low surface coverage but sorption diminishes regardless of the amount of adsorbate as surface area decreases. Such a relationship suggests a strong interaction between the P and the exchange surfaces and that the overall sorption was dependent on the properties of both components.

Conclusion

Soils in the southeastern United States are typically low in C due to the hot and humid climate, and agricultural production practices such as mold-board plowing and harrowing. Our studies indicate biochar have the potential to improve productivity in southeastern soils. Biochar additions to a low soil C loamy sand can increase CEC (15% at 22 Mg ha^{-1} char addition) and there also is potential for some biochars to serve as a source for K and possibly Ca and other nutrients. Some biochars also have the potential to increase P sorption. It is unknown at this point if there would be subsequent desorption of P by biochar and what affect this may have on crops. In some areas of the southeast with high soil test P due to repeated applications of animal manures, increased P soprtion could be an environmental benefit.

Biochar does not appear to a good source for N even in higher N chars. Additions of biochar at 11 and 22 Mg ha^{-1} with recommended N fertilizer did not decrease corn yields or cause N immobilization during the first growing season (Gaskin et al. 2006). However, the C:N ratios of biochar from several feedstocks was high and could serve as a potential sink for available N. Our preliminary work indicates biochar addition may have potential agricultural benefits, but a better understanding of changes in soil process is needed.

Milestone 1: Successful and reliable quantification of plant available nutrients in char and determination of crop yield completed.

Subtask E.2: Modification of production techniques and assessment of postproduction treatments to increase surface charges to pyrolysis-char.

Charges found on pyrolysis-char are suspected to be responsible for the increased capacity of char amended soils to retain nutrients and provide other beneficial properties. Aging of char is one postproduction treatment that is of great interest. Recent research suggests that positive charges disappear and negative charges evolve by natural oxidation of char in the environment. Biochar is a black, amorphous carbon similar to charcoal with a polycyclic structure and varying degrees aromaticity and surface oxidation. Evidence from black-carbon rich terra preta soils in the tropics indicates black carbon resists mineralization while increasing soil fertility and productivity (Glaser et al., 2002; Lehmann et al., 2003).

Biochars characteristically vary depending on the feedstock selected and conditions. Feedstock affects nutrient concentration, cation exchange capacity (CEC), and soluble carbon. Our work has shown that pyrolyzed poultry litter contains the highest nutrients, and CEC and pine chip the lowest (data not shown). Also, the higher pyrolysis temperature in the study, 500 °C, compared to lower temperature, 400 °C, decrease the CEC and increase most macronutrient concentrations in the biochar. Production temperature and feedstock results in biochars with varying concentrations of ash, volatiles, and fixed carbon content. Temperature and oxidation during or after the pyrolysis process can increase the size and continuity of pores in biochars. Black carbon has long been understood to be the most stable form of carbon in soil (Glaser et al., 2002) because of its aromatic structure; however, a small fraction of biochar, especially if produced at lower temperatures, may be mineralizable. Climate and temperature appear to determine the stability of biochar in soils.

While biochar may be unavailable for microbial mineralization, its porous structure and adsorptive capacity may benefit microbial populations. The presence of biochar may stimulate the mineralization of native soil organic matter. Charcoal may provide habitat and act as an absorbent for substrates, including phenolic compounds, promoting certain populations. Charcoal may also boost nitrification in forest ecosystems and reduce denitrification.

Research results

Our objective was to characterize two biochars, peanut hull (PH) and pine chip (PC), and correlate the results with C and N mineralization rates of a 136-day study. The methods to characterize the biochars were elemental, thermogravemetric, and proximate analysis, and Fourier transform infrared spectroscopy (FTIR). Peanut hull biochar contains significantly more moisture, three times more ash, and approximately 12 g kg^{-1} more estimated aliphatic compounds than PC biochar. However, PC contains more volatiles and fixed C.

The broad peaks from 3000 to 2800 and 900 to 700 cm^{-1} suggests an alkyl-aromatic structure (Figure E.3). Several O containing functional groups were detected in low concentrations in both fresh chars: OH (3700 – 2000 cm^{-1}), C=O (1700 cm^{-1}), and C-O-(C) (1275 cm^{-1}). Fresh PH had a slight response at 1050 cm^{-1} indicating C-O-(H) bonding. Both fresh PH and PC biochar contained C-H bonds (3000-2800 cm^{-1}) associated with aliphatic compounds.

Aged PH and PC biochars had a reduced peak intensity between 3000 and 2800 cm^{-1} compared to their respective fresh biochars indicating a reduction in aliphatic C-H bonds but more apparent between fresh and aged PH biochar. Aging also increased the concentration of oxygen containing groups. Carbonyl (1700 cm^{-1}) and C-O-(H) (1050 cm^{-1}) increased in PH and PC and C-0-(C) (1275 cm^{-1}) in PH. A slight shoulder around 2600 cm^{-1} in the aged biochar spectra may indicate the formation of some carboxylic acid functional groups. The aging process did not affect the concentration of aromatic bonds (1600 cm^{-1}) and associated aromatic C-H groups (900-700 cm^{-1}).

The reduction in aliphatic C-H bonds indicated by FTIR suggests that this fraction might have been the constituent of biochar degraded by microorganisms in soil. The aliphatic content of biochar may be a good indicator of potentially mineralizable C in biochar.

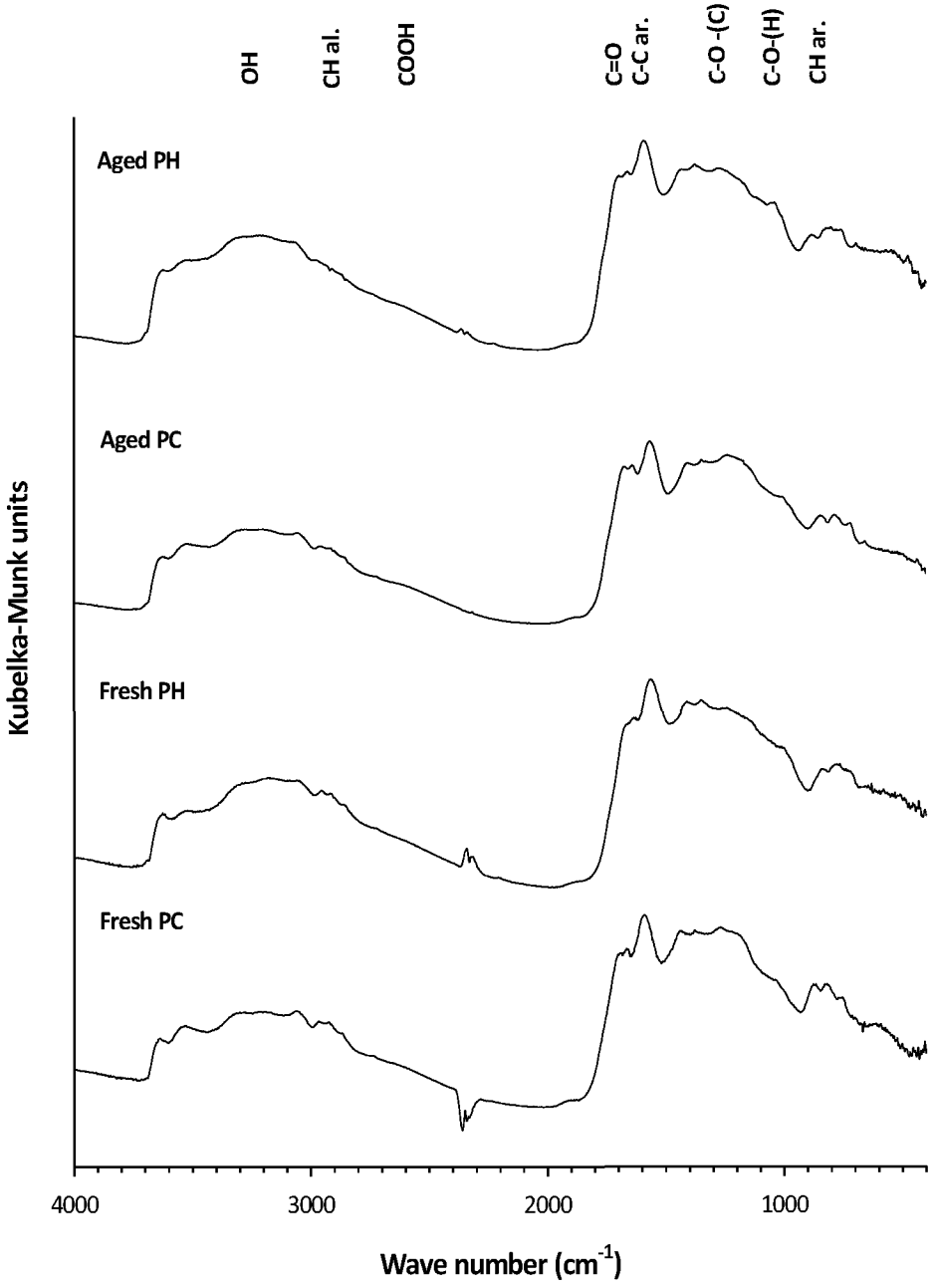

Figure E.3. FTIR spectra of fresh and aged PH and PC biochars.

Subtask E.4: The use of biochar in enhancing and odor reducing in composting.

Bulking agents are used in manure composting to provide optimal bulk density and aeration of the composting mix. Bulking agents also have an impact on the quality of the final product both in retaining nitrogen and improving degradability. Biochar (carbonized organic materials) seems to have ideal properties for use as bulking agent. We hypothesize that the use biochar as bulking agent for manure composing will improve aerobic biological activity and hence the speed of composting.

Methodology and results described and summarized below have independently been reported in the following peer-reviewed publications:

1. *Steiner, C., N.D. Melear, K. Harris, and K.C. Das. 2011. Biochar as bulking agent for poultry litter composting. Carbon Management, 2(3):227-230.*
2. *Steiner, C., K.C. Das, N.D. Melear, and D. Lakly. 2010. Reducing nitrogen losses during poultry litter composting using biochar. Journal of Environmental Quality, 39(4):1236-42.*

Methodology

Poultry litter (PL) is a mixture of accumulating manure and wood shavings used as bedding. The litter was obtained from a broiler house in North Georgia. Biochar was produced by pyrolysis of pine chips in a large batch reactor at 400°C. Pine chip biochar was used as obtained without further modification or particle size separation. Particle size fractionation showed that 82% of the biochar was present in a particle size between 1.2 and 16 mm. The majority (54%) was found between 4mm and 9.5 mm.

Three compost mixtures were prepared with poultry litter and biochar in different mix ratios on a dry weight basis. Treatments included:: I) 100% poultry litter (PL), II) 95% PL + 5% biochar and III) 80% PL + 20% biochar. Each treatment was replicated three times and individual experimental bioreactors had approximately the same weight of compostable material. Water was added to achieve a moisture content of 60% and the materials were mixed using a rototiller prior to placement in the bioreactors. The whole composting experiment of 9 bioreactors was repeated 3 times.

Three replicates of each treatment were placed in nine bioreactors to undergo composting for 42 days. The bioreactors are insulated stainless steel vessels with a diameter of 38 cm, a depth of 39.5 cm, and a volume of 0.057 m^3. Air was introduced every 20 minutes for 30 seconds, providing an effective aeration of 0.0425 $m^3 h^{-1}$. The compost was homogenized once a week by removing the contents of the bioreactor into a clean wheel barrow and thoroughly mixing with a shovel. At this time samples were taken for respiration measurements.

Respiration Measurements

The headspace gas in a bottle where the compost sample was placed was analyzed for CO_2 concentration at 2 hours intervals for a period of 72 hours using a computer controlled respirometer (Micro-Oxymas, Columbus Instruments Inc.). A sample of 10 to 15 g (DW) was placed in a sample bottle and then located into a water bath heated

to 37°C. The sample bottle and the gas analyzers are in a closed-circuit loop and headspace volumes and initial gas concentrations are measured automatically. The bottle was aerated with ambient air at a flow rate of 4 L m^{-3} each time the oxygen concentration changed by 5% within a sample interval. The air exiting the chamber was dehydrated by a condenser and condensed water returned to the samples. The procedure ensured a constant moisture content and temperature.

Under the assumption that biochar does not undergo significant decomposition we calculated respiration rate in mg-CO_2/g-PL/hr based on PL (volatile solids, VS). The changing ratio of biochar to poultry litter resulting from decompositon was calculated from the measured mass loss and the ratio was corrected every week.

Statistical Analysis

Treatment effects were analyzed by univariate general linear model (GLM) in a randomized complete block design. Significant differences between the treatments were marked by the LSD value ($p < 0.05$). Statistical analyses and plots were performed using SPSS Statistics 17.0 and SigmaPlot (SPSS Inc.).

Results and Discussion

Respiration rates were higher in the treatments with 20% biochar additions (Figure E.5). There is a direct relationship between VS and CO_2 respiration as noted in the literature. Literature suggests that carbonized ryegrass decomposed at a rate of 0.5% per year under optimal conditions therefore we assumed that biochar did not undergo significant decomposition but to which extent biochar does mineralize in such an environment would need further investigation. However, the first respiration peak was significantly ($p < 0.05$) higher in the treatment with 20% biochar addition in comparison to 5% and treatments without biochar (5.06, 4.32 and 4.38 CO_2 mg g^{-1} h^{-1}, respectively) even when the biochar mass was considered as VS and not deducted from the poultry litter mass. Availability of oxygen during the process is of primary importance and the presence of biochar particles in the mix might decrease bulk density and increase aeration.

The exponential increase in respiration also significantly increased with 20% biochar additions (Figure E.5a). This indicates a better substrate availability and thus faster microbial population growth.

Continued work in larger scale composting

Further work in evaluating the effects of biochar addition on the ammonia conserved during the composting was conducted. Detailed procedures are described in the reference cited above (Steiner et al., 2010). That study showed that pH, MC, and higher temperatures with greater degradation was seen when poultry litter was amended with biochar. The conservation of nitrogen, a key benefit to the quality of the compost, was highest in the higher biochar dosage treatments (Figure E.6 – mean value). The Run 3 showed lower differences because of the winter conditions.

Conclusion

Bulking agents are essential for enhancing aerobic conditions in manure composting. The recalcitrance against decomposition and ability to absorb moisture

makes biochar an exceptional bulking agent. Although the carbon seems to be unavailable for the microbial population, biochar amendments do increase respiration rates due to a better aeration of the compost mix. Nitrogen conservation occurred when biochar was added to the composting mixes.

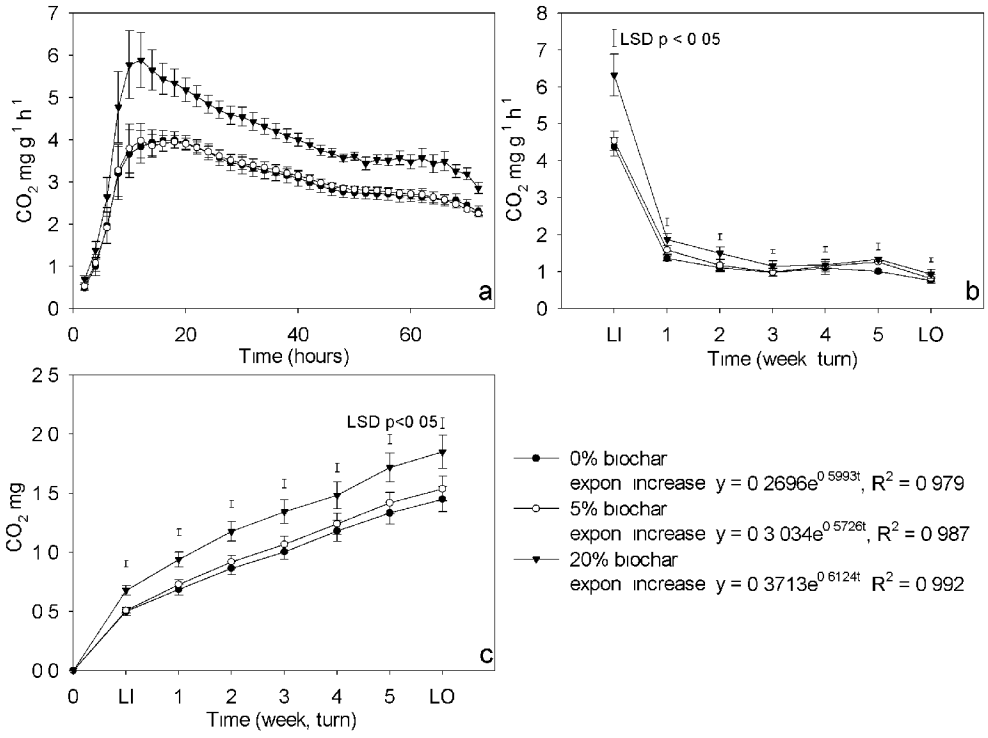

Figure E.5. Respiration of poultry litter during composting with biochar as bulking agent. The respiration refers to poultry litter mass only (CO_2 per g poultry litter per hour, n=9, LSD $p<0.05$). a) Respiration curve over the first 72 hours. The equation for the exponential increase is provided in the figure legend. B) Temperature maxima after weekly sampling from the compost pile and CO_2 measurements. c) Cumulative respiration calculated from the means in every week.

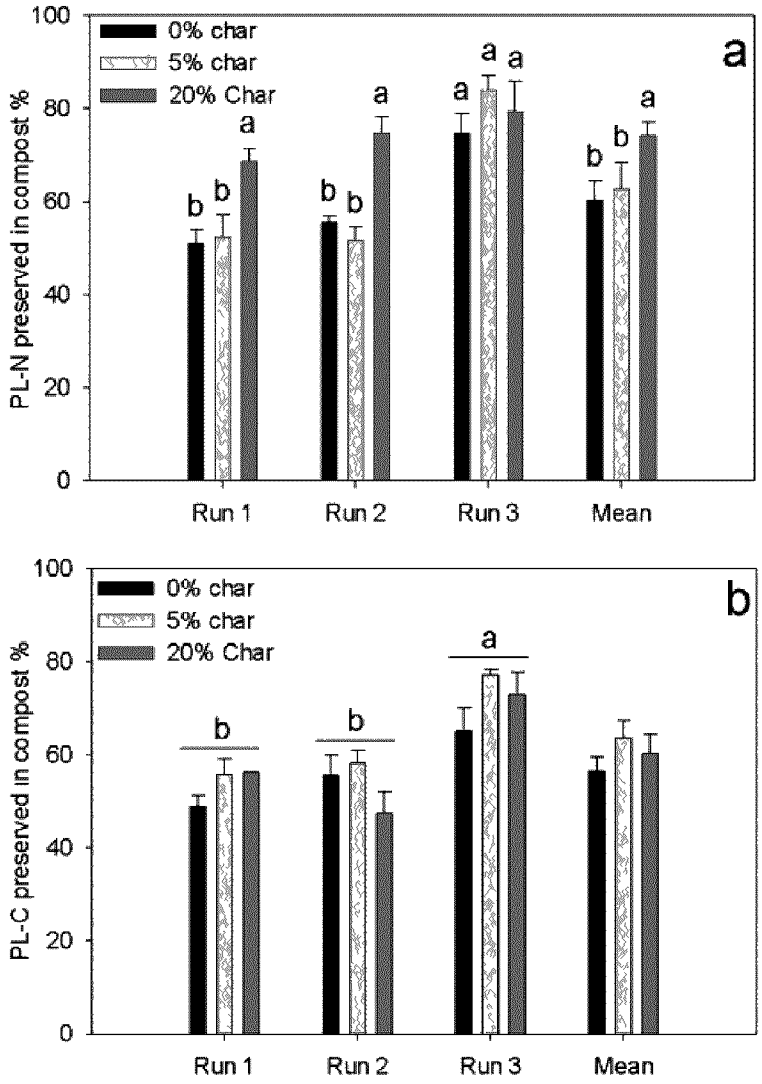

Figure E.6. Losses in (a) poultry litter nitrogen and (b) poultry litter carbon during composting. Char addition to the mix ranged from 0% (control) to 20% (high rate). Run 2 is higher due to lower decomposition rates in winter (ANOVA and Sudent-Newman-Keuls comparision – letters indicate significant difference at $p<0.05$)

Task F – Development of biomass feedstock resources

Subtask F.1: Selection of robust organisms and development of low cost, effective systems

This task is a continuation of work begun in a pervious project GO 85012 where municipal wastewater with a significant component of industrial wastewater was used

as growth media for algal cultivation. Several organisms were identified and selected from natural environments from the wastewater and local land application site, and cultured and characterized. Additional procedural details and results are given in the following two citations:

1. *Chinnasamy, S., A. Bhatnagar, R.W. Hunt, and K.C. Das. 2010. Microalgae cultivation in wastewater dominated by carpet mill effluents for biofuel applications. Bioresource Technology 101(9):3097-3105.*
2. *Chinnasamy, S., A. Bhatnagar, R. Claxton and K.C. Das. 2010. Biomass and bioenergy production potential of microalgae consortium in open and closed bioreactors using untreated carpet industry effluent as growth medium. Bioresource Technology, 101(17):6751-*60.

Our purpose in the present task was to further characterize the preferred consortium among those evaluated earlier and document their performance. Specifically we evaluated [1] the feasibility of growing consortium of native algal strains in industrial/municipal wastewater (CI) and [2] assess its biomass productivity in three reactor configuration, namely, raceways, vertical tank reactors (VTRs) and polybags.

Methodology and results described and summarized below have independently been reported in the following peer-reviewed publications:

1. *Chinnasamy, S., A. Bhatnagar, R. Claxton and K.C. Das. 2010. Biomass and bioenergy production potential of microalgae consortium in open and closed bioreactors using untreated carpet industry effluent as growth medium. Bioresource Technology, 101(17):6751-*60.

Methodology

Three algal strains, namely, *Chlamydomonas globosa, Chlorella minutissima* and *Scenedesmus bijuga* - isolates of industrial wastewater, were maintained in BG11 medium by frequent subculturing in a growth room at 25±2°C under ~80 µmol of photons m^{-2} s^{-1} light intensity with 12:12 h L/D cycle.

Raceways used in this study were made of opaque plastic and were 1.52 m wide, 2.44 m long and 0.61 m deep with a capacity of ~2000 L (Figure F.1). The working volume maintained in the raceway ponds was 950, 550 and 500 L in runs 1 & 2, 3 and 4, respectively. All the raceway ponds were powered by a paddle wheel and operated at 20-30 cm depth. The paddle wheel rotation was adjusted to generate a flow rate of ~21±3 cm s^{-1}. The vertical tank reactors (VTRs) were of 0.45 m diameter and 1.52 m height with 100 L working volume and made of transparent acrylic sheets (Figure F.1). A roll of low density polyethylene (LDPE - Uline-6-Mil heavy duty polytubing with 50.8 cm circumference) material was used to fabricate hanging polybags (95 cm deep, 15 cm diameter, 20 L working volume) (Figure F.1). All the reactors were attached with delivery tubings and air stones for bubbling 5-6% CO_2 and air mixture.

Upon receipt of the wastewater, approximately 175 mL of bleach containing 6.15% sodium hypochlorite was added to 1000 L of municipal/industrial (CI) untreated wastewater for sterilization. The wastewater totes were kept under tarps and

out of direct sunlight. For each round of the study the wastewater was filtered twice, first through a bag filter and then a diatomaceous earth filter. Wastewater was pumped from the storage tote through the diatomaceous earth filter into the raceways and VTRs. Algal inoculum was maintained in VTRs in BG11 medium for the purpose of inoculation. Biomass was harvested with a Lavin process centrifuge (model: 12-413V), operated at 2250x g, manually removed from the interior drum with a spoon and dried at 40 °C in a hot air oven for 72 h. It was stored at 4-5 °C subsequently. Detailed analytical procedures are described in the citation provided above. All methods were obtained from standard published methods in the literature.

Evaluation of biomass production potential of wastewater in raceways

In the first two runs of 10 and 12 d duration, raceway tubs were filled with 800 L of CI untreated wastewater. These were inoculated with 50 L each of exponentially growing cultures of *C. globosa, C.minutissima* and *S. bijuga* to assess the biomass productivity of the wastewater. After inoculation, the raceways were operated at 30 cm depth.

Comparison of vertical tube reactors with raceways

In the third run (11 days), CI untreated wastewater was used to compare the biomass productivity in raceways with VTRs. Raceways with 496 L wastewater were inoculated with 18 L of each of the three algal cultures mentioned above and operated at 20 cm depth with a total volume of 550 L. VTRs had 88 L wastewater and 4 L of each algal culture was added as inoculum. VTRs were operated with 100 L working volume and the depth of water column was maintained at 61 cm.

Comparison of raceways, VTRs and polybags

In the final run, CI untreated wastewater was used to compare biomass productivity in raceways (Working volume -500 L; Depth - 18 cm), vertical tank reactors (Working volume – 100 L; Diameter – 45 cm; Depth - 61 cm) and polybags (Working volume – 20 L; Diameter – 16 cm; Depth - 95 cm). Inoculum included equal volumes of *C. minutissima* and *S. bijuga* (Table 1). To each of the raceways, VTRs and polybags, 450, 90 and 18 L of CI untreated wastewater was filled and 25, 5 and 1 L of the consortium was added, respectively. Final volumes were: 500 L (18 cm deep) in raceways, 100 L (61 cm deep) in VTRs and 20 L (95 cm deep) in polybags.

Results and Discussion

The combined CI untreated wastewater was found to contain significant quantities of total nitrogen (~33 to 46 mg L^{-1}) and phosphorus (5 to 14 mg L^{-1}) to support algal growth. In the first run, algae grown in CI wastewater recorded a volumetric biomass productivity of 0.015 g L^{-1} d^{-1} in raceway ponds where the depth was maintained at 30 cm (Table F.1). However, the second run recorded a productivity of 0.021 g L^{-1} d^{-1} which was 40% higher than the first run. Average biomass productivity of the two raceways in the third run with 20 cm depth showed 153 and 81% increase when compared to the first and second runs, respectively. The raceways maintained with 18 cm depth recorded a maximum average productivity of 0.051 g L^{-1} d^{-1} which was 3.4, 2.4 and 1.3 times higher than the first, second and third runs, respectively (Table F.1).

Volumetric productivity of raceways was ~19 and 16% more than the productivity obtained in the VTRs in run 3 and 4, respectively. However, volumetric productivity obtained in the polybags was 0.07 g L^{-1} d^{-1}, which was significantly higher than the other two reactor systems (Table F.1). Decrease in the depth of water from 30 cm in the second run to 20 cm in raceways enhanced volumetric productivity by 81% whereas the areal productivity showed only 16% increase. Further decrease in depth from 20 cm to 18 cm showed 34 and 23% increase in volumetric and areal productivities, respectively. In the 4th run which made the direct comparison of all reactors, polybag reactors recorded ~37 and 59% increase in volumetric productivity and ~621 and 142% increase in areal productivity over raceways and VTRs, respectively (Table F.1).

Changes in the temperature impacted biomass productivity. Green house temperature from 12 to 4 PM was 6 ^{o}C higher than ambient. Polybags recorded highest temperatures up to 43^{o}C. They also showed broadest range of variation in diurnal temperature. From 10 AM to 4.45 PM, for a 5^{o}C increase in atmospheric temperature, green house recorded 9.7 ^{o}C increase while polybags showed 17.5^{o}C increase (Data not shown). Temperature however, varied with the type of reactors also. As expected, a rise in temperature from 16 to 24^{o}C led to increase in productivity of the raceways (Figure F.2). In the fourth run where the direct comparison was made between all 3 reactors, the average temperature was 24, 27.5 and 32.1^{o}C for the raceways, VTRs and polybags, respectively. Compared to raceways, polybags recorded 8.1^{o}C and VTRs recorded 3.5^{o}C increase in the culture temperature. It was interesting to note that the average culture temperature of polybags was 4.6^{o}C higher than VTRs. It was evident from the results that the polybags maintained higher temperature that favored higher biomass productivity (Figure F.2). However, in contrast to the polybags, the average volumetric productivity obtained in the VTRs was less than that of raceways. Growth was also directly proportional to increase in pH from 7.0 - 7.9 (Figure F.2). However, this could be a consequence of higher growth of algae.

Apart from temperature and solar irradiation, the variation in the nutrient quality of the wastewater used in all the runs for raceways and VTRs might also have varied the productivity that is evident from Table F.1. In general, productivity of an algae cultivation system can be evaluated through four parameters viz. volumetric productivity (VP), i.e. productivity per unit reactor volume (g L^{-1} d^{-1}); illuminated surface productivity (ISP) , i.e. productivity per unit of illuminated surface area of the reactor (g m^{-2} d^{-1}); areal productivity (AP), i.e. productivity per unit of ground area occupied by the reactor (g m^{-2} d^{-1}); and overall areal productivity (OAP) expressed as g m^{-2} d^{-1} , i.e. the productivity obtained from the overall ground area including empty spaces required for equipment access and space between reactors in a mass cultivation system (Tredici, 2004). OAP has greater meaning and a useful method to evaluate productivity between different kinds of cultivation systems and reactors for scale-up operations.

Superior performance of the closed systems was essentially due to: (1) Better temperature profile: i.e. the culture in the polybags and VTRs reached the optimal temperature for growth earlier in the morning when compared to the raceway ponds.

Moheimani and Borowitzka (2006) opined that the productivity of *Pleurochrysis carterae* can be improved by heating the ponds in the morning, presumably because this allows the algae to photosynthesize faster in the low [O_2] conditions which occur in the early morning.

Contrary to our expectation, the volumetric productivities of VTRs were lower than raceways. Though the light-receiving surface to volume ratio of VTRs was more than the raceway, the walls of the tubes caused a 30% decrease of sunlight penetration from the outer to the inner face of the walls. Significantly larger light penetration depth (~2.5 times as deep for the tubes compared to the raceways) and the light attenuation of the vertical tank walls could have resulted in the poor volumetric productivity despite large surface to volume ratio, less variation in temperature and efficient CO_2 mass transfer conditions.

Biomass analysis of algal consortium

The mean carbon content of all harvested biomass was 49.8 % whereas the mean nitrogen content was 9.6 % (Figure F.3). This narrow C/N ratio of 5.2 suggested that a large percentage of the biomass was protein (~53.8%). The hexane extracted neutral lipids were only 5.3% and the total carbohydrate was ~15.7%. However, the harvested biomass does possess a significant amount of energy per unit mass. The observed calorific value of 23.6 KJ g^{-1} for the mixed algal biomass was within the values cited in other literature which range from 20 to 25 kJ g^{-1} (Huntley and Redalje, 2006; Sheehan et al., 1998).

Conclusions

Out of three reactor configurations tested for overall areal and volumetric biomass productivity, polybag reactors appear to be the best followed by VTRs and raceways.

References cited in this section:

Huntley, M., Redalje, D., 2006. CO_2 mitigation and renewable oil from photosynthetic microbes: a new appraisal. Mitig. Adapt. Strategies Glob. Chang. 12, 573-608

Moheimani, N.R., Borowitzka, M.A., 2006. The long-term culture of the coccolithophore *Pleurochrysis carterae* (Haptophyta) in outdoor raceway ponds. J Appl Phycol. 18, 703-712.

Sheehan, J., Dunahay, T., Benemann, J., Roessler, P., 1998. Look back at the U.S. Department of Energy's Aquatic Species Program: biodiesel from algae; Close-Out Report. NREL Report No. TP-580-24190.

Tredici, M.R., 2004. Mass production of microalgae: photobioreactors. In: Richmond A, editor. Handbook of microalgae culture: biotechnology and applied phycology. Oxford, Blackwell Publishing, pp 178-214.

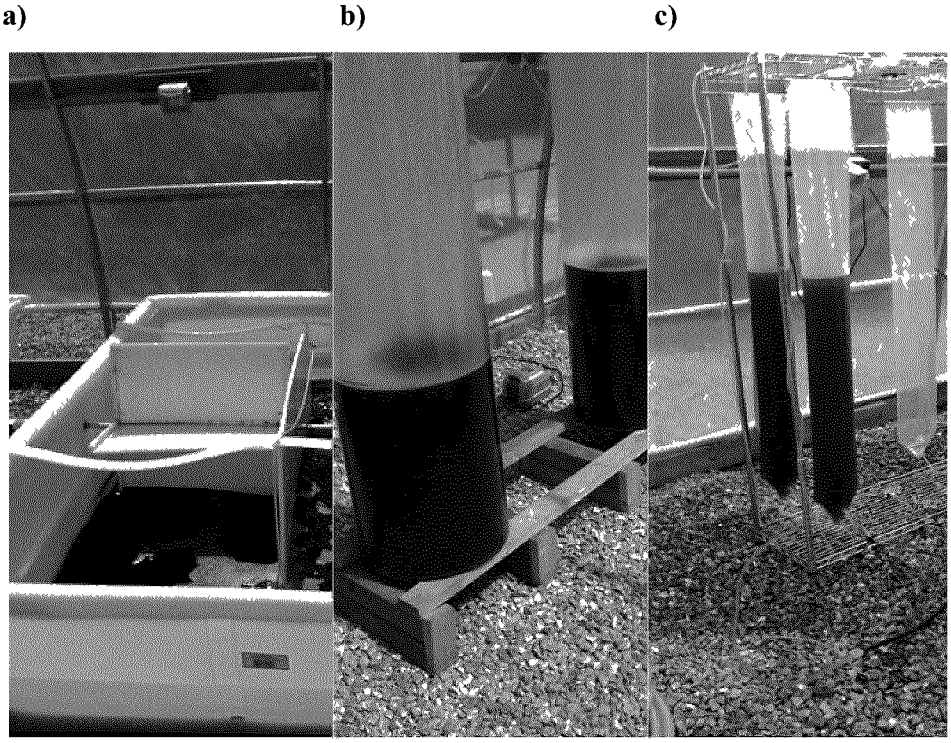

Figure F.1. Algae cultivation systems viz. a) raceways, b) vertical tank reactors (VTRs) and c) polybags used for evaluating biomass productivity in carpet industry untreated wastewater.

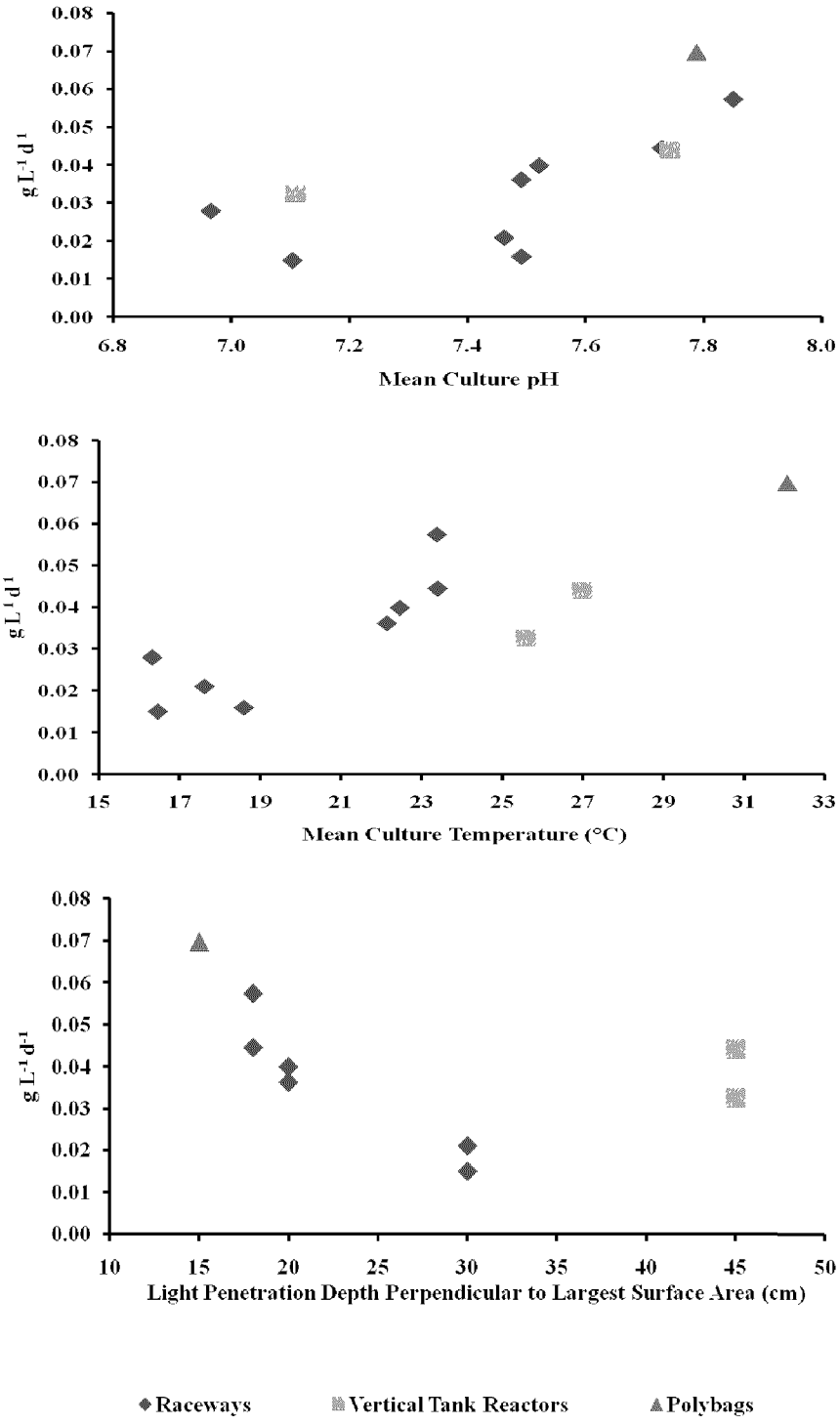

Figure F.2. Productivity of algae consortium with respect to changes in pH, temperature and light penetration in raceways, vertical tube reactors and polybags

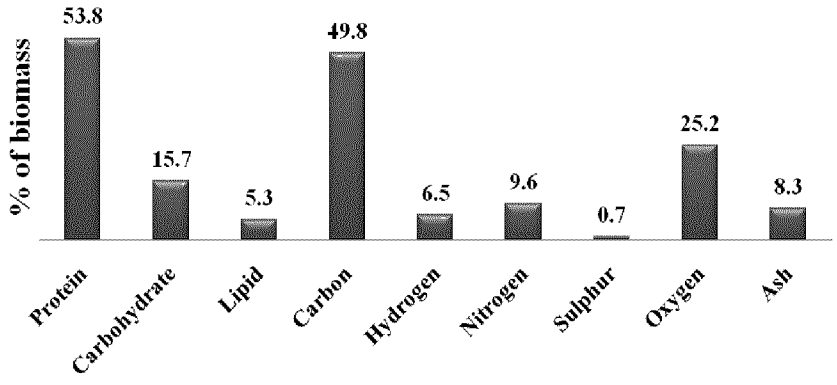

Figure F.3. Composition of algal biomass grown in wastewater. Results indicate that the microalgae consortium was rich in proteins and low in carbohydrates and lipids.

Table F.1. Volumetric and areal biomass productivity of algal consortium in carpet industry untreated wastewater

Run	Type	Depth[a]	Vol	Reactor surface area			Biomass productivity		Run time
				Floor Area	Lighted Area	Surface to volume ratio	Volumetric	Areal	
		(cm)	(m^3)	(m^2)	(m^2)	(m^{-1})	g L^{-1} d^{-1} Mean	g m^{-2} d^{-1} Mean	days
1	RW	30	0.95	3.1	3.1	3.3	0.015	4.42	10
2	RW	30	0.95	3.1	3.1	3.3	0.021	6.43	12
3	RW	20	0.55	2.8	2.8	5.1	0.04	7.79	11
	RW	20	0.55	2.8	2.8	5.1	0.036	7.13	11
	VTR	45	0.1	0.16	1	10	0.032	20.3	11
4	RW	18	0.5	2.8	2.8	5.6	0.057	10.36	8
	RW	18	0.5	2.8	2.8	5.6	0.045	8.04	8
	VTR	45	0.1	0.16	1	10	0.044	27.4	8
	PB	15	0.02	0.021	0.5	25	0.07	66.4	8

RW- Raceways; VTR- Vertical tank reactors; PB- Polybags.

[a] *Light penetration depth perpendicular to largest surface area*

Subtask F.2: Evaluating processing and conversion characteristics of algae biomass

In algal processing there are steps including harvesting, drying, extraction, and conversion. In this task we focused on the drying process. Drying is a critical step in algal biomass production as it improves shelf life, facilitates easier transport and enhances extraction efficiency of lipids and other value added compounds. Understanding the compositional changes and drying behavior of microalgae are essential in developing economical microalgae based biorefinery. We investigated production rate, chemical compositions and drying characteristics of microalgae consortium (*scenedesmus, chlamydomonas* and *chlorella)* grown in a raceway pond in the southern US climate. Page model predicted experimental moisture loss data well and satisfactorily described the drying process based the statistical evaluation of three mathematical drying kinetics models.

Methodology and results described and summarized below have independently been reported in the following peer-reviewed publications:

2. *Vishwanathan, T., S. Mani, K.C. Das, S. Chinnasamy, and A. Bhatnagar. 2011. Thin layer drying kinetics and chemical composition of microalgae consortium. Transactions of the ASABE, 54(6):2245-2252*

Methodology

Biomass Production

Isolates of green algal species *Chlorella globosa*, *Chlamydomonas minutissima*, *Scenedesmus bijuga* was inoculated in simulated raceway ponds of 1.52 meters wide, 2.44 m long, and 0.61 m deep mixed by a paddle wheel. The working volume was 550 L. The individual cultures of these three species were scaled up from 4 L flasks to the 150 L vertical tubes prior to cultivation in the raceway ponds. The culture was supplemented with BG11 medium and 5-6% CO2 - air mixture bubbled through two air stones at a rate of 10 L min^{-1}. After 10 days of growth, the biomass was harvested using a centrifuge (AML Industries Inc. Model 12-413V) with an inlet flow rate of 230 L h^{-1}. All centrifugation was performed at the 2250 x g. The centrifuged slurry is subjected to thin layer drying as shown in Figure F.4.

Drying Experiments

Initial moisture content was determined gravimetrically by drying a known weight of microalgal slurry at 103° C for 24 hr in a convective hot air oven. The thin layer drying kinetics study was carried according to the ASABE standards (ANSI/ASAE S448.1 JUL2001). 10 g of algal slurry was spread in to a 2.85 mm thin-layer on a circular aluminum tray with uniform edges and subjected to drying in a convective oven with a constant parallel air flow velocity of 0.3 m/s at different ambient air temperatures 30°, 50°, 70° and 90° C. The weight loss was measured manually for every one minute initially for the first 30 minutes and the time interval between weight measurements are gradually relaxed to 3, 5, 10 and 30 minutes till the equilibrium moisture content was reached. Each drying experiment was carried out in triplicates.

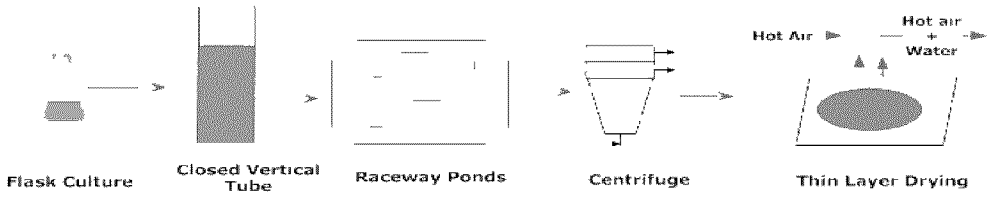

Figure F.4. Biomass production and Drying.

Biomass Compositional analysis

The microalgal diversity in the biomass produced was determined using light microscopy. Biomass density, lipid content, and all other analytical testing was done using standard methods reported in the literature. Detailed procedures are listed in the reference cited above

Modeling the Drying kinetics

The kinetics of dehydration was modeled using three semi-theoretical and empirical models commonly applied for biological materials; Henderson-Pabis model (equation 1) (Henderson and Pabis, 1961), Newton's model (equation 2) (Lewis, 1921)and Page model (equation 3).

$$MR = \frac{M(t) - M_{eq}}{M_o - M_{eq}} = A\exp(-kt) \quad (1)$$

$$MR = \frac{M(t) - M_{eq}}{M_o - M_{eq}} = \exp(-kt) \quad (2)$$

$$MR = \frac{M(t) - M_{eq}}{M_o - M_{eq}} = \exp(-kt^n) \quad (3)$$

Where MR, the dimensionless moisture ratio, is the unaccomplished moisture change defined as the ratio of free water still to be removed at any time t to the total free water initially available, Mt is the instantaneous moisture content, Mo is the initial moisture content and Me is the equilibrium moisture content, k is the drying constant, A is related to the effective diffusivity of water from the sample and n is the product constant. K varies with drying air temperature where n varies with the nature of the product. All these drying models represent the transport properties like moisture diffusivity, thermal conductivity, density, specific heat and interphase mass transfer coefficients (Doymaz and Pala, 2002; Karathanos and Belessiotis, 1999; Panchariya et al., 2002; Sokhansanj, 1984) by a single drying constant K. As the exact drying process is a complex problem that involves simultaneous mass and energy transfer in a hygroscopic shrinking system (Ratti, 2001), a complete description of the actual mechanisms involved is usually not obtainable or extremely complex (Carbonell et al., 1986; Hawlader et al., 1991; Mazza and LeMaguer, 2007) and hence these thin

layer drying kinetics models are used to approximately estimate the drying parameters.

The experimental drying data were fitted to the models and the statistical parameters are estimated using the non linear regression analysis. Best model was selected based on R^2, Chi-square, SSE and RMSE values.

Determination of effective diffusivity

Ficks second law of non uniform diffusion can be applied to explain the dehydration behavior and effective diffusivity of biological materials that normally follows a falling-rate drying period where the moisture migration is defined by diffusion (Babalis and Belessiotis, 2004; Doymaz and Pala, 2002).

$$\frac{\partial Ml}{\partial t} = \nabla(D_{ef} \nabla Ml) \qquad (4)$$

where Ml is the local moisture content, t is the drying time and D_{ef} is the effective diffusivity. The theoretical solution series to equation (1) for infinite slab geometry is given as (Crank 1975)

$$MR = \frac{M(t) - M_{eq}}{M_o - M_{eq}} = \frac{8}{\pi^2} \sum_{n=1}^{\alpha} \frac{1}{(2n+1)^2} \exp(-(2n+1)^2 \pi^2 \frac{Dt}{4L^2}) \qquad (5)$$

Where MR is the moisture ratio, D is the effective moisture diffusivity, L is the thickness of the thin slab and n is the number of terms in the expansion series. For long dehydration periods, only the first term (n=1) in the series expansion as given in (3) is sufficient to explain the drying mechanism (Riva and Peri, 1985).

$$MR = \frac{M(t) - M_{eq}}{M_o - M_{eq}} = \frac{8}{\pi^2} \exp(-\frac{\pi^2 D_{ef} t}{4L^2}) \qquad (6)$$

The effective diffusivity, D_{ef} is a lumped parameter resulting from the contribution of all mass transport mechanisms like gas diffusion, capillary flow, and bound water migration occurring in the different phases (Silva et al., 2000; Zogzas et al., 1994).The value of effective diffusivity can be derived from (3) either by non-linear regression or by using methods of slopes for the linearized equation (Ait Mohamed et al., 2008; Vega-Galvez et al., 2008). The coefficient of effective diffusivity obtained in above methods is found to be comparable to that of the exact values obtained by iterative techniques (general implicit Euler's method of finite differences) to solve the Ficks second law of diffusion, in materials where liquid diffusion is predominant (Karathanos and Belessiotis, 1999).

Effect of drying temperature on effective diffusivity or the drying rate can be expressed by an Arrhenius type equation (Karatas, 1997; Madamba et al., 1996; Maskan et al., 2002; VACCAREZZA and CHIRIFE, 1978)

$$\theta = \theta o \exp(-E / RT) \qquad (7)$$

Where θ, denotes the drying rate or effective diffusivity, E denotes the activation energy (kcal mol); R denotes the universal gas constant (kcal mol^{-1} K^{-1}); and T the

absolute temperature (K). The value *E* was calculated from the slope and k0 from the intercept of the linearized Arrhenius type equation (Barreiro et al., 1997).

Results and discussion

The results of biomass composition analysis are discussed in terms of its likelihood to support each energy conversion process that requires drying viz, transesterification, transesterification with anaerobic digestion and flash pyrolysis (Amin, 2009). The biomass composition of the consortium was high in protein, moderate in lipids and low in carbohydrate as the consortium is dominated by the protein rich species, scenedesmus (Table F.2). Total lipid content of the consortium is 16.10% which falls in the range reported for species like *Dunaliella salina*, *Scenedesmus obliquus, Scenedesmus dimorph, Isochrysis galbana* but lesser than the prominent lipid producers like botryoccous braunii, nanochloropsis, dunaliella (Chisti, 2007; Chisti, 2008; Deng et al., 2009; Li et al., 2008; Mata et al.). These results support the hypothesis that the native microalgae consortium can be developed to almost match the lipid production achieved by slow growing high lipid producing strains in open ponds that suffer severe drawbacks due to weed species invasion. It should also be noticed that the lipid content reported in this study includes triacylglecerol, the ideal feedstock for biofuel production along with poor biodiesel feedstock like free fatty acids and polar lipids that form water and gum respectively, during conventional alkaline catalyzed transesterification process (Canakci and Sanli, 2008; Knothe et al., 2005). Detailed lipid profiling studies are warranted to precisely determine the exact proportion of each lipid class and critical efforts are required to utilize the polar lipid portion of the microalgae rather than targeting the neutral lipid portion alone which was the focus in earlier studies (Hu et al., 2008; Pienkos and Darzins, 2009). The presence of free fatty acids and polar lipids may make the feedstock less attractive for the conventional transestrification process, but it was responsible for high energy content of the consortium. The calorific value of the consortium was 22.75 KJ/g which was falls in the range to that of scendesmus species (Matsunaga et al., 2009) chlorella species (Illman et al., 2000)and the other values reported in the literature (Chinnasamy et al.; Huntley and Redalje, 2007). Anaerobic digestion of the whole biomass, without any prior lipid extraction, may be an attractive option given the high calorific value. Even after the lipid extraction for biodiesel production, the spent biomass of the consortium can be a viable feedstock for anaerobic digestion as it produces not only methane but also recycle nitrogen and phosphorous and can supplement algal growth itself (Phang et al., 2000; Sialve et al., 2009). The high protein content, on the other hand may cause ammonium toxicity in the digesters which demands essential pretreatment methods before loading in the digester. The high protein content is also responsible for a low C/N ratio of 5.5 for the consortium in comparison to that of 20-25 which is considered ideal for higher methane production (Angelidaki and Ahring, 1993). Nevertheless, our consortium may be used as an efficient feedstock for anaerobic digestion, if preprocessing steps like chemical treatments, thermal treatment and ultrasonic treatments (Bougrier et al., 2006) that improve the disintegration of the recalcitrant cell walls of chlorella scenedesmus species (Okuda, 2002) is applied. The low carbohydrate content 6.63% makes the consortium less attractive for bioethanol fermentation. Flash pyrolysis , which involves heating the of the dried algal biomass in presence of a catalyst, at high

heating rate (103–104 K/s), short gas residence time to crack into short chain molecules and rapid cooling can directly produce liquid biocrude with efficiency ranging as high as 80% (Miao et al., 2004; Zhang et al., 2007).

Table F.2. Composition of oven dried algal consortium

Parameter	Values
Biochemical Composition (% of dry weight)	
Carbohydrate	6.63±1.07
Lipid	16.10±1.47
Protein	56.74±0.99
Ultimate Analysis (%)	
Carbon	49.94±0.55
Hydrogen	7.66±0.16
Nitrogen	9.08±0.16
Sulphur	0.5±0.02
Proximate Analysis (%)	
Ash	5.32±0.29
Volatile	80.09±0.81
Fixed Carbon	14.59±0.52
Heating value (Mj Kg^{-1})	22.75±0.10

Drying Characterization

The initial moisture content of the algal slurry was 757.39% on a dry weight basis and the density was 0.99246 g/ml. The relative humidity achieved at each drying air temperature of 30, 50 70 and 90 C was 23.9%, 15%, 6.5% and 3.9% respectively. The equilibrium moisture content, which determines the limit of moisture reduction in a material for a given ambient condition, decreased with increase in air temperature. Equilibrium moisture content (EMC) was determined as the moisture content at which there was no significant change in the subsequent weight measurements or the decrease of dry basis moisture content remained 0.1% consistently for successive readings. In all the drying air temperature the EMC reached was less than 18% (wet basis) which proves that the dried biomass is commercially stable (Vega-Galvez et al., 2008). The EMC achieved for drying air temperature of 30, 50, 70, 90° C were 13.01%, 10.15%, 1.52%, 1.54% respectively. The dehydration curves showed a clear exponential tendency (Figure 5.a) and it was observed that the drying time decreases with increase in the air temperature. The drying time for air temperature 30°, 50°, 70° and 90° C to achieve EMC was 1620, 1020, 690 and 440 minutes respectively. These results were similar to other few reports on algae drying for individual species like gelidium sesquipdale (Ait Mohamed et al., 2008), Aphanothece microscopica Nageli

(Jacob Lopes et al., 2007), spirulina plantis (Desmorieux and Decaen, 2006; Lemus et al., 2008; Oliveira et al., 2009) Gracilaria (Lemus et al., 2008) and macrocytis pyrifera (Vega-Galvez et al., 2008). A plot of drying rate against dry basis moisture content shown in Figure 5.b illustrates the absence of constant rate drying period and the whole drying process took place in falling rate drying period even though the biomass had high initial moisture content. This may be attributed to the fact that the biomass has high protein content (Chirife, 1983). This result also showed that diffusion was the dominant physical mechanism responsible for moisture movement within the samples.

Drying Kinetics modeling and effective diffusivity

The instantaneous moisture content of the slurry for all drying experiments were converted to dimensionless moisture ratio and plotted against drying time. Statistical parameters evaluated for each model through non-linear regression showed that all three drying kinetics model proposed in this research were useful. Nevertheless the page model best described the dehydration kinetics based on the high R^2, and closeness of RMSE and SSE to zero. Page's equation has been reported to adequately predict the thin layer drying of bagasse (Vijayaraj et al., 2007), pistachio (Midilli and Kucuk, 2003), shell corn, peanuts, and rapeseeds(Pathak et al., 1991), sunflower seeds (Syarief et al., 1984). The drying constant k, determined from page equation increased with increase in the drying temperature and it was found to be in the range of 0.002 to 0.035 min^{-1}. Similarly, the effective diffusivity calculated based on linearlized form of equation 6, increased with increase in drying temperature obtaining values between 2.70 and 11.00 x 10-^{10} m^2/s. Applying Arrhenius-type equation for effective diffusivity and drying rate constant resulted in activation energy of 41.19 and 21.37 Kj/mol respectively (Table F.3, Figure F.6). The values of effective diffusivity obtained for our consortium is lesser than that of the microalgae gracilaria (2.76-22.41x10-9), macrocytis pyrifera (5-10x10^{-9}), aphanothece microscopic nageli (8.1-8.8x10^{-8}) but higher than spirulina plantis (2.8- 4.2x10^{-11}). At the same time, the Def values was found similar to the food product like red pepper (3.2-11.2 x 10^{-9}), kale (14.9-55.9 x 10^{-10}), dill (6.70-14.34x10^{-10}), parsley (9-23.37 x 10^{-10}) (Vega-Galvez et al., 2008) and biofuel feedstock like sugarcane bagasse (1.63X10^{-10} to 3.2X10^{-10}) (Vijayaraj et al., 2007), olive oil bagasse (1.9-3.3x10^{-9}) (Freire et al., 2001), The drying rate constant and effective diffusivity for each temperature differed statistically from each other based on the p-value obtained (<0.05) for a confidence interval of 95% in one way ANOVA. Thus drying temperature has a significant effect on both drying rate constant and effective diffusivity. Similar statistical analysis (ANOVA) on the empirical constant n of the page equation showed lesser significant interaction (p=0.02) on the drying air temperature (Table F.3).

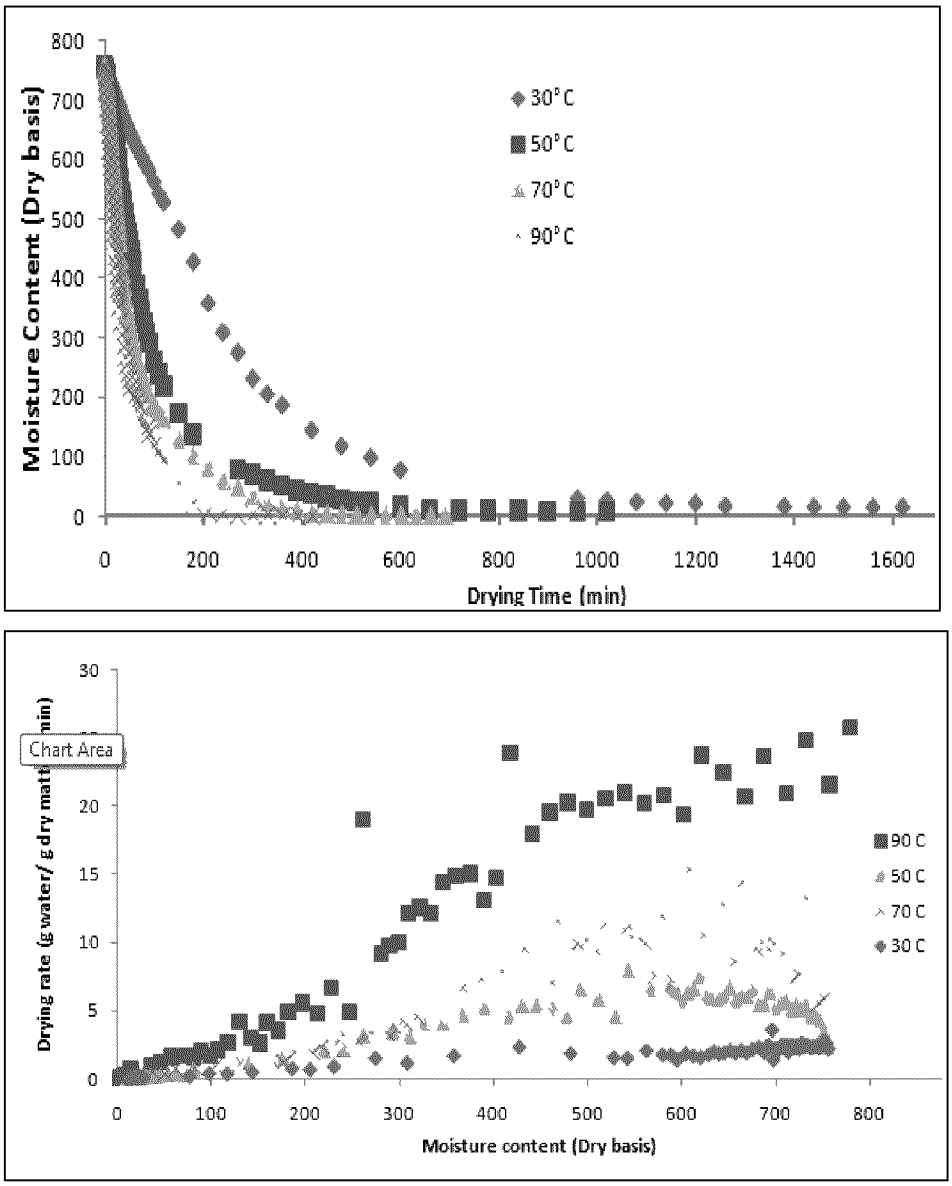

Figure F.5. (a) Drying curves (b) drying rate curves for the microalgal consortium

Table F.3. Values of kinetic parameters and statistical evaluation of each model

Model		30°	50°	70°	90°
Newton					
	k	0.0040	0.0117	0.0164	0.0314
	R2	0.9968	0.9963	0.9939	0.9959
	RMSE	0.0210	0.0216	0.0265	0.0190

	SSE	0.0359	0.0347	0.0476	0.0218
Henderson-pabis					
	a	1.0177	1.0142	1.0074	1.0056
	k	0.0048	0.0121	0.0166	0.0317
	R2	0.9980	0.9970	0.9940	0.9961
	RMSE	0.0182	0.0192	0.0265	0.0186
	SSE	0.0266	0.0274	0.0467	0.0209
Page Model					
	k	0.0021	0.0122	0.0197	0.0348
	n	1.1283	1.0101	0.9505	0.9699
	R2	0.9994	0.9971	0.9944	0.9966
	RMSE	0.0095	0.0189	0.0254	0.0176
	SSE	0.0070	0.0265	0.0434	0.0181
Diffusivity		2.708E-10	4.539E-10	7.218E-10	1.100E-09

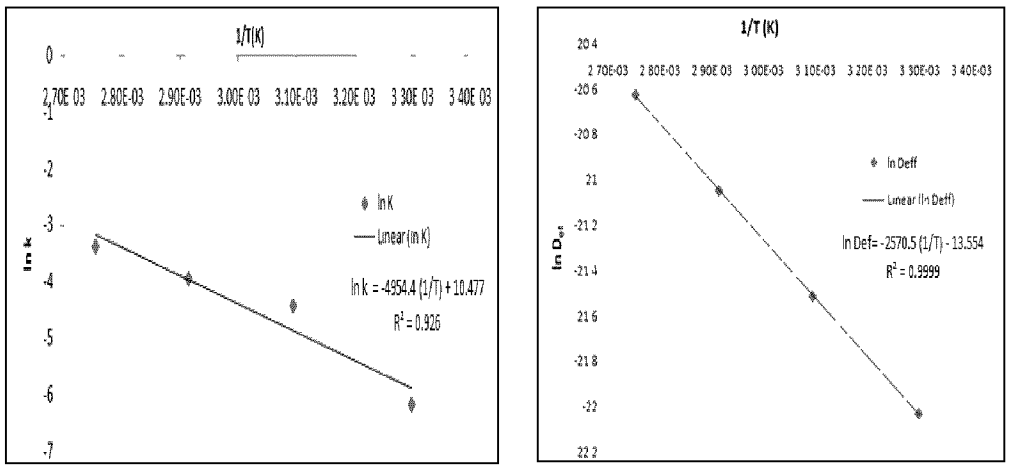

Figure F.6. Arrhenius-type relation between (a) drying rate constant and (b) effective diffusivity with temperature (Kelvin)

Key findings and conclusions

The desorption characteristics of the microalgae consortium suitable for biofuel application showed that the page model can satisfactorily simulate the drying behavior of the consortium. The effective diffusivity showed significant dependence on drying temperature with activation energy of 41.19 kJ/mol based on Arrhenius type equation. In spite of high initial moisture content, the constant rate drying period was not observed and the whole drying process occurred in first stage falling-rate

period, probably due to the high protein content of the consortium. The consortium is also found to be applicable for different biofuels conversion strategies based upon the biochemical composition.

Subtask F.3: Integrating algae biomass production with an integrated biorefinery.

Modification of plans: Our original plan was ambitious and was to develop the technology for multiple products from algae, thereby taking the algae into an integrated biorefinery. We believe that only modest steps towards this direction were achieved.

The task of cultivating algae in a wastewater stream itself was very challenging. However, we were able to demonstrate that several algae and a consortium was able to grow well providing attractive biomass productivity. Further research is required to convert these harvested algae to further products, thus leading to formation of a biorefinery. Our work thus far indicted that thermochemical liquefaction is an attractive candidate, however no work was done in this project towards evaluating this pathway.

Task G – Educational outreach and technology transfer program

Our team was actively involved in continuously transferring technology and recent findings through outreach and education during this project. These activities included, direct one-on-one talks with industry partners and entrepreneurs interested in the areas of work in integrated biorefineries, conference presentations, site visits and presentations to larger industries, and service in state agency based outreach functions. In education, the laboratories involved in this research directly trained undergraduate and graduate students, post-doctoral fellows, technical staff, and collaborators not directly funded out of this project.

Over the period of this grant (which overlapped with GO 85012), 22 students were trained, including 5 PhD and 13 Masters degree research along with 4 formal undergraduate student research training. The biorefinery research conducted provided training opportunity for 14 research technicians, 6 postdoctoral scientists and 34 research collaborators. The total persons trained in this project were 76 persons.

Listing of conference proceedings, peer reviewed journal articles and patents that came out of this work are listed in the following sections.

Products developed under the award and technology transfer activities

Publications (list journal name, volume, issue), conference papers

3. Schomberg, H.H., J.W. Gaskin, K. Harris, K.C. Das, J.M. Novak, W.J. Busscher, D.W. Watts, R.H. Woodroof, I.M. Lima, M. Ahmedna, D. Rehrah, and B. Xing. 2011. Influence of biochar on nitrogen fractions in a coastal plain soil. Journal of Environmental Quality [In Press]
4. Jena, U., K.C. Das, and J.R. Kastner. 2012. Comparison of the effects of

Na_2CO_3, $Ca_3(PO_4)_2$, and NiO catalysts on the thermochemical liquefaction of microalga *Spirulina platensis*. Applied Energy. In press.

5. Novak, J.M., I. Lima, B. Xing, J.W. Gaskin, C. Steiner, **K.C. Das**, M. Ahmedna, D. Rehrah, D.W. Watts, W.J. Busscher, and H. Schomberg. 2011. Development of designer biochar to remediate specific chemical and physical aspects of degraded soils: influence of biochars on availability of fixed N fractions. Journal of Environmental Quality [In Press]
6. Mattos, E., R. Hunt, M. van Iersel, M. Cabrera, and K.C. Das. 2011. Changes in chlorophyll fluorescence parameters in different growth stages of *Chlorella sorokiniana*. ABO Summitt, Minneapolis, 25-27 Oct 2011.
7. Vandenbrink, J.P., R.N. Hilten, **K.C. Das**, A.H. Paterson, and F.A. Feltus. 2011. Analysis of crystalline index and hydrolysis rates in the bioenergy crop *Sorghum bicolor*. Bioenergy Research [In Press] DOI: 10.1007/s12155-011-9146-2.
8. Jena, U. and **K.C. Das**. 2011. Comparative evaluation of thermochemical liquefaction and pyrolysis for BioOil production from microalgae. Energy & Fuels, 25(11):5472-5482
9. Hunt, R.W., S. Chinnasamy, and **K.C. Das**. 2011. The effect of naphthalene-acetic acid on biomass productivity and chlorophyll content of green algae, coccolithophore, diatom and cyanobacteria cultures. Applied Biochemistry and Biotechnology, 164(8):1350-1365.
10. Singh, M., D.L. Reynolds, and **K.C. Das**. 2011. Microalgal system for treatment of effluent from poultry litter anaerobic digestion. Bioresource Technology, 102(23):10841-10848.
11. Steiner, C., N.D. Melear, K. Harris, and **K.C. Das**. 2011. Biochar as bulking agent for poultry litter composting. Carbon Management, 2(3):227-230.
12. Putt, R., M. Singh and **K.C. Das**. 2011. An efficient system for carbonation of high-rate algae pond water to enhance CO2 mass transfer. Bioresource Technology, 102(3):3240-45
13. Garcia, S., K. Jangid, W.B. Whitman, and **K.C. Das**. 2011. Transition of microbial communities during the adaptation of anaerobic digestion of carrot waste. Bioresource Technology, 102(15):7249-7256.
14. Jena, U., **K.C. Das** and J.R. Kastner. 2011. Effect of operating conditions of thermochemical liquefaction on biocrude production from *Spirulina platensis*. Bioresource Technology, 102(1):6221-6229.
15. Bhatnagar, A., S. Chinnasamy, M. Singh and **K.C. Das**. 2011. Renewable biomass production by mixotrophic algae in the presence of various carbon sources and wastewater. Applied Energy, 88(10):3425-3431.
16. Jena, U., N. Vaidyanathan, S. Chinnasamy, and **K.C. Das**. 2011. Evaluation of microalgae cultivation using recovered aqueous co-product from

thermochemical liquefaction of algal biomass. Bioresource Technology, 102(3):3380-87.

17. Liesh, A.M., S.L. Weyers, J.W. Gaskin and **K.C. Das**. 2010. Impact of two different Biochars on earthworm growth and survival. Annals of Environmental Science, 4:1-9.
18. Hunt, R.W., S. Chinnasamy, A. Bhatnagar, and **K.C. Das**. 2010. Effect of biochemical stimulants on biomass productivity and metabolite content of the microalga, *Chlorella sorokiniana*. Applied Biochemistry and Biotechnology, 162(8):2400-2414.
19. Singh, K., M. Risse, J. Worley, **K. C. Das**, and S. Thompson. 2010. Effect of fractionation and pyrolysis on fuel properties of poultry litter. Journal of Air and Waste Management, 60(7):875-883
20. Singh, K., K. Lee, J. Worley, L.M. Risse and **K.C. Das**. 2010. Anaerobic digestion of poultry litter – a Review. Applied Engineering in Agriculture, 26(4):677-688.
21. Vishwanathan, T., S. Mani, K.C. Das, S. Chinnasamy, and A. Bhatnagar. 2011. Thin layer drying kinetics and chemical composition of microalgae consortium. Transactions of the ASABE, 54(6):2245-2252
22. Hilten, R., R. Speir, J. Kastner and K.C. Das. 2011. Production of gasoline-like fuel via catalytic pyrolysis of acidulated peanut oil soap stock. Bioresource Technology 102(17):8288-8294
23. Doydora, S., M. Cabrera *, K.C. Das, J. Gaskin, L. Sonon, and W. Miller. 2011. Release of nitrogen and phosphorus from poultry litter amended with acidified biochar. IJERPH Special issue: Soil Pollution – Preventaion and Mitigation, 8(5):1491-1502.
24. Das, K.C., K. Singh, B.P. Bibens, R. Hilten, S.A. Baker, W.D. Greene and J.D. Peterson. 2011. Pyrolysis characteristics of forest residues obtained from different harvesting methods. Applied Engineering in Agriculture, 21(1):107-113.
25. Ormsby, R.V. 2011. Levoglucosan transformation and kinetics of hemicellulose hydrolysis using carbon supported solid acid catalysts. Unpublished M.S. Thesis, Biological Engineering, The University of Georgia, Athens GA 30602.
26. Lakshmanaswamy, A., E. Rajaraman, M. A. Eiteman, E. Altman. 2011. Microbial removal of acetate selectively from sugar mixtures. *Journal of Industrial Microbiology and Biotech.,* in press (2011) doi: 10.1007/s10295-010-0932-1
27. Garcia-Perez, M., T.T. Adams, J.W. Goodrum, K.C. Das, and D.P. Geller. 2010. DSC studies to evaluate the impact of bio-oil on cold flow properties and oxidation stability of biodiesel. Bioresource Technology, 101(15):6219-24.

28. Chinnasamy, S., A. Bhatnagar, R. Claxton and K.C. Das. 2010. Biomass and bioenergy production potential of microalgae consortium in open and closed bioreactors using untreated carpet industry effluent as growth medium. Bioresource Technology, 101(17):6751-60.

29. Hilten, R., R. Speir, J.R. Kastner, and K.C. Das. 2010. Production of fuel from the catalytic cracking of pyrolyzed poultry DAF skimmings. Journal of Analytical and Applied Pyrolysis 88(1):30-38.

30. Hilten, R. and K.C. Das. 2010. Comparison of three accelerated aging procedures to assess bio-oil stability. Fuel 89(10): 2741-2749.

31. Steiner, C., K.C. Das, N.D. Melear, and D. Lakly. 2010. Reducing nitrogen losses during poultry litter composting using biochar. Journal of Environmental Quality, 39(4):1236-42.

32. Chinnasamy, S., A. Bhatnagar, R.W. Hunt, and K.C. Das. 2010. Microalgae cultivation in wastewater dominated by carpet mill effluents for biofuel applications. Bioresource Technology 101(9):3097-3105.

33. Bhatnagar, A., M. Bhatnagar, S. Chinnasamy and K.C. Das. 2010. *Chlorella minutissima*-A promising fuel alga for cultivation in municipal wastewaters. Applied Biochemistry and Biotechnology 161(8):523-536.

34. Gaskin, J.W., R.A. Speir, D. Lee, K. Harris, L.A. Morris, K.C. Das and D. Fisher. 2010. Effect of peanut hull and pine chip biochar on soil nutrients, corn nutrient status and yield. Agronomy Journal, 102, 623-633.

35. Hilten, R., B. Bibens, J.R. Kastner and K.C. Das. 2010. In-line esterification of pyrolysis vapor with ethanol improves bio-oil quality. Energy & Fuel 24(1):673-682.

36. Risse, L. M., K. Singh, K.C. Das, J. Worley and S. Thompson, 2010. Value Added Poultry Litter Products through Fractionation and Pyrolysis. Poster abstract for the National Animal and Poultry Waste Management Symposium, Greensboro, NC, September 26-28, 2010.

37. Das, K.C., M. Singh, M. Garcia-Perez, and S. Chinnasamy. 2010. Biorefinery Technologies – an overview. International Conference on Bioengineering, SRM University, Chennai, India, July 29-31 [Presentation and Proceedings]

38. Chinnasamy, S., M. Singh, and K.C. Das. 2010. Microalgae technology for integrated waste management with bioenergy production. International Conference on Bioengineering, SRM University, Chennai, India, July 29-31 [Presentation and Proceedings]

39. Almeida, A., K.C. Das, and N. Balagurusamy. 2010. Biochemical methane potential of desert plants: *Aloe vera* and *Opuntia robusta* in Comarca Lagunera, Mexico. Proceedings of the 3rd Intl Symposium on Energy from Biomass and Waste, Venice, Italy, Nov 8-11.

40. Alvarado, A., S. Chinnasamy, K.C. Das, and N. Balagurusamy. 2010. Opportunities for co-digestion of industrial and agricultural substrates for

anaerobic digestion. Proceedings of the 3rd Intl Symposium on Energy from Biomass and Waste, Venice, Italy, Nov 8-11.

41. Steiner, C., K.C. Das, N. Melear, J. Gaskin, K. Harris, and D. Lakly. 2010. Biochar use in the poultry industry. 3rd Intl Biochar Conference, Rio de Janeiro, Brazil, Sept 12-15.
42. Viswanathan, T., S. Mani, S. Chinnasamy, K.C. Das. 2010. Effect of cell rupturing methods on the drying characteristics of microalgae. Society of Industry Microbiology, 32nd Symposium on Biotechnology for Fuels and Chemicals, Clearwater beach FL, April 19-22.
43. Novak, J.M., I. Lima, B. Xing, J.W. Gaskin, C. Steiner, K.C. Das, M. Ahmedna, D. Rehrah, D.W. Watts, W.J. Busscher, and H. Schomber. 2009. Characterization of designer biochar produced at different temperatures and their effects on a loamy sand. Annals of Environmental Science, 3, 195-206.
44. Hunt, R.W., A. Zavalin, A. Bhatnagar, S. Chinnasamy and K.C. Das. 2009. Electromagnetic biostimulation of living cultures for biotechnology, biofuel, and bioenergy applications. International Journal of Molecular Science 10, 4515-4558.
45. Chinnasamy, S., B. Ramakrishnan, A. Bhatnagar, S.K. Goyal and K.C. Das. 2009. Carbon and nitrogen fixation under elevated levels of CO_2 and temperature by Anabena fertilissima. Journal of Freshwater Ecology 24(4):587-596.
46. Singh, K., M. Risse, J. Worley, K. C. Das, and S. Thompson. 2009. Studying compaction behavior of fractionated poultry litter and use of pyrolysis condensate as a binder during pelletizing. Transactions of ASABE 52(3):949-956.
47. Smith, J.S., M. Garcia-Perez, and K.C. Das. 2009. Producing fuel and specialty chemicals from the slow pyrolysis of poultry DAF skimmings. Journal for Analytical and Applied Pyrolysis 86(1):115-121
48. Chinnasamy, S., B. Ramakrishnan, A. Bhatnagar, and K.C. Das. 2009. Biomass production potential of a wastewater alga Chlorella vulgaris ARC 1 under elevated levels of CO2 and temperature. International Journal of Molecular Sciences 10(2):518-532.
49. Kastner, J.R., J. Miller, P. Kolar, and K.C. Das. 2009. Catalytic ozonation of ammonia using biomass char and wood fly ash. Chemosphere 75, 739-744.
50. Gaskin, J.W., C. Steiner, K.R. Harris, K.C. Das, and B. Bibens. 2008. The effect of low-temperature pyrolysis conditions on the characteristics of poultry litter, peanut hull, and pine chip biochars for agricultural use. Transactions of the ASABE 51(6):2061-2069
51. Das, K.C., S. Chinnasamy, G. Hawkins and C. Steiner. 2009. Organic waste management - Bioproducts and Biofuel Opportunities. AgriINTEX International Conference - Next Generation of Indian Agriculture,

Coimbatore, India, October 2-5, 2009 [International Invited Keynote Presentation]

52. Singh, K., K.C. Das, M. Risse, and J. Worley. 2009. Determination of Composition of Cellulose and Lignin Mixture using Thermo Gravimetric Analysis (TGA). Journal of Energy Resource Technology 131(2): DOI: 10.1115/1.3120349
53. Kastner .J.R, J. Miller, and K.C. Das. 2009. Pyrolysis conditions and ozone oxidation effects on ammonia adsorption in biomass generated chars. Journal of Hazardous Materials, 164(2-3):1420-1427.
54. Jena, U., and K.C. Das. 2009. State of the art thermochemical liquefaction of biomass for biofuel generation. Annual meeting of American Society Agricultural and Biological Engineering, Reno, Nevada, USA. June 20-24.
55. Eiteman, M.A., S. A. Lee, R. Altman, E. Altman. 2009. A substrate-selective co-fermentation strategy with *Escherichia coli* produces lactate by simultaneously consuming xylose and glucose. *Biotechnology and Bioengineering*, 102(3):822-827.
56. Vairavapandian, D. 2009. Formation of platinum thin films by electrochemical ALD and 2nd network of carbon nanotubes for electrochemical applications. PhD Dissertation, The University of Georgia, Department of Chemistry.

Web site or other Internet sites that reflect the results of this project

This project hosted a website www.biorefinery.uga.edu that was intended to provide an overview of activities in the project. Listing of publications is provided on this site, however no direct description of research results are shown.

Networks or collaborations fostered

Through this project we fostered a very effective partnership with USDA-ARS represented by laboratories/centers in Georgia, South Carolina and Illinios. Several publications have resulted from this partnership and research work is continuing in a partnership at the time of writing this report.

Several on-campus partnerships between Engineering (lead), Crop and Soil Science, Microbiology, Forestry, and other fields have resulted.

Technologies/Techniques

Technologies developed in activities that included this grant were in pyrolysis, algal production in wastewaters and in fermentation. University of Georgia has partnered with Dalton Utilities (Dalton, Georgia) in developing a method of removing phosphorus from wastewater while cultivating algae for biofuel applications. The work includes laboratory scale testing and onsite pilot testing at the company site. Although this interaction started prior to the initiation of this grant, a bulk of the work continued on during the period of this grant, and is ongoing beyond the end of this grant. Funding for these efforts have been through multiple sources including direct

funding from Dalton Utilities, this DOE grant (GO88144), and Appalachian Regional Council.

Inventions/Patent Applications, licensing agreements

A listing of patent applications that came out of this effort is shown below. Of these applications, some have been licensed and are described later.

1. U.S. Utility Patent Application 2011. Biological optimization systems for enhancing photosynthetic efficiency and methods of use. Publication No. US 2011/0179706A1; Application No: 13/014,464 Filed Jan 26, 2011. UGARF. Inventors: R.W. Hunt, S. Chinnasamy, K.C. Das, and E.R de Mattos.
    - U.S. Provisional Patent Application. 2010. Biostimulants for enhancing biomass productivity and other metabolites in algae for biofuel and other commercial applications. K.C. Das, R.W. Hunt, S. Chinnasamy. Docket No. 222102-8990. Utility Patent Application Filed, Jan 16, 2011 (listed above).
    - Patent Disclosure: 2010. Biostimulants for enhancing biomass productivity and other metabolites in algae for biofuel and other commercial applications. Inventors: K.C. Das, R.W. Hunt, S. Chinnasamy. Provisional Patent Application Field (listed above).
2. U.S. Utility Patent Application. 2010. Algal lipid harvest using mollusk for biofuel production. Publication No. US 2011/0045556; Application No. 12/862,246. Filed Aug 24, 2010. UGARF. Inventors: K.C. Das, S. Chinnasamy, J. Shelton, S.B. Wilde, R.S. Haynie and J.A. Herrin.
    - Patent Disclosure: 2009. A novel biobased method of harvesting microalgae for biofuels production. Inventors: K.C. Das, S. Chinnasamy, J. Shelton, S. Wilde, R. Haynie, J. Herrin.
3. U.S. Utility Patent Application. 2010. Method of increasing biomass productivity, lipid induction, and controlling metabolites in algae for production of biofuels using biochemical stimulants. Publication No. US 2011/0091945 A1; Application No. 12/907,206. Filed Oct 19, 2010. UGARF. Inventors: K.C. Das, R.W. Hunt, S. Chinnasamy, R. Claxton, and P. Raber.
4. Patent Disclosure: 2009. Process and product for minimizing nitrogen losses, enhancing microbial activity and accelerating stabilization of organic wastes during composting. Inventors: C. Steiner (4/10), K. C. Das (4/10), N.D. Melear (2/10).